TECHNICAL REPORT STANDARD TITLE PAGE

1. Report No.	2. Government Accession No.	3. Recipient's Catalog No.
CFHR 1-8-69-123-16		

4. Title and Subtitle	5. Report Date
"Fatigue and Stress Analysis Concepts for Modifying the Rigid Pavement Design System"	January 1973
	6. Performing Organization Code
7. Author(s)	8. Performing Organization Report No.
Piti Yimprasert and B. Frank McCullough	Research Report 123-16
9. Performing Organization Name and Address	10. Work Unit No.
Center for Highway Research The University of Texas at Austin Austin, Texas 78712	11. Contract or Grant No. Research Study 1-8-69-123
	13. Type of Report and Period Covered
12. Sponsoring Agency Name and Address	Interim April 1971 - October 1972
Texas Highway Department 11th & Brazos Austin, Texas 78701	14. Sponsoring Agency Code

15. Supplementary Notes

Research performed in cooperation with DOT, FHWA.
Research Study Title: "A System Analysis of Pavement Design and Research Implementation"

16. Abstract

Traffic associated fatigue of concrete is a significant influence on the distress of the rigid pavement system. This study reports the fatigue property of concrete as well as a stress analysis of reinforced and nonreinforced sections at the AASHO Road Test. The concrete fatigue equation was developed for the prediction of the allowable number of applications on concrete at any applied stress level. In the stress analysis, the effect of load transfer and the loss of support of pavement slab were taken into consideration for both pavement types.

The load transfer analysis shows that the reductions in bending and twisting stiffness at the joint of reinforced sections are 97 percent of the full stiffness value at two adjacent stations, and 81 percent at one station, respectively. For nonreinforced sections, the reduction in bending stiffness is 100 percent at one station and there is no reduction in twisting stiffness. The influence of load transfer on the behavior of rigid pavement is highly important.

The loss of support analyses explain the differences in distress and performance histories of the rigid pavement sections which have the same design variables at the AASHO Road Test. The shape of the eroded area beneath the two adjacent slabs was developed to simulate the pumping condition in the field. The maximum principal stress was predicted at any pumping index and usually increases as the pumping index increases.

17. Key Words	18. Distribution Statement
fatigue, envelope curve, shakedown limit, load transfer, pumping index, eroded area, maximum principal stress	

19. Security Classif. (of this report)	20. Security Classif. (of this page)	21. No. of Pages	22. Price
Unclassified	Unclassified	137	

Form DOT F 1700.7 (8-69)

FATIGUE AND STRESS ANALYSIS CONCEPTS FOR MODIFYING THE RIGID PAVEMENT DESIGN SYSTEM

by

Piti Yimprasert
B. Frank McCullough

Research Report Number 123-16

A System Analysis of Pavement Design
and Research Implementation

Research Project 1-8-69-123

conducted for

The Texas Highway Department

in cooperation with the
U. S. Department of Transportation
Federal Highway Administration

by the

Highway Design Division
Texas Highway Department

Texas Transportation Institute
Texas A&M University

Center for Highway Research
The University of Texas at Austin

January 1973

The contents of this report reflect the views of the authors, who are responsible for the facts and the accuracy of the data presented herein. The contents do not necessarily reflect the official views or policies of the Federal Highway Administration. This report does not constitute a standard, specification, or regulation.

PREFACE

This report is one of a series that describes work done under the project entitled "A System Analysis of Pavement Design and Research Implementation." The project is a joint effort by the Texas Highway Department; Center for Highway Research, The University of Texas at Austin; and the Texas Transportation Institute, Texas A&M University.

This report presents the development of a mathematical model for simulating the behavior of rigid pavement in the field under repeated loads. The effects of load on different sizes of slabs were determined by analyses of load transfer across the joints. Included herein is the development of a model to predict the fatigue life of concrete.

Special appreciation is extended to Mrs. Nancy Braun and to the rest of the Center for Highway Research personnel for their cooperation and contributions.

Piti Yimprasert

B. Frank McCullough

January 1973

LIST OF REPORTS

Report No. 123-1, "A Systems Approach Applied to Pavement Design and Research," by W. Ronald Hudson, B. Frank McCullough, F. H. Scrivner, and James L. Brown, describes a long-range comprehensive research program to develop a pavement systems analysis and presents a working systems model for the design of flexible pavements.

Report No. 123-2, "A Recommended Texas Highway Department Pavement Design System Users Manual," by James L. Brown, Larry J. Buttler, and Hugo E. Orellana, is a manual of instructions to Texas Highway Department personnel for obtaining and processing data for flexible pavement design system.

Report No. 123-3, "Characterization of the Swelling Clay Parameter Used in the Pavement Design System," by Arthur W. Witt, III, and B. Frank McCullough, describes the results of a study of the swelling clay parameter used in pavement design system.

Report No. 123-4, "Developing A Pavement Feedback Data System," by R. C. G. Haas, describes the initial planning and development of a pavement feedback data system.

Report No. 123-5, "A Systems Analysis of Rigid Pavement Design," by Ramesh K. Kher, W. R. Hudson, and B. F. McCullough, describes the development of a working systems model for the design of rigid pavements.

Report No. 123-6, "Calculation of the Elastic Moduli of a Two Layer Pavement System from Measured Surface Deflections," by F. H. Scrivner, C. H. Michalak, and W. M. Moore, describes a computer program which will serve as a subsystem of a future Flexible Pavement System founded on linear elastic theory.

Report No. 123-6A, "Calculation of the Elastic Moduli of a Two Layer Pavement System from Measured Surface Deflections, Part II," by Frank H. Scrivner, Chester H. Michalak, and William M. Moore, is a supplement to Report No. 123-6 and describes the effect of a change in the specified location of one of the deflection points.

Report No. 123-7, "Annual Report on Important 1970-71 Pavement Research Needs," by B. Frank McCullough, James L. Brown, W. Ronald Hudson, and F. H. Scrivner, describes a list of priority research items based on findings from use of the pavement design system.

Report No. 123-8, "A Sensitivity Analysis of Flexible Pavement System FPS2," by Ramesh K. Kher, B. Frank McCullough, and W. Ronald Hudson, describes the overall importance of this system, the relative importance of the variables of the system and recommendations for efficient use of the computer program.

Report No. 123-9, "Skid Resistance Considerations in the Flexible Pavement Design System," by David C. Steitle and B. Frank McCullough, describes skid resistance consideration in the Flexible Pavement System based on the testing of aggregates in the laboratory to predict field performance and presents a nomograph for the field engineer to use to eliminate aggregates which would not provide adequate skid resistance performance.

Report No. 123-10, "Flexible Pavement System - Second Generation, Incorporating Fatigue and Stochastic Concepts," by Surendra Prakash Jain, B. Frank McCullough, and W. Ronald Hudson, describes the development of new structural design models for the design of flexible pavement which will replace the empirical relationship used at present in flexible pavement systems to simulate the transformation between the input variables and performance of a pavement.

Report No. 123-11, "Flexible Pavement System Computer Program Documentation," by Dale L. Schafer, provides documentation and an easily updated documentation system for the computer program FPS-9.

Report No. 123-12, "A Pavement Feedback Data System," by Oren G. Strom, W. Ronald Hudson, and James L. Brown, defines a data system to acquire, store, and analyze performance feedback data from in-service flexible pavements.

Report No. 123-13, "Benefit Analysis for Pavement Design System," by W. Frank McFarland, presents a method for relating motorist's costs to the pavement serviceability index and a discussion of several different methods of economic analysis.

Report No. 123-14, "Prediction of Low-Temperature and Thermal-Fatigue Cracking in Flexible Pavements," by Mohamed Y. Shahin and B. Frank McCullough, describes a design system for predicting temperature cracking in asphalt concrete surfaces.

Report No. 123-15, "FPS-11 Flexible Pavement System Computer Program Documentation," by Hugo E. Orellana, gives the documentation of the computer program FPS-11.

Report No. 123-16, "Fatigue and Stress Analysis Concepts for Modifying the Rigid Pavement Design System," by Piti Yimprasert and B. Frank McCullough, describes the fatigue of concrete and stress analyses of rigid pavement.

ABSTRACT

Fatigue of concrete is a significant influence on the distress of the rigid pavement system. This study reports the fatigue property of concrete as well as the stress analysis of reinforced and nonreinforced sections at the AASHO Road Test. The concrete fatigue equation was developed for the prediction of the allowable number of applications on concrete at any applied stress level. In the stress analysis, the effect of load transfer and the loss of support of pavement slab were taken into consideration for both pavement types. The reinforced and nonreinforced sections are 24-by-40-foot and 24-by-15-foot slab panels, respectively.

The analysis of load transfer serves to accomplish the discontinuity of reinforced and nonreinforced sections. The analyses are based on the corner deflections obtained from the theoretical analyses and the AASHO Road Test equations (Ref 32). The results show that the reductions in bending and twisting stiffness at the joint of reinforced sections are 97 percent of the full stiffness value at two adjacent stations and 81 percent at one station, respectively. For nonreinforced sections, the reduction in bending stiffness is 100 percent at one station and there is no reduction in twisting stiffness. The influence of load transfer on the behavior and performance of rigid pavement is highly important. The maximum principal stress usually increases as the reduction in twisting stiffness increases, while no significant change in deflection is encountered. The reduction in bending stiffness causes significant increases in deflection, while there is no significant change in stress. These results were analyzed to cover the simulations of the characteristics of reinforced and nonreinforced sections at the AASHO Road Test.

The loss of support analyses explain the differences in distress and performance histories of the rigid pavement sections which have the same design variables at the AASHO Road Test. The shape of the eroded area beneath the two adjacent slabs was developed to simulate the pumping condition in the field. The maximum principal stress was predicted at any pumping index and usually increases as the pumping index increases. The analyses provide the predictions of the maximum principal stresses for each month during the test period at the AASHO Road Test.

KEY WORDS: fatigue, envelope curve, shakedown limit, load transfer, pumping index, eroded area, maximum principal stress.

SUMMARY

A mathematical model for predicting the maximum stress at any pumping index in rigid pavement has been developed. The analyses techniques and transformations in the model are simulations of pavement observations at the AASHO Road Test. As a part of the model, a fatigue equation of portland cement concrete has been developed to predict the fatigue life of a concrete pavement using laboratory test data.

The development has the advantage of clarifying the histories of rigid pavement performance where subbase erosion and pumping have been experienced and gives the background for further improvements in the rigid pavement design methods.

IMPLEMENTATION STATEMENT

A mathematical model has been developed in this paper for simulating the behavior of rigid pavements in the field under repeated loads. This stress analysis system predicts the maximum principal stress for any condition of subbase pumping or erosion for both reinforced and nonreinforced pavements in varying degrees of load transfer. A fatigue equation for portland cement concrete was developed considering most of the available concrete fatigue research. Laboratory data can be used to quantify the parameters of fatigue equation. In addition, varying the model also considers varying degrees of load transfer, thus permitting the designer to select optimum system considering load transfer.

The developed system has the capability of explaining the nature of induced stresses due to traffic application with varying subsurface conditions, thus it can be used to explain the differences in performance histories of various pavement types. For the first time the value of stabilized subbases can be justified on the basis of design procedures. Also the relative value of various load transfer systems may be evaluated to permit the engineer to select an optimum system.

The development system may be combined with other improvements in the rigid pavement design system (RPS) to give a more complete rigid pavement design method that takes into account fatigue of the concrete, the joint spacing, load transfer simulation and variations of subsurface. Before the system can be fully implemented with a new subbase material, a test method must be evaluated for predicting the erodibility characteristics of a subbase material.

TABLE OF CONTENTS

C H A P T E R I

INTRODUCTION

As the present methods of pavement design require more exact solutions, the characteristics, mechanism, and behavior of the materials and design variables become increasingly important to highway engineers. In this report, the theoretical analysis and the data from the controlled field experiment from the AASHO Road Test were analyzed and collected to obtain the best information for the prediction of fatigue distress in rigid pavement. Most materials in rigid pavement possess the characteristic of failing by progressive fracture. This fracture is started by the application of loads and increases as the load applications increase. After a certain number of load repetitions, it fails in fatigue.

It is well known that rigid pavement distress under repeated load involves the number and the interaction of variables such as loading variables, material characteristics, and the environmental conditions. The response of the pavement to the load repetitions is usually characterized by measured stresses, strains, deflections,

and observed distress manifestations. Therefore, a more rational method of pavement design in rigid pavement is needed, which could predict the fatigue life and the maximum principal stress under various stages of pavement and subbase conditions.

Objective

The primary objective of this report is to develop fatigue and stress analysis concepts for modifying the rigid pavement system. The more specific objectives of this development are:

(1) To review and summarize the information pertaining to the fatigue properties of concrete and develop fatigue equations from the laboratory test data, and

(2) data analyses to obtain the best procedure for the prediction of stress in rigid pavement.

Scope

The concrete fatigue equation was developed by using computer program, the stepwise regression analysis STEP 01. This computer program was used to correlate the

relationship between the number of applications, applied stress ratio, and the speed of testing. Only the failed sections were selected to perform the concrete fatigue equation.

The stress analysis used the discrete-element SLAB program to evaluate the maximum principal stresses in rigid pavement (AASHO Road Test). Many variables were taken into consideration in the evaluation of maximum principal stresses and are listed below:

(1) joint spacing,

(2) variation of subsurface materials, and

(3) pumping of subsurface materials.

The importance of each of these variables was determined on the basis of changes of maximum principal stresses and deflections due to traffic applications only. This study excludes the effect of temperature on slab performance.

Chapter II summarizes a literature review on the fatigue properties of concrete from laboratory tests and the development of the fatigue equation from laboratory test data.

Chapter III presents the data collected from the AASHO Road Test for the analysis of the following chapters.

Chapter IV presents the analysis of load transfer effects to accommodate the differences in distress and performance histories of reinforced and nonreinforced sections.

Chapter V presents the transformations of pumping index at the AASHO Road Test to the eroded area beneath slab for the feasible use of discrete-element slab program in predicting maximum principal stresses during the test period.

Chapter VI presents the prediction of maximum principal stresses for reinforced and nonreinforced sections at any pumping index during the test period.

Chapter VII presents conclusions and future research needs in this area.

C H A P T E R I I

FATIGUE OF CONCRETE

Studies have shown that fatigue of concrete is one of the major distress mechanisms in rigid pavement (Ref. 32). The purpose of studying the fatigue property of concrete is not only for economical and proper design, but also to obtain a better understanding of the characteristics of concrete failure after years of service. Fatigue failure of concrete may be caused by flexural stress, compressive stress, or the combination of these.

The fatigue of concrete is defined as "the process of progressive localized permanent structural change occurring in the material subjected to conditions which produce fluctuating stresses and strains at some point or points and which may culminate in cracks or complete fracture after sufficient number of fluctuations" (Ref. 10). The manner in which the test specimens are subjected to fluctuating stresses and strains in the fatigue test has been categorized in terms of load conditions and mode of loading. If the load conditions remain constant throughout the life of the specimen, the specimen is said to be

subjected to simple loading condition. If the load condition changes during repeated stressing in some described manner, the specimen is subjected to compound loading. Usually in fatigue tests of concrete, the stress level, expressed in terms of the ratio between the maximum applied stress and the strength of concrete, remains constant throughout the test period. Figure 2.1 shows the typical characteristic of the material under repeated load at the constant stress level. The results show that at the certain stress level, the strain usually increases as the number of applications increase.

Recently, continuously reinforced concrete pavement design has greatly increased the use of concrete in highway construction. Rigid pavement design system usually uses a rather low factor of safety in design because of economic purposes. It is believed that the flexural stress in concrete slab due to traffic applications is one factor that might lead to distress of rigid pavement. Therefore, to simulate the behavior of a slab under repeated loading, the fatigue of concrete in flexure will be presented in this report. The concrete fatigue equation was also developed to predict the allowable number of applications which can be applied to the specimens at any stress level.

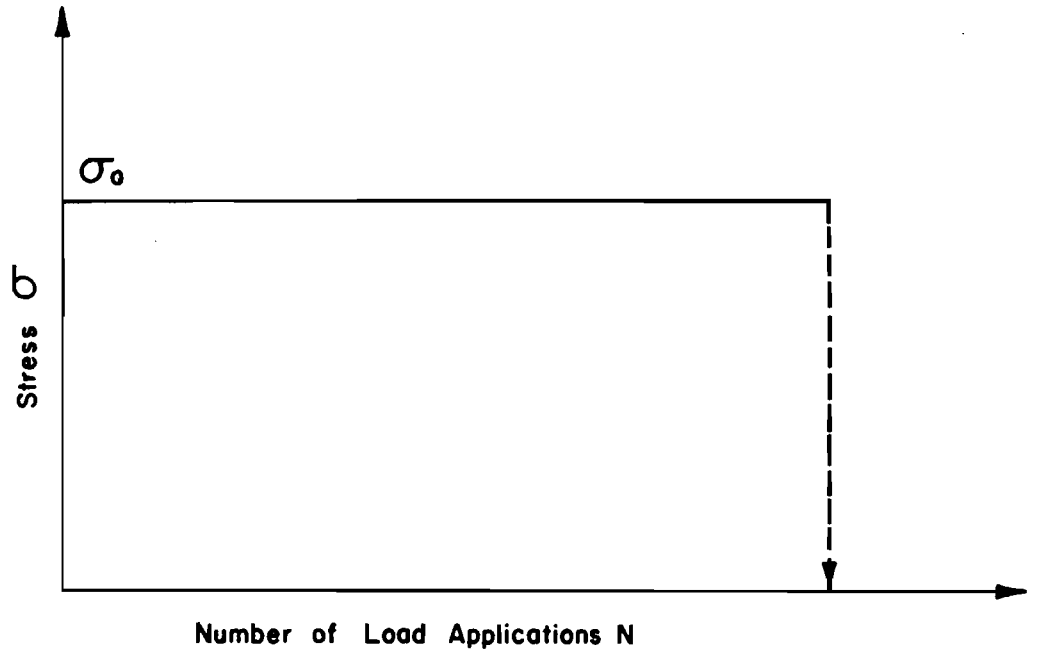

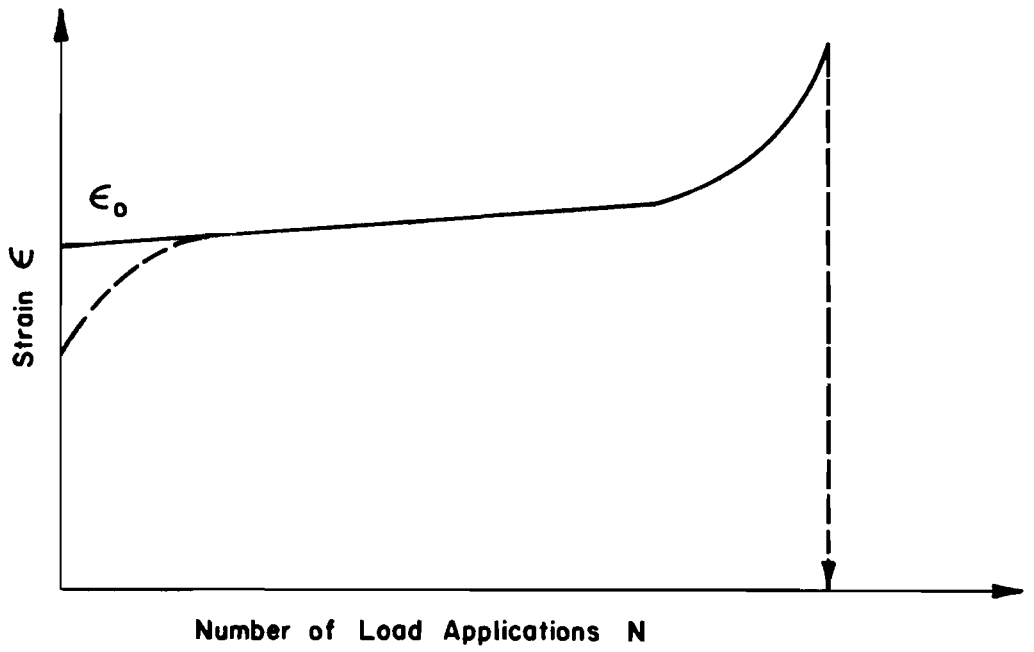

Fig 2.1. Typical behavior of various materials in controlled stress fatigue test.

Concrete fatigue investigations have been made by many researchers. The results of these tests are usually presented in the form of stress level versus the logarithm of the number of load repetitions. If there is a change in the curve and it becomes asymptotic to a line parallel to the horizontal axis, the bounding is called the fatigue limit (Fig. 2.2). The fatigue limit of concrete may not be obtained in the first five million applications, and it is possible that the fatigue limit will never be obtained. To better understand the study in fatigue of concrete, it will be helpful to discuss the mechanism and boundary variables of the initial repeated loads on the concrete.

Mechanism of Repeated Loads of Concrete

Existing theory of concrete design structure mostly is restricted to monotonic increases in loads. In fact, the effects of loads on structure can be divided into fatigue effects due to a large cycle of loading at relatively low stress level or due to a small cycle of loading of rather high stress level, each of which causes additional deformation to the structure. The mechanism

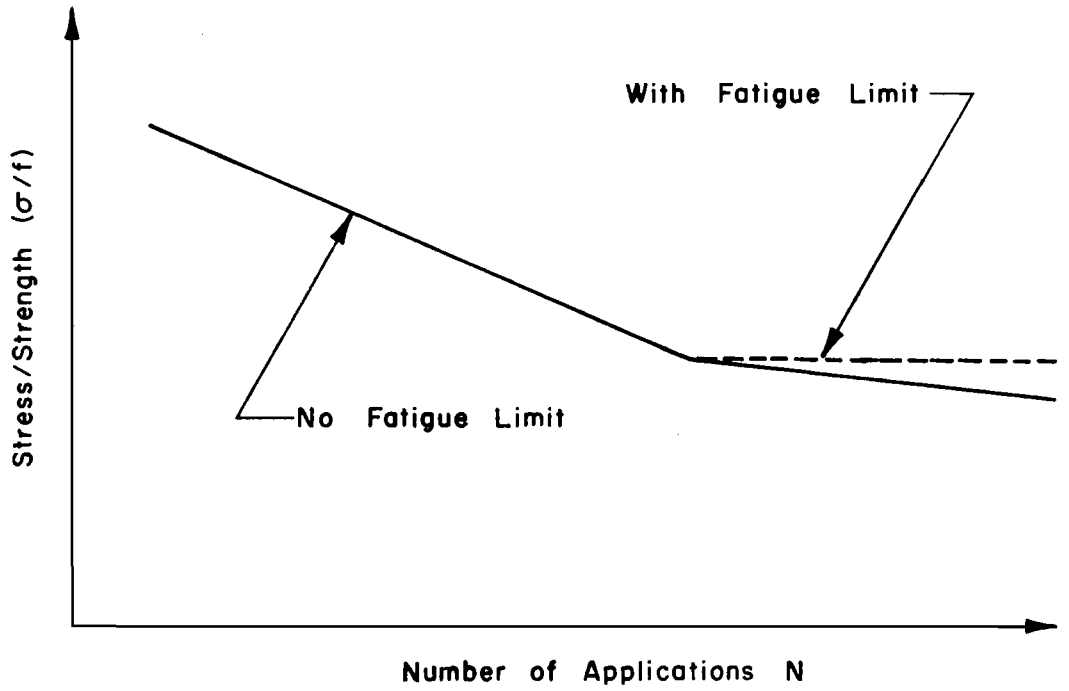

Fig 2.2. Typical characteristic of various materials under repeated load.

of repeated load (as shown in Fig. 2.3) consists of loading, unloading, and reloading conditions.

Figure 2.3 shows the stress-strain curve of concrete under repeated load. The normal stress-strain curve is a plot of the relationship between stress and strain obtained by increasing the strain monotonically. The unloading curve is the curve that is traced in the stress-strain plane when the strain is decreased from the value above the elastic limit of the material. After unloading, the strain is increased again from a certain stage of unloading. A curve will be traced which will be called a reloading curve. The locus of the broken curves joining the end of the reloading curve to the start of an unloading curve is called an envelope curve. The locus of points where the reloading portion of any cycle crosses the unloading portion is called the shakedown limit. The value of shakedown limit depends on the minimum stress in the cycle of loading and unloading. For complete unloading, the shakedown limit is near the envelope curve, whereas for partial unloading, the shakedown limit occurs at a lower value of stress. It follows that the value of shakedown limit (in terms of stress) depends to a considerable extent on the stress amplitude of the cycle. The maximum

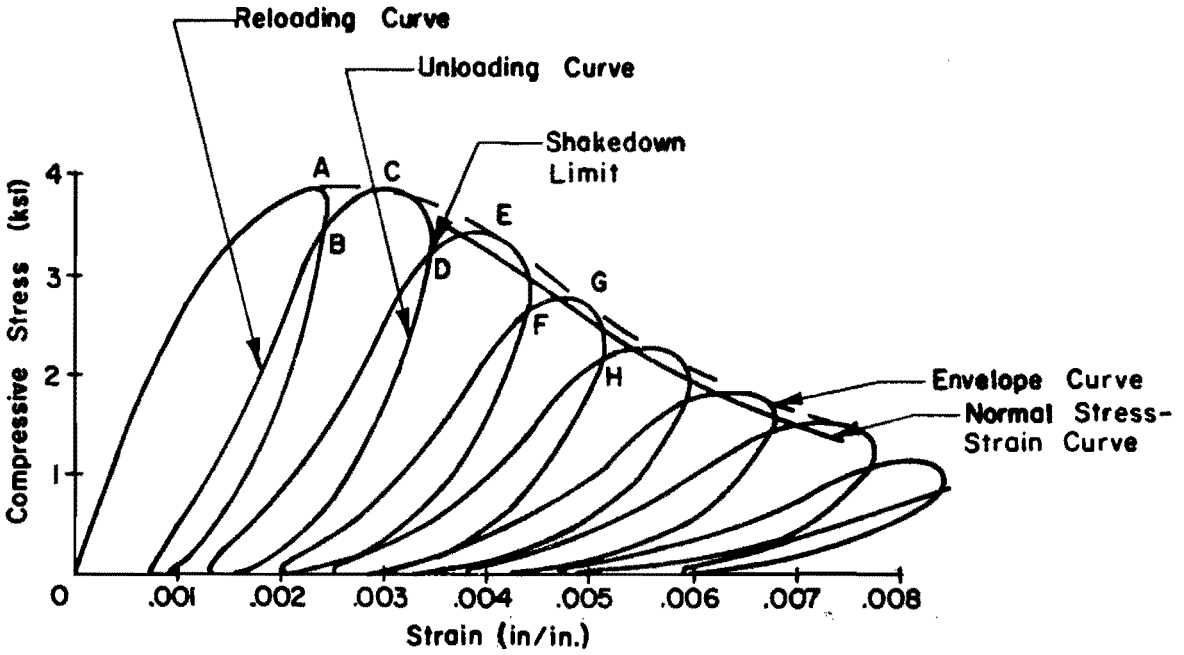

Fig 2.3. Stress-strain curve of concrete under repeated load (after Ref 6) (complete unloading).

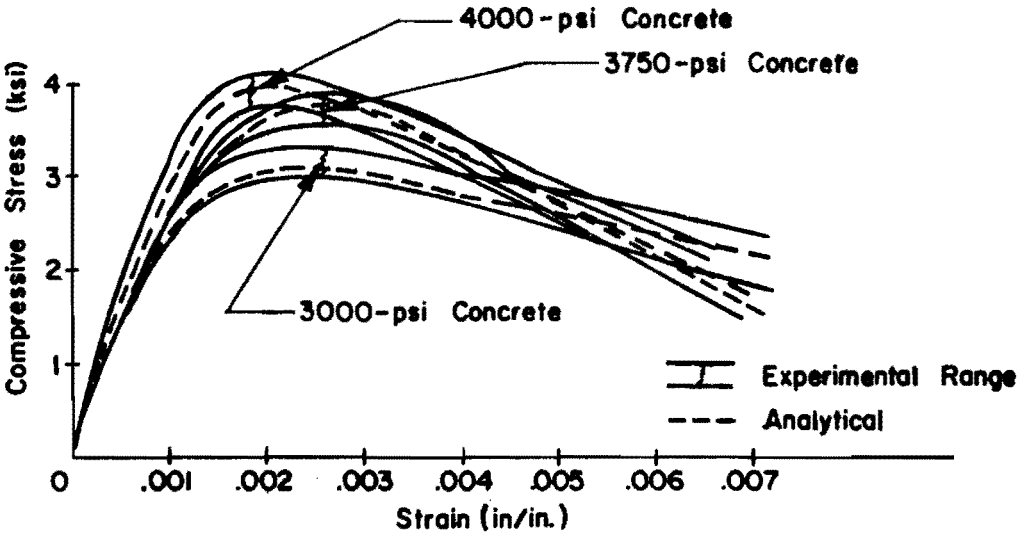

Fig 2.4. Envelope curves for three different concretes (after Ref 6).

stresses above shakedown limit lead to the additional strains which may cause failure at a small number of cycles, while maximum stresses at or below shakedown limit lead to fatigue failure after a large number of cycles (Ref. 6).

Figure 2.4 illustrates that as the strength of concrete increases, the rate of reduction in strength capacity of concrete under repeated load increases. This result shows a good agreement with the fatigue test which was performed by Kesler (Ref. 7).

Boundary Variables Affecting Fatigue Behavior of Concrete

The design of rigid pavements is based to a large extent on data obtained from static tests. To consider the fatigue properties of concrete, many variables must be evaluated. These variables may be separated into three groups, as listed below:

A. Material Variables
    1. Concrete properties
        a. Moisture content
        b. Condition of concrete
        c. Age of concrete
        d. Strength of concrete
        e. Elastic modulus of concrete

2. Aggregate properties

B. Load Variables

1. Mode of loading

a. Magnitude of loads (stress level)

b. Range of stresses

c. Speed of loading

2. Load condition

a. Simple loading

b. Compound loading (mixed traffic)

C. Environmental Variables

1. Moisture

2. Temperature

Since fatigue tests generally extend over a considerable period of time, it is recommended that the test be conducted on aged concrete specimens to minimize the effect of strength gain of concrete during the test period. The number of load applications to failure largely depends on the ratio of applied stress to concrete strength. The higher the ratio, the lower the allowable number of applications. The most severe condition occurs when the applied stress changes from flexural stress to compressive stress or reverse loading conditions.

Fatigue of Concrete in Flexure

Performance studies have shown that one of the contributors to failure of concrete pavement by cracking is the repeated application of flexural stresses. Thus, the flexural fatigue characteristics of concrete are of primary concern, since it is well known that concrete is stronger in compression than in flexure. In the following paragraphs, the effect of concrete properties, range of applied stresses, and speed of testing on fatigue life are studied.

Concrete Properties. The importance of concrete properties on the fatigue behavior of concrete has been reported by Kesler (Ref. 7). The tests were performed at speeds of 70 cycles per minute (cpm), 230 cpm, and 440 cpm with aged specimens, to avoid strength gain of concrete during the test period. The results for all speeds show that the decrease in fatigue life for high strength concrete is considerably faster than low strength concrete.

The applied load in percent of static strength versus fatigue life was plotted for tests performed at all speeds and is shown in Figure 2.5. These results

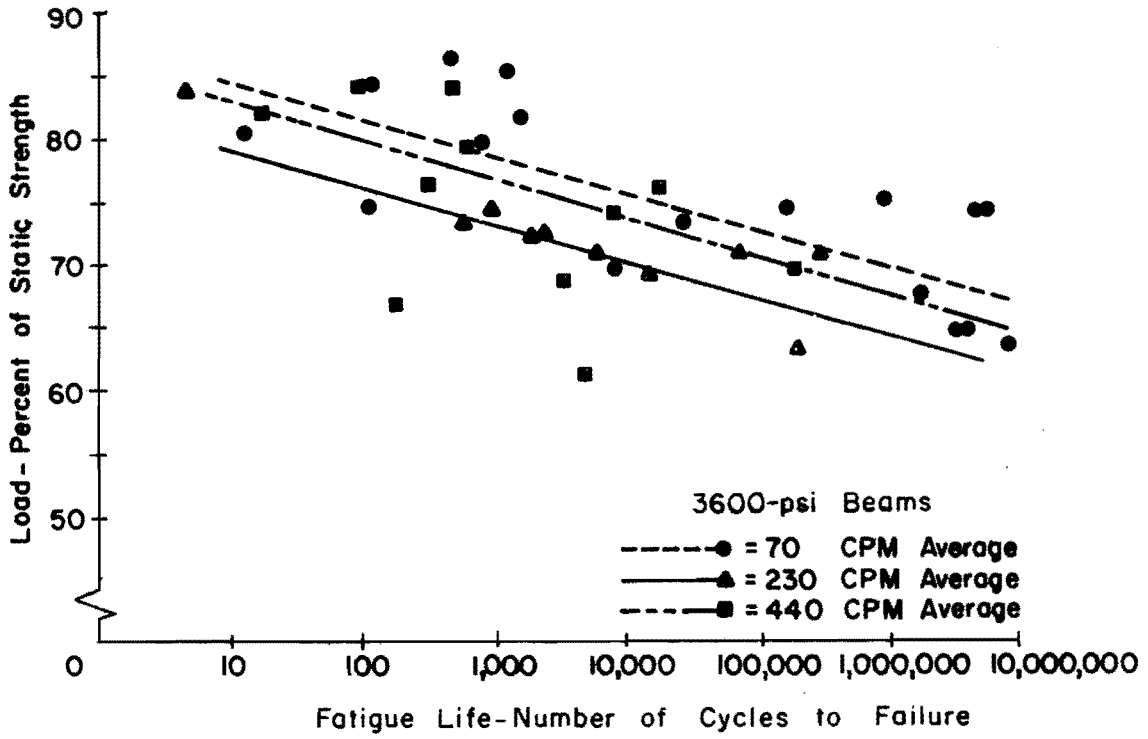

(a)

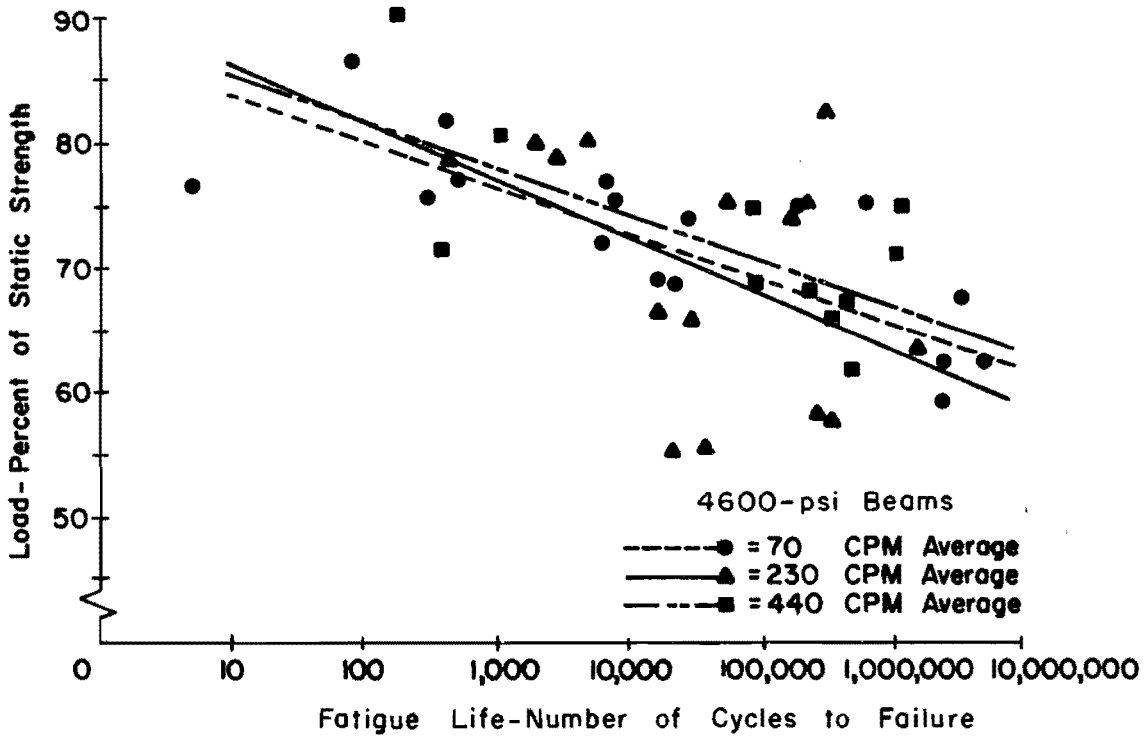

(b)

Fig 2.5. Fatigue tests of concrete from Kesler (after Ref 7).

point out that the most pronounced difference in fatigue life occurs at extremely low applications (ten applications). The maximum difference between the 3600 psi and 4600 psi concrete (compressive strength) in fatigue life is approximately 7 percent. From these results, it may be concluded that if considering the other functions which can influence fatigue life and strength of concrete, the effect of strength of concrete in fatigue is taken into account by normalizing. Thus, in modeling the concrete fatigue equation, the data from both types of concrete will be used.

Since concrete pavements are likely to be wet on the bottom from saturated subgrades (worse condition), the information of fatigue tests of concrete in a wet or saturated condition is desirable. Tests by the Testing Material Laboratory at Purdue University (Ref. 10) were performed on a continuously saturated specimen (age four months) and temporarily saturated specimen (age 19 months, immersed in water 200 hours before the test). The record of the tests, although limited, indicates an interesting and important feature of fatigue action on concrete specimens. The temporarily saturated and continously saturated specimens under repeated loading showed the fatigue life 89 percent and 83 percent of the dry specimens, respectively.

Murdock and Kesler (Ref. 8) concluded in their test that inadequately aged and cured concrete is less resistant to fatigue than well aged and cured concrete. In addition, they found that fatigue life decreases slightly for lean-mixed concrete than for concrete with a high water cement ratio.

Purdue University (Ref. 10) also performed the tests to study the effect of age on fatigue life of concrete. The tests were performed on 28-day, 4-month, and 6-month specimens at the speed of loading 10 cycles per minute. The fatigue lives were equal to 40 to 60 percent, 50 to 55 percent, and 54 to 55 percent of concrete strength, respectively. It is doubtful that fatigue life of concrete increases with an increase in age. However, the variance of fatigue life decreases with an increase in age of specimens.

Range of Stresses. It has been found that plain concrete does not exhibit a fatigue limit when subjected to repeated loads without stress reversals. Fatigue life up to ten million applications for each of several stress ranges were investigated and it was found that these fatigue lives depend on the range of stresses to which the specimens were subjected.

The fatigue strength can be defined as the ratio between applied stress and concrete strength at any number of applications. It was found to decrease as the number of load applications is increased. Figure 2.6 shows the effect of stress range on the fatigue life of concrete developed by Murdock and Kesler (Ref. 8). The R-term on the graph is equal to the ratio between the minimum flexural stress and the maximum flexural stress applied to the specimens during the test period. Tests were made at an age of more than 90 days to reduce effect of strength gain during the test period. None of the tests showed a fatigue limit, although many specimens sustained more than ten million applications without failure. The results from the test show a significant increase in the number of applications as the R-value increases. Fatigue strengths at ten million applications for R equal to 0.13-0.18, 0.25, 0.5, and 0.75, were 61, 63, 73, and 85 percent of concrete strength, respectively.

Clemmer (Ref. 9) determined a fatigue strength after three million applications to be approximately 55 percent of the strength of the concrete for the specimens subjected to stresses ranging from zero to the maximum. These results were confirmed by Hatt and Crepps (Ref. 9)

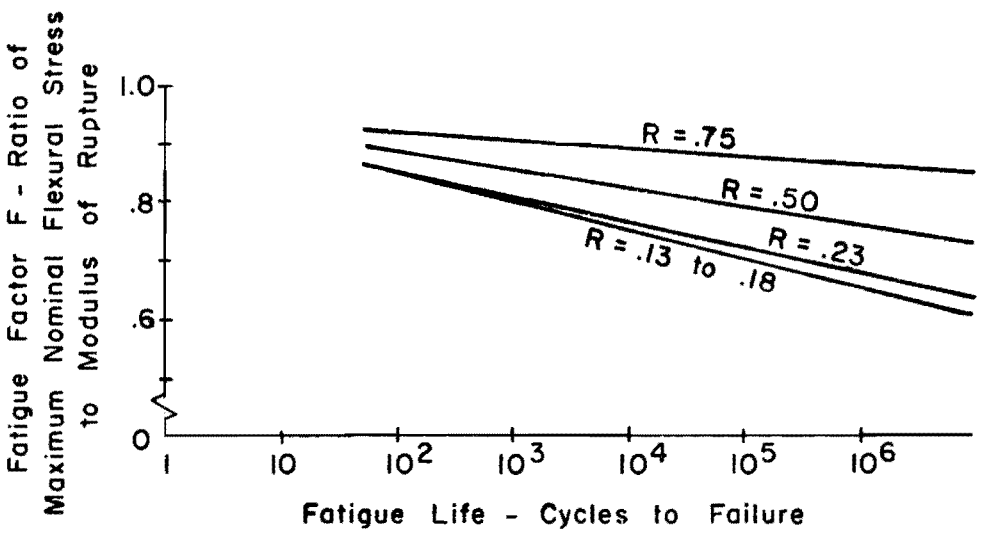

Note: All Tests Were Performed at Constant Minimum Stress of 70 psi.

$$R = \frac{\text{Minimum Flexural Applied Stress}}{\text{Maximum Flexural Applied Stress}}$$

Fig 2.6. Effect of the range of applied stress on the behavior of plain concrete under fatigue loading (after Ref 8).

when they obtained the same fatigue life for stress reversal condition.

The tests by the Illinois Division of Highways reported by Clemmer and Older were aimed to duplicate the actual condition occurring at the corner of the pavement. Tests were performed on 15 specimens at 40 cpm with the stress ratio (flexural stress to flexural strength of concrete) equal to 0.5, 0.61, and 0.70. The results show that for a stress ratio equal to 0.5, applications up to 1,130,000 can occur without failure, but for stress ratios of 0.61 and 0.70, failure usually occurs under 50,000 and 91,000 applications, respectively.

Yoshimoto and Ogino (Ref. 11) confirmed that concrete does not have a fatigue limit in the range up to 10^7 cycles of load. The fatigue limit may be found in the range over 10^7 cycles of load. The effect of repeated load on flexural strength of the survival concrete specimens had been investigated. The strength of concrete was measured at the beginning of the test and after the test. Tests were performed at the load range (ratio of stress and flexural strength of concrete) of 0.42, 0.625, and 0.835 and at a speed of 660 cpm. Specimens were divided into two groups based on the number of total

load cycles applied during the testing period. Group A was for tests with up to 200,000 cycles and Group B for those with up to 10^7 cycles. The average strength of the specimens which did not fail was not significantly different after the number of load cycles was increased from 200,000 to 10,000,000, as shown in Figure 2.7. The specimens which failed due to fatigue and the damaged specimens were neglected in this figure. It was also found that when the stress level was less than the first breaking point of the stress-strain curve, there was no permanent deformation after several loading repetitions and Young's modulus was constant. The first breaking point of the stress-strain curve can be defined as the first point at which the stress-strain relation of concrete is considered to be out of linear relation. Whenever the major stress was greater than the first breaking point, permanent deformation had developed in the specimens.

For the effect of applied stress on fatigue life, it may be concluded that either an increase in maximum applied stress or a decrease of the ratio between minimum and maximum applied stresses causes the decrease in the fatigue life of concrete.

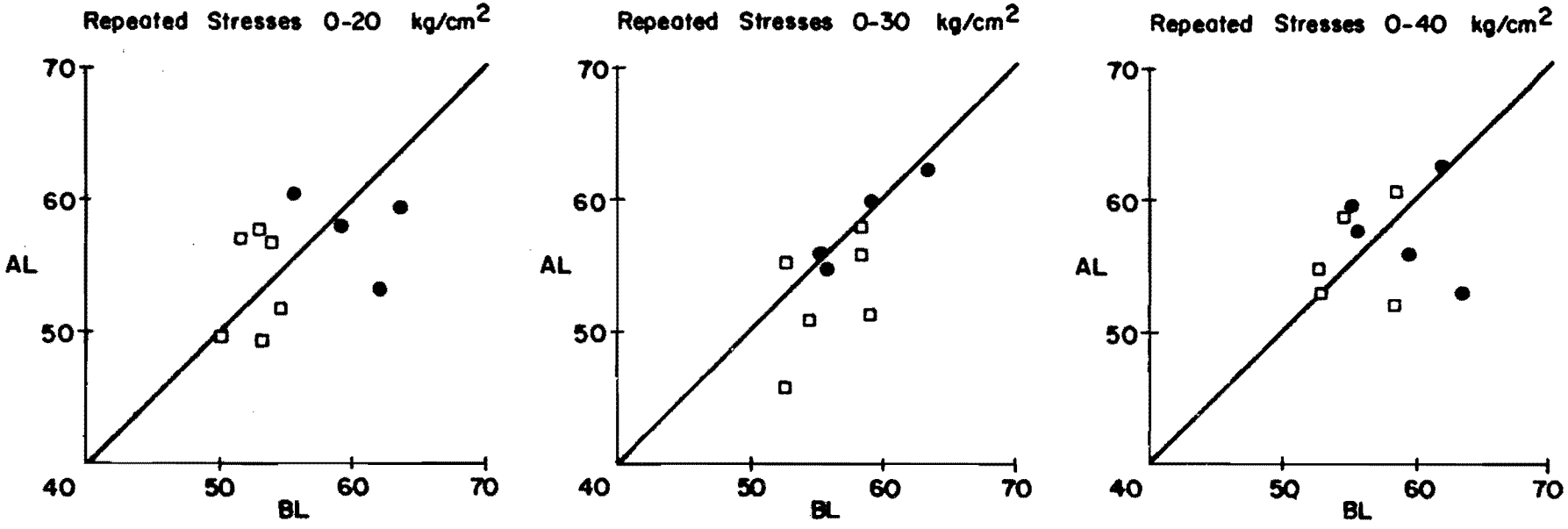

BL = Flexural Strength of Concrete Before Loading.
AL = Flexural Strength of Concrete After Loading.

□ = Load Applications $\leq 10^7$
● = Load Applications $\leq 2 \times 10^5$

Fig 2.7. Comparison of flexural strength of concrete before and after repeated load at various levels of applied load (after Ref 11).

Speed of Testing. Kesler investigated the effect of rate of load applications on concrete fatigue life (Ref. 7). The specimens were divided into two groups, one having the average compressive strength of 3600 psi and the other 4600 psi, with both groups tested with third-point loading. Tests were conducted at 70, 230, and 440 cpm. The results of Kesler's test are shown in Figure 2.5. The maximum variation in fatigue life is approximately 5 percent at ten million applications. Figure 2.8 was plotted to show the effect of the loading speed on the concrete fatigue life at various numbers of the ratios between applied stress and flexural concrete strength. The curve shows a decrease in fatigue life of concrete with an increase in the speed of the test up to the certain point. After this certain point, the fatigue life begins to increase with an increase in speed. From these test results, it may be concluded that the speed of testing is not a significant factor influencing the fatigue life of concrete when the other variables were considered.

Probability of Fatigue Failure

As might be expected, specimens tested at the same stress level failed at different numbers of cycles.

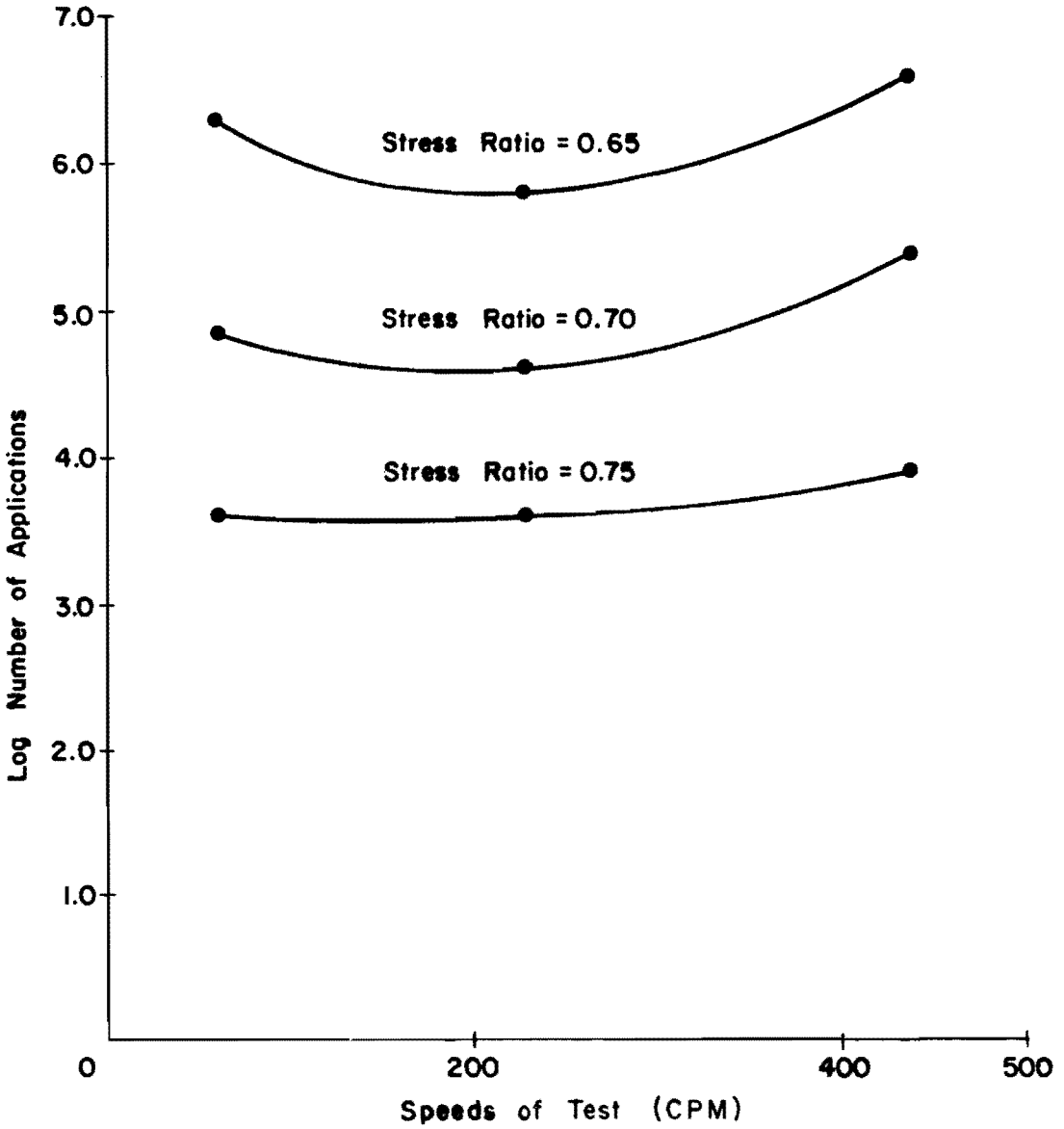

Fig 2.8. Effect of speed of test on fatigue life of concrete at various applied stress ratios (from Fig 2.5(b)).

For this reason, to successfully predict the fatigue life of concrete, it is required that the probability of fatigue failure be considered as a criterion in design.

McCall (Ref. 15) conducted tests to study the relation between the stress level, the number of load applications, and the probability of fatigue failure. These tests were with a complete reverse loading in flexure at the rate of 1800 cycles per minute. The stress levels varied from 45 to 70 percent of the modulus of rupture. The beams were tested to failure or 20 million applications, whichever occurred first. With this approach to probability of fatigue failure, he analyzed his data by ranking the specimens in the order of the number of cycles to failure and calculating the probability of failure, P, by dividing the rank of each specimen by the number of specimens, plus one. The reason for adding one was to avoid a probability of failure equal to one. The results of the tests are shown in Figure 2.9 and it was concluded that, as the stress level and number of load applications increase, the probability of fatigue failure increases.

Figure 2.10 presents the effect of applied stress levels to the chance of survival of the tested specimens after 20 million applications. The results of

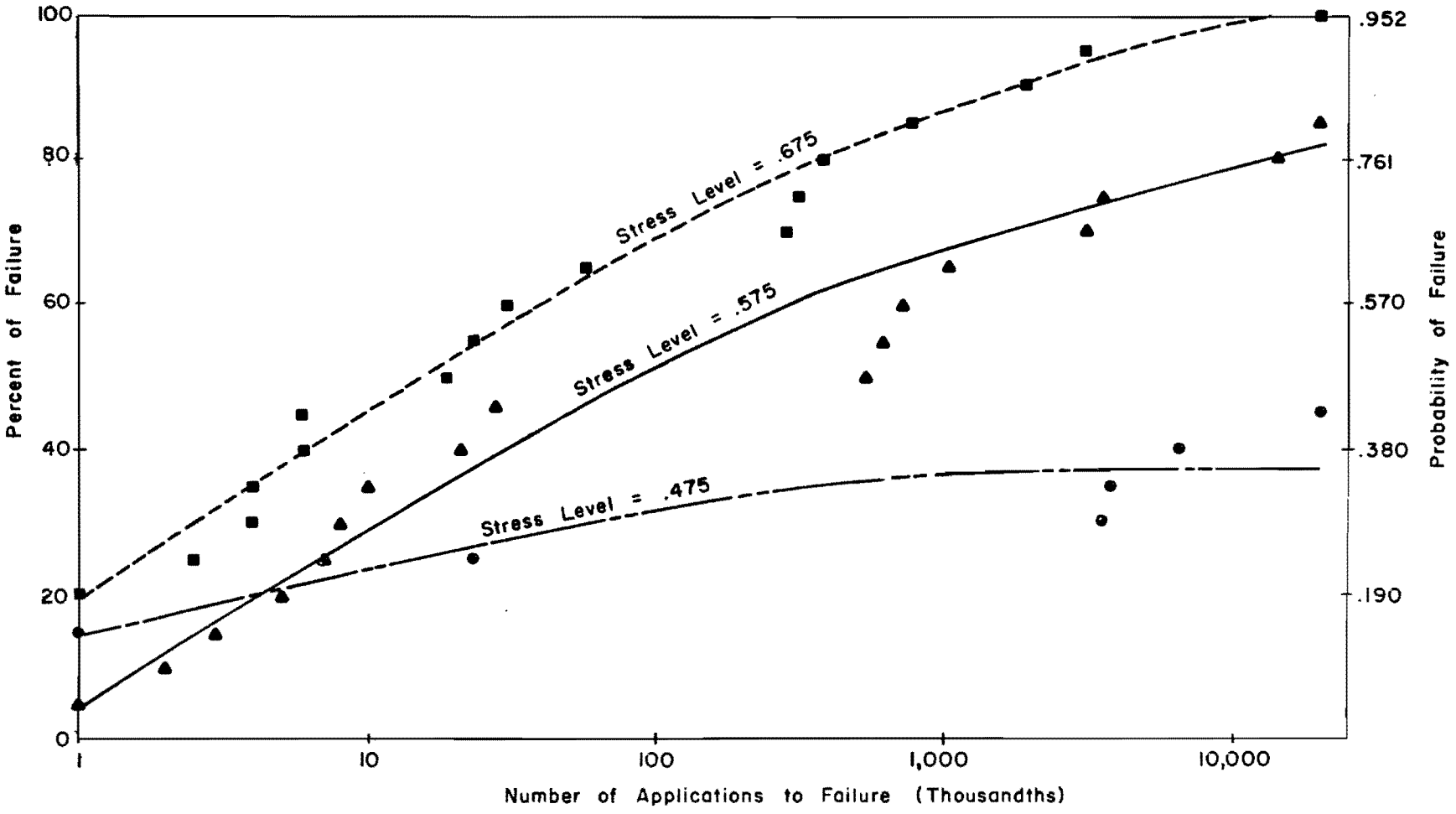

Fig 2.9. Probability of fatigue failure at various stress levels (after Ref 15).

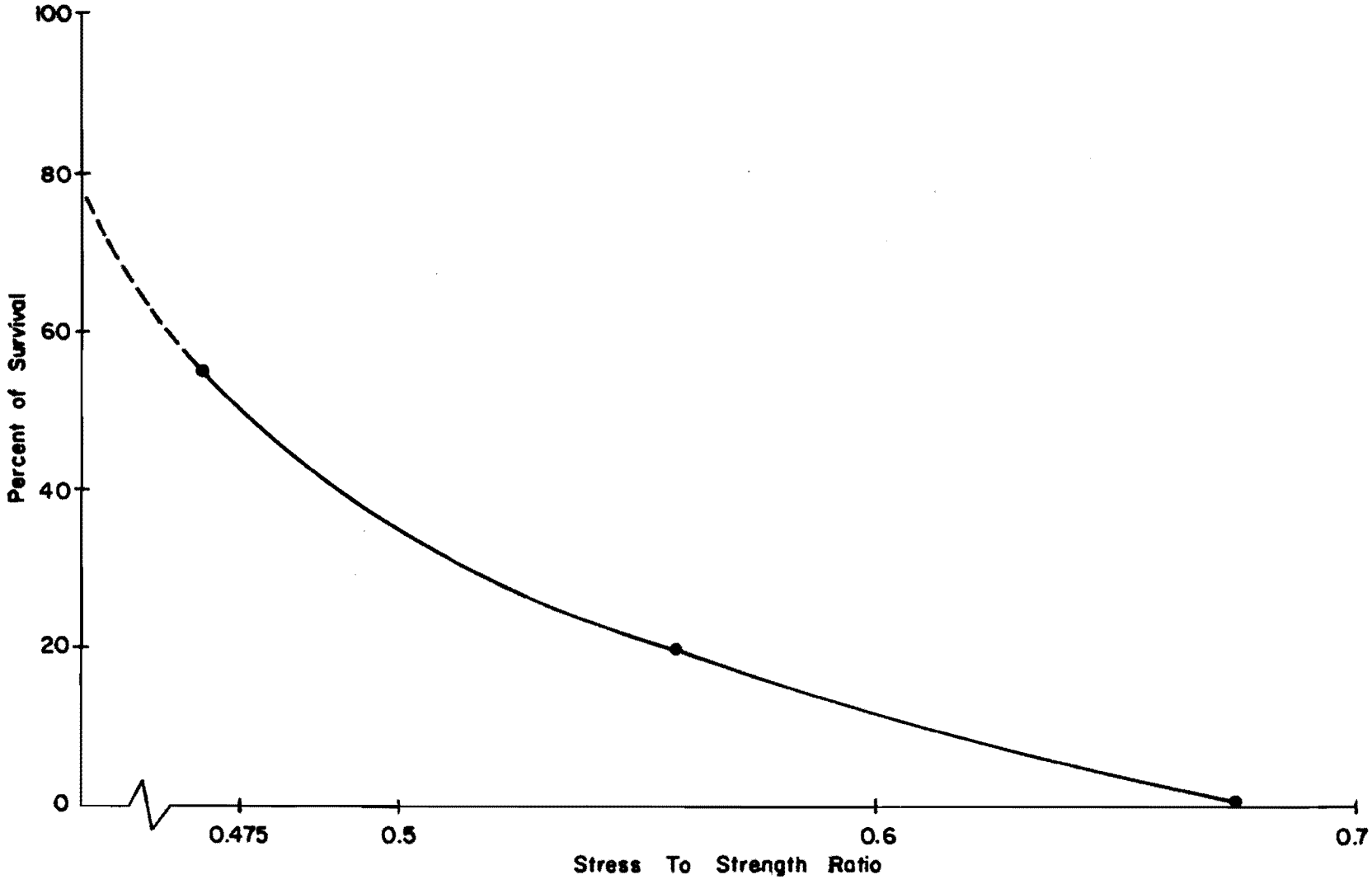

Fig 2.10. Effect of stress ratio on percent of survival of the specimens after 20 million applications (after Ref 15).

the analysis showed that the increasing in the stress level caused the significant drop in the chance of survival of the specimens after 20 million applications. From the results of this plot, it may be concluded that concrete always has a chance to fail, even though the applied stress is only 0.45 of the flexural strength.

Development of Concrete Fatigue Equation

To develop the theoretical concrete fatigue equation, the laboratory test performed by Kesler (Ref. 7) has been selected to model the fatigue life of concrete because

(1) the tests were conducted up to ten million applications,
(2) repeated load started from near zero to maximum,
(3) the tests are performed for different types of concrete,
(4) the specimens were made of plain concrete, and
(5) the tests were performed for various speeds of testing.

The specimens used were 64 inches long with a cross section 6-by-6 inches. They were supported on a

60-inch span loaded at third points to produce flexural stresses in the middle third. The repeated load is applied to the specimen through the loading plate. The specimens were divided into two groups with

(1) an average compressive strength of 3600 psi, and

(2) an average compressive strength of 4600 psi.

The machine was run at different speeds: 70 cpm, 230 cpm, and 440 cpm.

Figure 2.5 shows the results of the test. To obtain data for the prediction of the fatigue equation of concrete, only failed specimens were selected from the test. Since the average compressive stress (f'_c) from the AASHO Road Test was approximately 4000 psi, the data from both types of concrete from Kesler's test were selected.

To predict the number of applications, an attempt was made to relate the number of applications to

(1) stress ratio (ratio between induced stress and flexural strength of concrete), and

(2) speed of testing.

Stepwise regression (STEP 01) was selected to predict the fatigue equation of concrete. This program computes a sequence of multiple linear regression equations in a stepwise manner (Ref. 29). At each step, one

variable is added to the regression equation. The variable added is the one making the greatest reduction in error sum of squares. Equivalently, it is the variable which has the highest partial correlation with the dependent variable partial on the variables which have already been added; equivalently, it is the variable which, if it were added, would have the highest F-value. In addition, variables can be forced into the regression equation. Nonforced variables are automatically removed when their F-values become too low (Ref. 29).

Transformations. Before performing the regression analyses, a careful study of the data scatter of each independent variable versus the dependent variable was made in order to achieve the best equation. The data for 31 specimens plotted in Figure 2.11 from the laboratory test were selected.

An attempt was made to relate the log number of load applications to speed of testing, stress ratio, and strength of concrete. The following transformations are the inputs in STEP 01 program:

Variable 1: the number of load applications--Log N

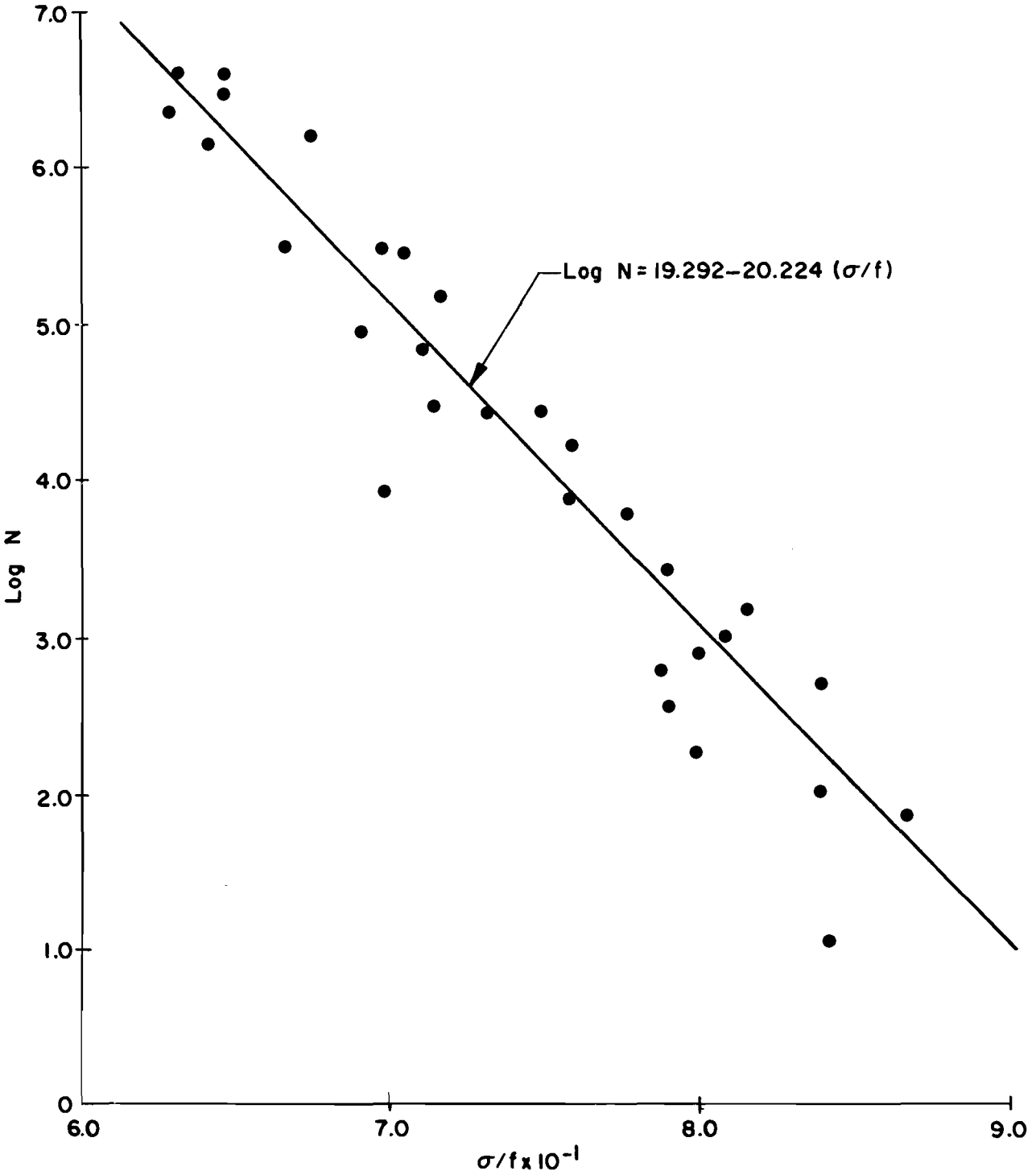

Fig 2.11. Number of applications versus stress ratio from laboratory test (after Ref 7).

Variable 2: the stress ratio--σ/f, Log σ/f,

$(\sigma/f)^{1/2}$, $(\sigma/f)^4$, f/σ.

Variable 3: the speed of testing--s, 1/s, Log s

where

f = flexural strength of concrete, psi;

σ = stress level of testing, psi;

s = speed of testing, cycles per minute.

Model Development. From the stepwise regression analysis for the 31 specimens, it was found that the effect of speed of testing has no effect on predicting the fatigue equation. The results of STEP 01 are summarized below:

Step Number 1:

$$\text{Log } N = 19.292 - 20.224\,(\sigma/f) \qquad (2.1)$$

Standard error for residuals = 0.4186 (in log term)

Multiple R = 0.9599

Step Number 2:

$$\text{Log } N = 15.261 - 17.497\,(\sigma/f) + 1.477\,(f/\sigma) \qquad (2.2)$$

Standard error for residuals = 0.4257 (in log term)

Multiple R = 0.9600

The tolerances for the other transformative variables are not sufficient enough for further computation by STEP 01. From summary results, the recommended equation is:

$$\text{Log } N = 19.292 - 20.224\ (\sigma/f) \tag{2.3}$$

$$N = \frac{10^{19.292}}{10^{20.224(\sigma/f)}} \tag{2.4}$$

where

N = allowable number of load applications;

σ = maximum principal stresses, psi;

f = flexural strength of concrete for third-point loading, psi.

The reasons for selecting this equation are as follows:

(1) minimum in the number of complicated terms,

(2) smallest standard deviation, and

(3) high correlation coefficient.

The standard error of estimate is the best estimate of the standard deviation. This means that the predicted log number of applications will be within ± 0.4186. Figure 2.12 shows the correlation of actual number of

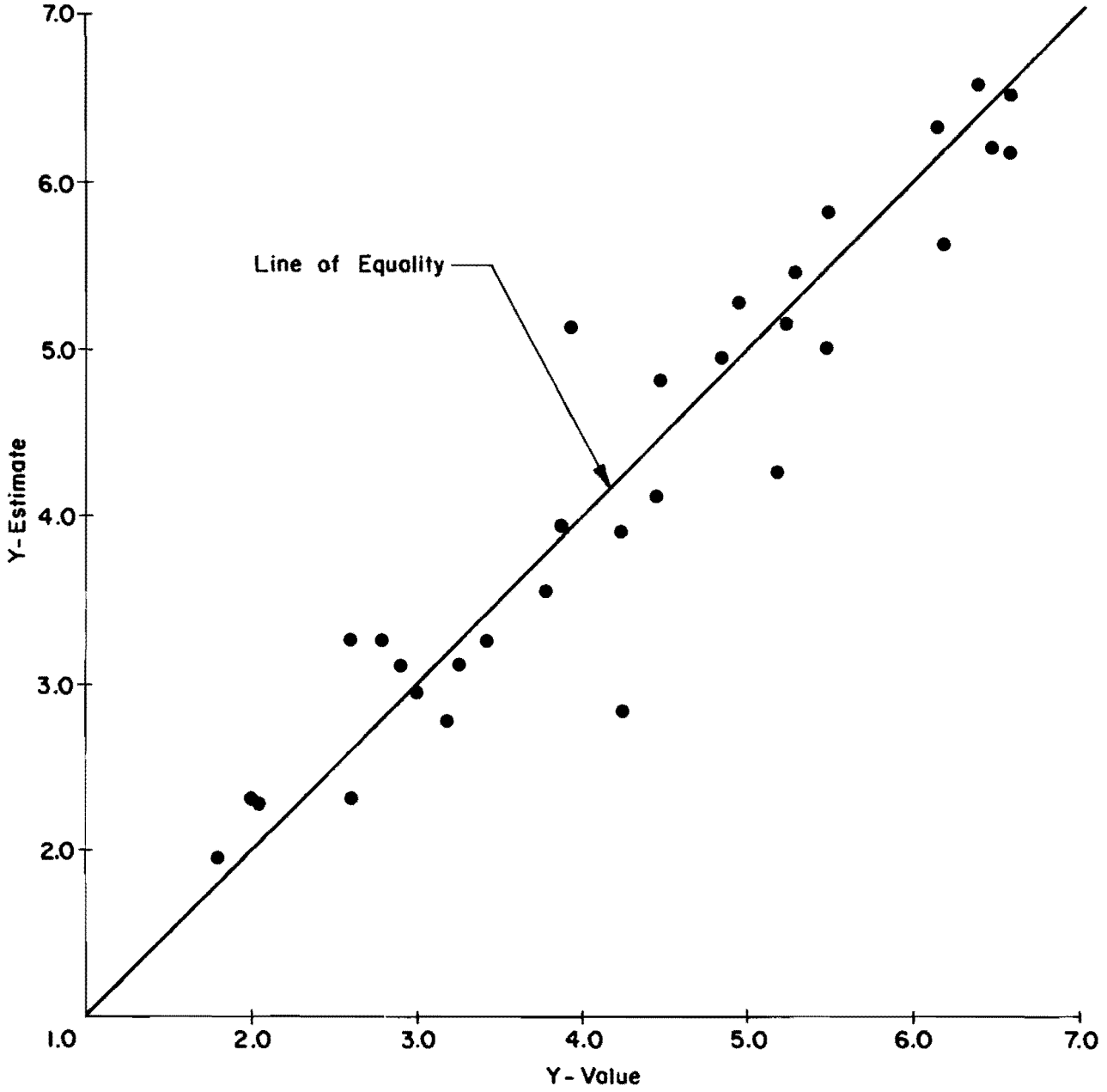

Fig 2.12. Comparison between actual and predicted number of applications.

applications from laboratory tests versus the predicted number of applications from the model equation, and the plot exhibits no abnormalities.

Comparison between Field and Laboratory Fatigue Tests. Pavements in actual service are subjected to mixed traffic containing different wheel loads and axle load configurations, thereby producing various stress levels during the pavement life. The variations of the stresses in rigid pavement depend on the magnitude of wheel loads, position of loading, and the environmental effects. To compare the fatigue property of concrete from laboratory tests to a field test, the data from the AASHO Road Test were selected.

The AASHO Road Test presented the fatigue life of pavement as a function of thickness of the pavement, magnitude and configuration of the axle load, design variables (reinforced or nonreinforced section), and the cracking index. Figure 2.13 shows the effect of the magnitude of the single-axle load on the fatigue life of rigid pavement for reinforced and nonreinforced sections at various levels of cracking index for a 6.5-inch pavement thickness. The results obtained from the graphs are presented below:

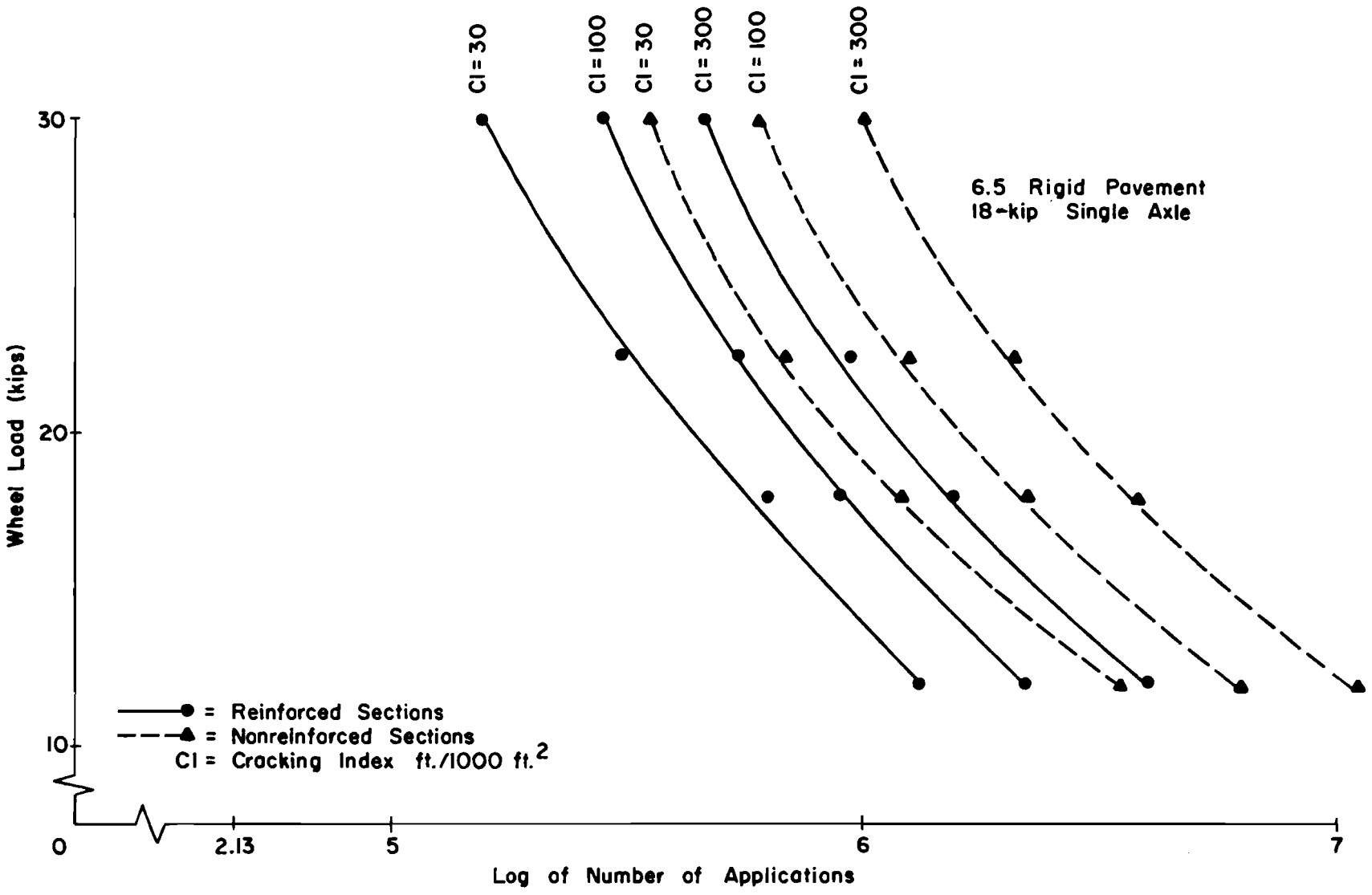

Fig 2.13. Effect of wheel load on fatigue life of rigid pavement at AASHO Road Test from AASHO Road Test equation (Ref 32).

(1) The fatigue life of the nonreinforced sections are longer than reinforced sections for any cracking index.

(2) The allowable number of applications increases as the cracking index increases.

(3) The allowable number of applications decreases as the magnitude of wheel load increases.

Vesic (Ref. 33) has developed a fatigue equation for rigid pavements from the AASHO Road Test data (at a serviceablility index equal to 2.5) as the function of the strength of concrete and the induced stress in the pavement slab. The fatigue equation is:

$$N_{2.5} = 225{,}000\ (f_c/\sigma)^4 \qquad (2.5)$$

where

f_c = flexural strength of concrete, in psi;

σ = induced flexural stress in concrete slab, in psi.

Hudson and Scrivner (Ref. 22) also developed a fatigue equation from the AASHO Road Test data and presented the fatigue life of the pavement as a function of the edge stress where the axle load was applied at 17 to 22 inches from the pavement edge. Their fatigue equation for single-axle load is:

$$N = \frac{10^{16.52}}{\sigma_c^{4.34}} \qquad (2.6)$$

where

σ_c = pavement edge stress with load applied 2 ft. from pavement edge in psi.

The author modified this equation to predict the fatigue life of the rigid pavement as the function of the edge stress and strength of concrete. The purpose of this development is to introduce the strength of concrete into the original equation, so that the rational comparison can be made. The modification was achieved by considering the strength of concrete to be 790 psi; the modified equation is:

$$N = 8750 \, (f_c / \sigma_c)^{4.34} \qquad (2.7)$$

where

f_c = flexural strength of concrete, in psi.

A comparison between field and laboratory concrete fatigue tests is presented in Figure 2.14. The curves from the laboratory tests which were performed by Kesler, Murdock, and Clemmer show straight-line relations in fatigue behavior. This characteristic means that concrete does not exhibit a fatigue limit in the laboratory test. The field experiment obtained, PCA method, shows the tendency for a fatigue limit to develop at some number of applications, but Vesic's and Hudson's exhibit no

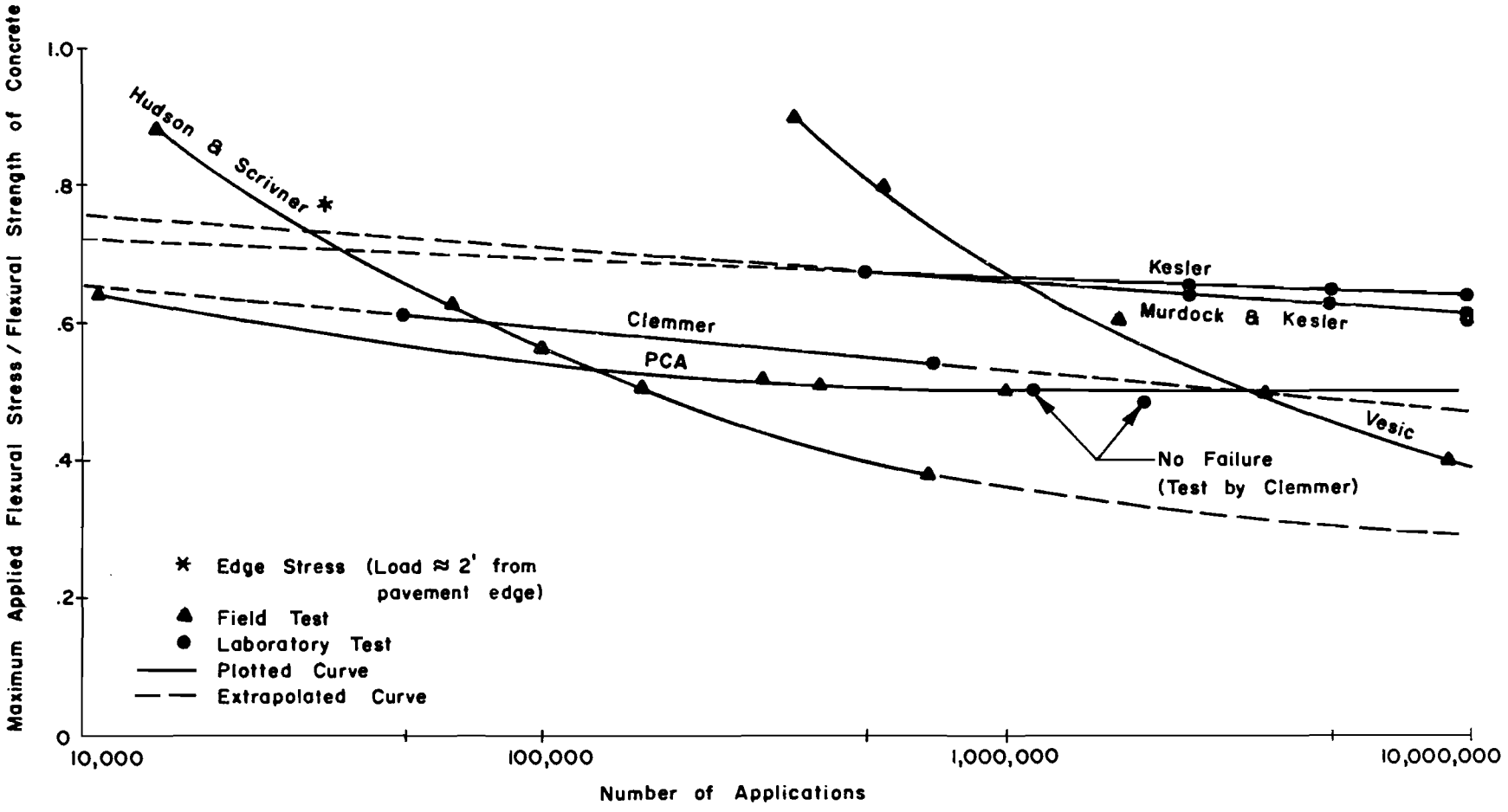

Fig 2.14. Comparison between field and laboratory test on fatigue of concrete.

fatigue limit. In general, at the same stress level, the laboratory tests show a higher number of applications than for a field test. Explanations for these results are as follows:

(1) The laboratory test usually has better environmental conditions, such as the control of temperature and moisture, than the field tests.

(2) The number of applications from laboratory tests are determined at the failure of the specimens, whereas the number of applications from the field tests are determined when the serviceability index drops below a certain specified minimum level.

(3) In the field tests, there are many stress levels produced by the wheel load applications, while in the laboratory tests, there is only one stress level.

Summary

From all of the studies, it was found that the applied stresses are the most significant factor influencing fatigue life of concrete. As the applied stresses increase, the fatigue life always decreases. The interval of the maximum and minimum applied stresses is also significant. The wider the stress intervals, the smaller the fatigue life. Types of concrete and the test speeds have small effects on fatigue life and are considered

negligible. The studies of the probability of fatigue failure confirm that the concrete exhibits no fatigue limit.

A comparison between the field and laboratory tests gives the reasonable results. The field tests have the initial stresses produced by the fluctuation of moisture and temperature. When the loads are applied, the additional stress due to load stresses and environmental stresses will result. In laboratory tests, the induced stresses are usually caused by the applied load only. Therefore, with the specimens subjected to the same load level, the field tests will allow a smaller number of load applications than the laboratory test.

C H A P T E R I I I

DATA FROM AASHO ROAD TEST

The principal purpose of presenting the data collected from the AASHO Road Test is to provide the information for

(1) load transfer study of the jointed pavement at the AASHO Road Test,

(2) prediction of the maximum principal stresses of the reinforced and nonreinforced sections during the test period, and

(3) future criteria for predicting fatigue distress in rigid pavement design system.

The AASHO Road Test performed the test for the 25 months of regular traffic. There were various types of axle loads applied to the jointed pavement but only single-axle load applications were selected because of their relative analysis simplicity. The actual average wheel path position of the traffic application varied between 17 and 22 inches from the pavement edge. For the feasible use of the discrete-element slab program, it was assumed that the average wheel path position at the AASHO

Road Test was 24 inches from the pavement edge. All the data below were obtained and analyzed from the AASHO Road Test (Ref. 26):

(1) concrete slab properties during the test period,

(2) subsurface variation in terms of k-value, and

(3) traffic applications.

In the analysis, these principal variables will be briefly discussed. Additional information on materials used in the rigid pavement test sections and the method of construction may be obtained from Reference 26.

Concrete Slab Properties and Dimensions

The slab thickness for the test sections varied from 2-1/2 inches to 12-1/2 inches. Sections with non-reinforced slabs had transverse contraction joints spaced at 15 feet, thus forming 12-by-15-foot slab panels. The reinforcement of these sections consisted of single-welded wire fabric placed 1-1/2 inches to 2 inches from the surface in the pavement slabs. The size of dowels in transverse joints was increased according to the slab thickness from 3/8-inch in diameter and 12 inches in length to 1-5/8 inches in diameter and 18 inches in length. Longitudinal

joints were reinforced with tie bars increasing in size with slab thickness from No. 3, 20 inches long, to No. 5, 30 inches long.

The pavement concrete was made with Type 1 portland cement, coarse aggregate, natural sand, water, and air-entraining agent. Standard procedures were followed in the mixing and placing of the concrete. The typical mean strength of concrete for each month during the test period of loops 4, 5, and 6 is presented in Table 3.1. The minimum age of the concrete when the test traffic started was equal to three months for loops, 4 and 5 and 3-1/2 months for loop 6 (Ref. 26).

Variation of Subsurface Conditions for AASHO Road Test

During the test period, the subsurface conditions of rigid pavement varied from time to time. Only the variation of subsurface condition due to seasonal change of loop 1 was studied and plotted. Since the tests were performed at the same location for all loops, it was assumed that the variation of subsurface conditions of loops 4, 5, and 6 due to seasonal changes is the same as loop 1. The tests for loops 4, 5, and 6 of the elastic

TABLE 3.1. FLEXURAL STRENGTH OF CONCRETE IN PSI: DURING TRAFFIC TEST PERIOD AASHO ROAD TEST

Year	Month											
	Jan.	Feb.	Mar.	Apr.	May	Jun.	Jul.	Aug.	Sept.	Oct.	Nov.	Dec.
1958	-	-	-	-	-	-	510	600	650	762	770	775
1959	780	782	784	785	786	787	789	789	789	789	789	789
1960	789	789	789	789	789	789	789	789	789	789	789	789

Note: Data from AASHO Road Test

Third point loading

modulus of subsurface reaction were performed from April 23 to May 25, 1960. The variations of elastic modulus of subbase reaction due to seasonal change during the test period of all loops are shown in Figure 3.1. The ranges of k-value for study loops are shown below (Ref. 32):

(1) loop 4 varied from 110 to 155 pci,

(2) loop 5 varied from 103.5 to 148.5 pci, and

(3) loop 6 varied from 117.5 to 162.5 pci.

The average minimum and maximum k-values for all loops were 108 and 155.5 pci, respectively. The minimum value of k occurred in the spring, while the maximum usually occurred in the winter. The highest value of elastic modulus of subsurface was recorded in September and assumed to be constant through March because of the lack of test data during this period.

Traffic Distribution and Application

During the 25 months of the regular traffic test, a total of 556,880 vehicle application trips (1,113,760 axle applications) were made in each traffic lane. Details of the traffic distribution for each month, which are used in this chapter for the prediction of fatigue distress, are shown in Table 3.2.

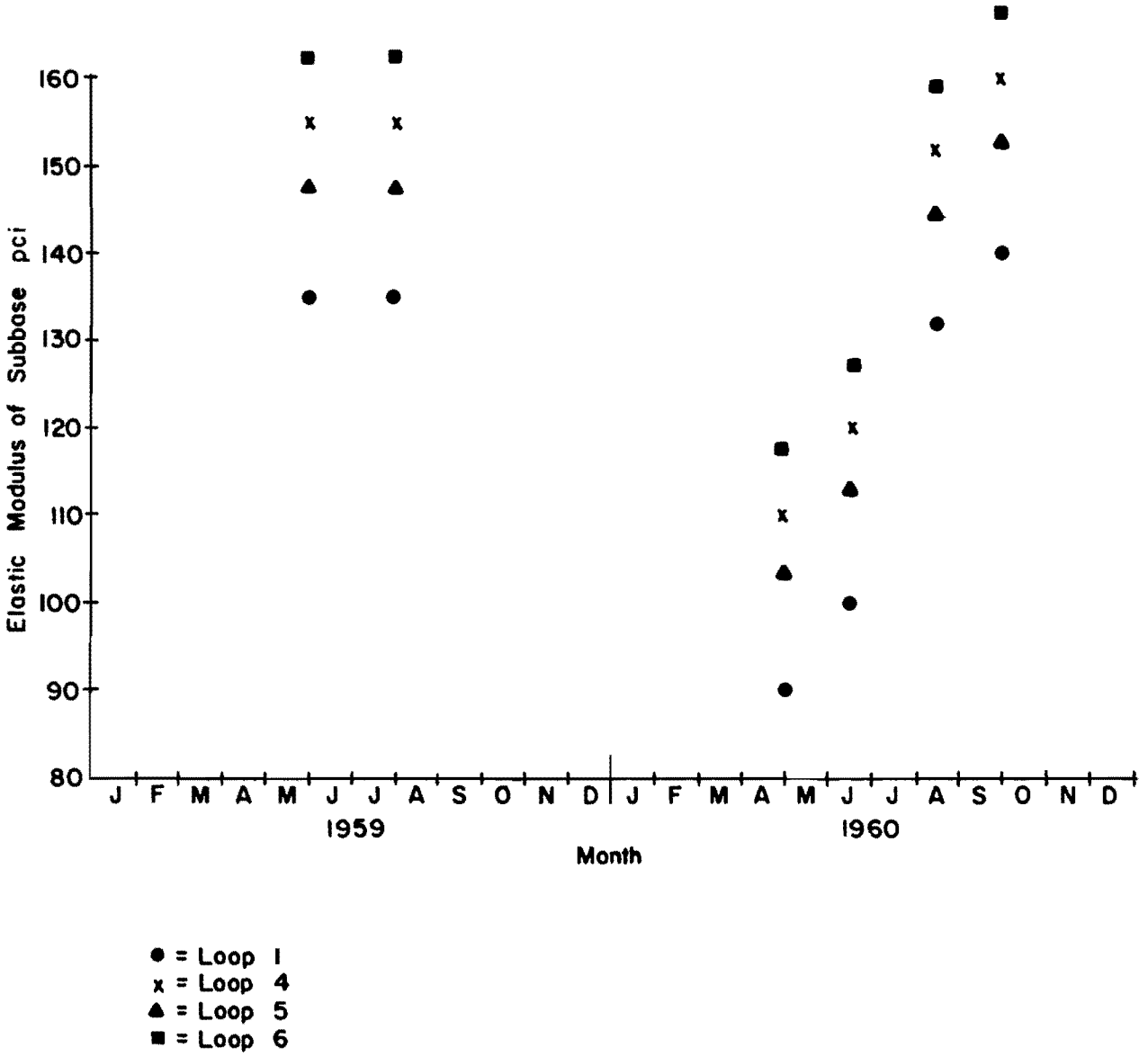

Fig 3.1. Condition of subbase during the test period at AASHO Road Test (after Ref 32).

TABLE 3.2. LOAD APPLICATIONS FOR EACH MONTH AT AASHO ROAD TEST (In thousands)

Year	Loop	Month											
		Jan.	Feb.	Mar.	Apr.	May	Jun.	Jul.	Aug.	Sept.	Oct.	Nov.	Dec.
1958	4	-	-	-	-	-	-	-	-	-	0.8	7.5	21.7
		-	-	-	-	-	-	-	-	-	0.8	8.3	30.0
	5	-	-	-	-	-	-	-	-	-	0.8	7.5	21.7
		-	-	-	-	-	-	-	-	-	0.8	8.3	30.0
	6	-	-	-	-	-	-	-	-	-	0.8	7.5	21.7
		-	-	-	-	-	-	-	-	-	0.8	8.3	30.0
1959	4	19.8	20.2	16*	16	31	35	37	37	43	35	30	37
		49.8	70	86**	102	133	168	205	242	285	320	350	387
	5	19.5	20.5	14	18	29	34	31	38	44	42	30	37
		49.5	70	84	102	131	165	196	234	278	320	350	387
	6	20	20	16	16	29	37	36	38	43	35	30	37
		50	70	86	102	131	168	204	242	285	320	350	387
1960	4	70	63	65	78	72	80	67	58	72	71	30	1
		457	520	585	663	735	815	882	940	1012	1083	1113	1114
	5	70	60	65	81	64	81	69	63	67	72	34	1
		457	517	582	663	727	808	877	940	1007	1079	1113	1114
	6	70	58	65	85	70	75	67	63	65	72	36	1
		457	515	580	665	735	810	877	940	1005	1077	1113	1114

* Load applied during the month

** Summation of applied loads from the start

At the beginning of the test, the drivers were instructed to follow a programmed placement as follows: travel one trip (10 percent) with the outside of the dual tires on the guide lines nearest the edge, seven trips (70 percent) with the tire edge between the guide lines, and two trips (20 percent) with the tires on the lines nearest the center line. However, later the drivers were instructed to drive between the guide lines at all times with the expectation that the random driving position of each different driver would accomplish the programmed result.

Selected Test Sections for Analysis

Three of the main loops, loops 4, 5, and 6, were selected because of their significant change in performance histories for the first level of their thickness. For the prediction of the maximum principal stresses, all three loops for nonreinforced sections were analyzed, but only loop 4 was analyzed for reinforced sections because all reinforced sections can be analyzed by the same process. Reinforced and nonreinforced sections were considered as 40-by-24-foot and 15-by-24-foot slab panels,

respectively. All loops were studied under single load applications. The details of each loop are:

(1) loop 4--5-inch pavement thickness, 18-kip single-axle load;

(2) loop 5--6.5-inch pavement thickness, 22.4-kip single-axle load; and

(3) loop 6--8-inch pavement thickness, 30-kip single-axle load.

C H A P T E R I V

EFFECT OF LOAD TRANSFER

The load transfer device is a mechanical means of carrying the load across the joint and usually utilizes dowel bars. The results of the AASHO Road Test show a considerable difference in performance for reinforced and nonreinforced sections. It is hypothesized that this difference may be explained by differential values of load transfer for the two pavement types. Therefore, this chapter has the objective of developing load transfer criteria for the slabs at the AASHO Road Test. This, of course, would provide future design criteria for jointed concrete pavements.

The reinforced sections were 240 feet long with sawed-doweled transverse contraction joints spaced at 40 feet. Nonreinforced sections were 120 feet long with sawed-doweled transferse contraction joints spaced at 15 feet (no expansion joints were provided). In both types, the size of dowels varied with thickness.

Discontinuity in structural members causes severe localized stress due to reduction in stiffness of

the sections. Previous work by Abou-Ayyash (Ref 23) showed the effect on deflection of bending stiffness reduction in cracked slabs for continuously reinforced concrete pavement. The amount of stiffness reduction depends on the percentage of longitudinal reinforcement and type of concrete. According to Ref 23, the range of reduction in bending stiffness for 4000-psi concrete (compressive strength) is between 85 and 95 percent. Since jointed pavement has less load transfer than continuously reinforced concrete pavement (Ref 35), it is anticipated that reduction in stiffness will be greater.

The basic background of the assumptions on slab stiffness will be briefly discussed. Figure 4.1 is a pictorial representation of the finite-element model of the slab, as suggested by Hudson (Ref 37). The torsion bars represent the real torsional stiffness of the slab and are always active in the system. The Poisson's ratio effects and the bending stiffness of the plate are represented by elastic blocks at the node points of the slab. The elastic blocks have a stress-strain relationship equivalent to the real plate and have Poisson's ratio equal to that of the plate. If the beams in the x-direction are bent up, the beams in the orthogonal y-direction bend down due to Poisson's ratio. More information may be obtained from Refs 36 and 37.

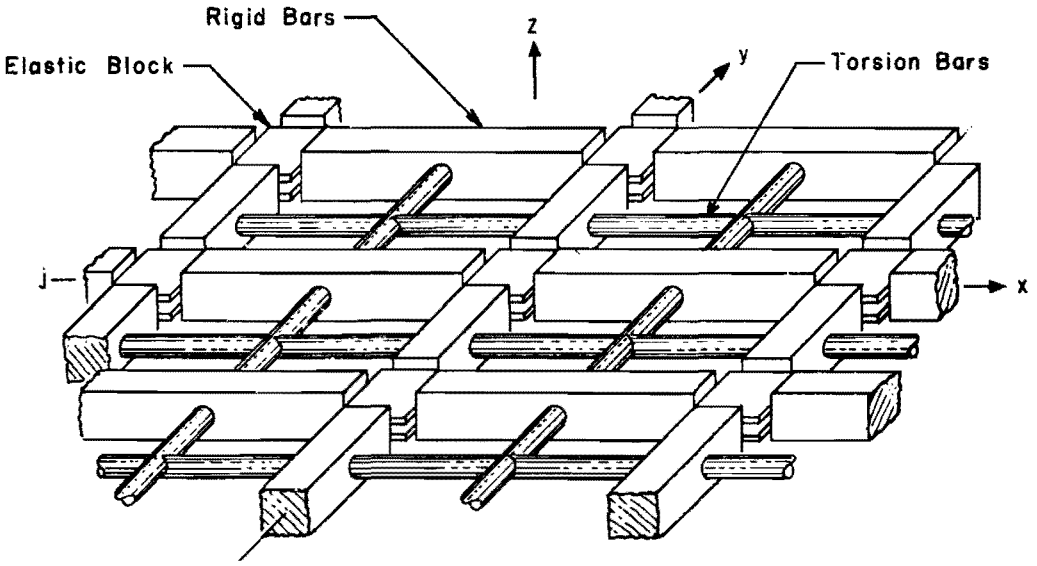

Fig 4.1. Finite-element model of a plate or slab (after Ref 36).

To study the effect of load transfer for jointed pavement at the AASHO Road Test, typical loading conditions for both pavement types shown in Fig 4.2 were selected. The analysis in the following paragraphs illustrates the effect of reduction in twisting stiffness and bending stiffness on the maximum principal flexural stresses and deflections.

Effect of Twisting Stiffness Reduction

To study the effect of reduction in twisting stiffness, a typical pavement section was selected from loop 4 and the loads were placed at the anticipated wheel path positions, i.e., approximately 2 feet from the pavement edge. The first consideration is a pure reduction in twisting stiffness, i.e., no reduction in bending stiffness. SLAB 40 was used to calculate the maximum stresses and deflection at zero percent, 75 percent, and 100 percent reduction in twisting stiffness. The results are plotted in Figs 4.3 and 4.4. As shown by Figs 4.3 and 4.4, the maximum principal stresses of the slab, as well as the maximum deflections, usually increase as the percent of reduction in twisting stiffness increases. Comparing the

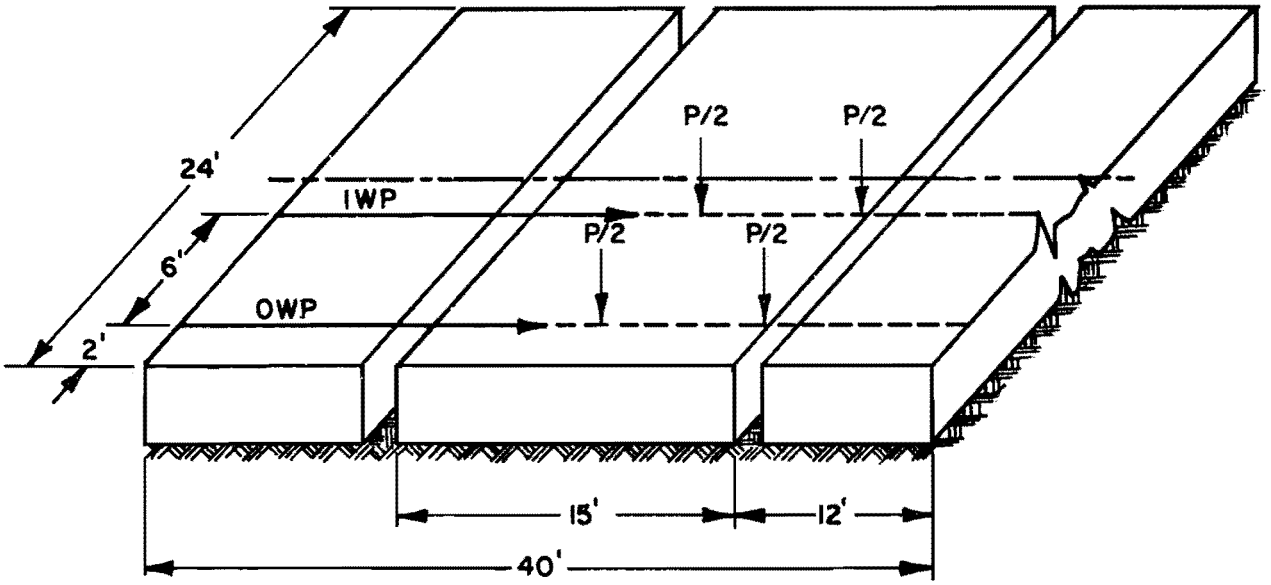

IWP = Inside Wheel Path
OWP = Outside Wheel Path
P = Axle Load Pounds

(a) Nonreinforced section.

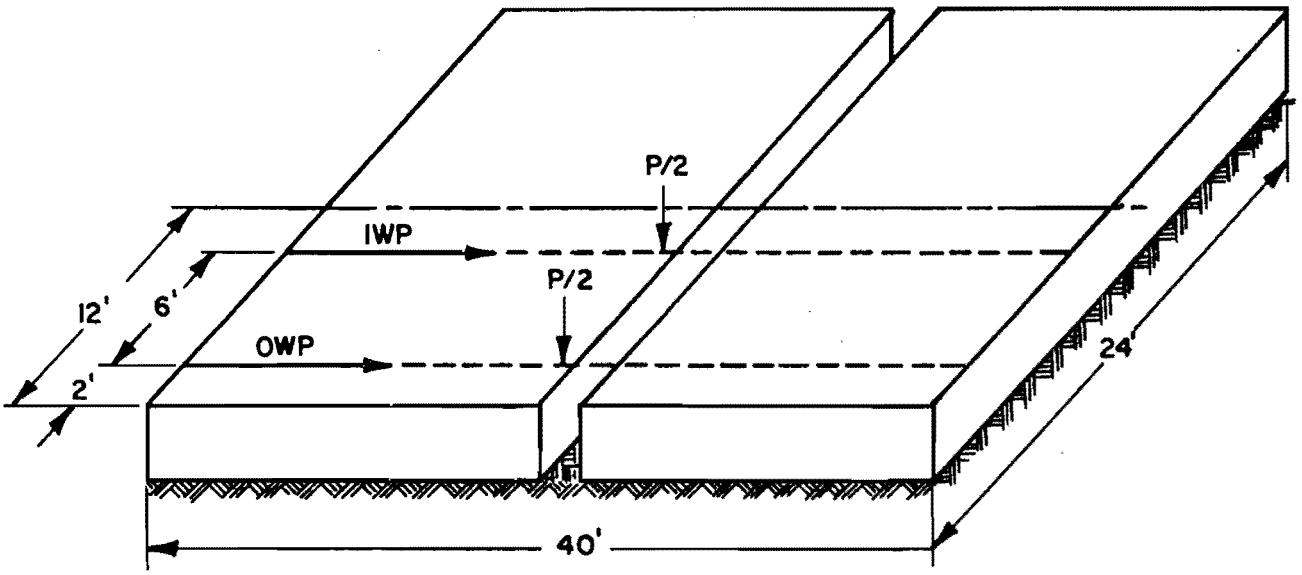

IWP = Inside Wheel Path
OWP = Outside Wheel Path
P = Axle Load Pounds

(b) Reinforced section.

Fig 4.2. Typical selected sections and loading conditions.

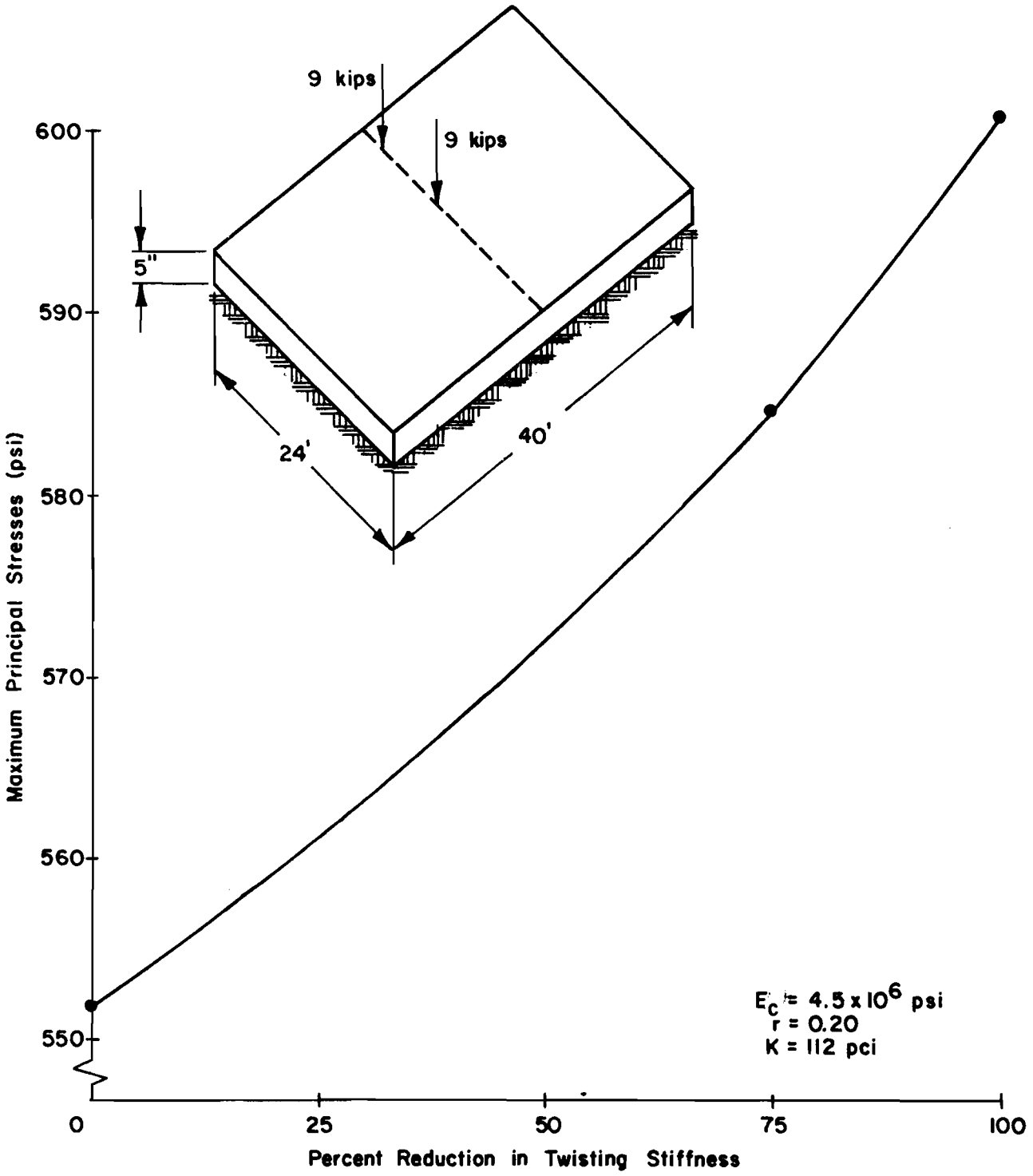

Fig 4.3. Effect of reduction in twisting stiffness on maximum principal stress.

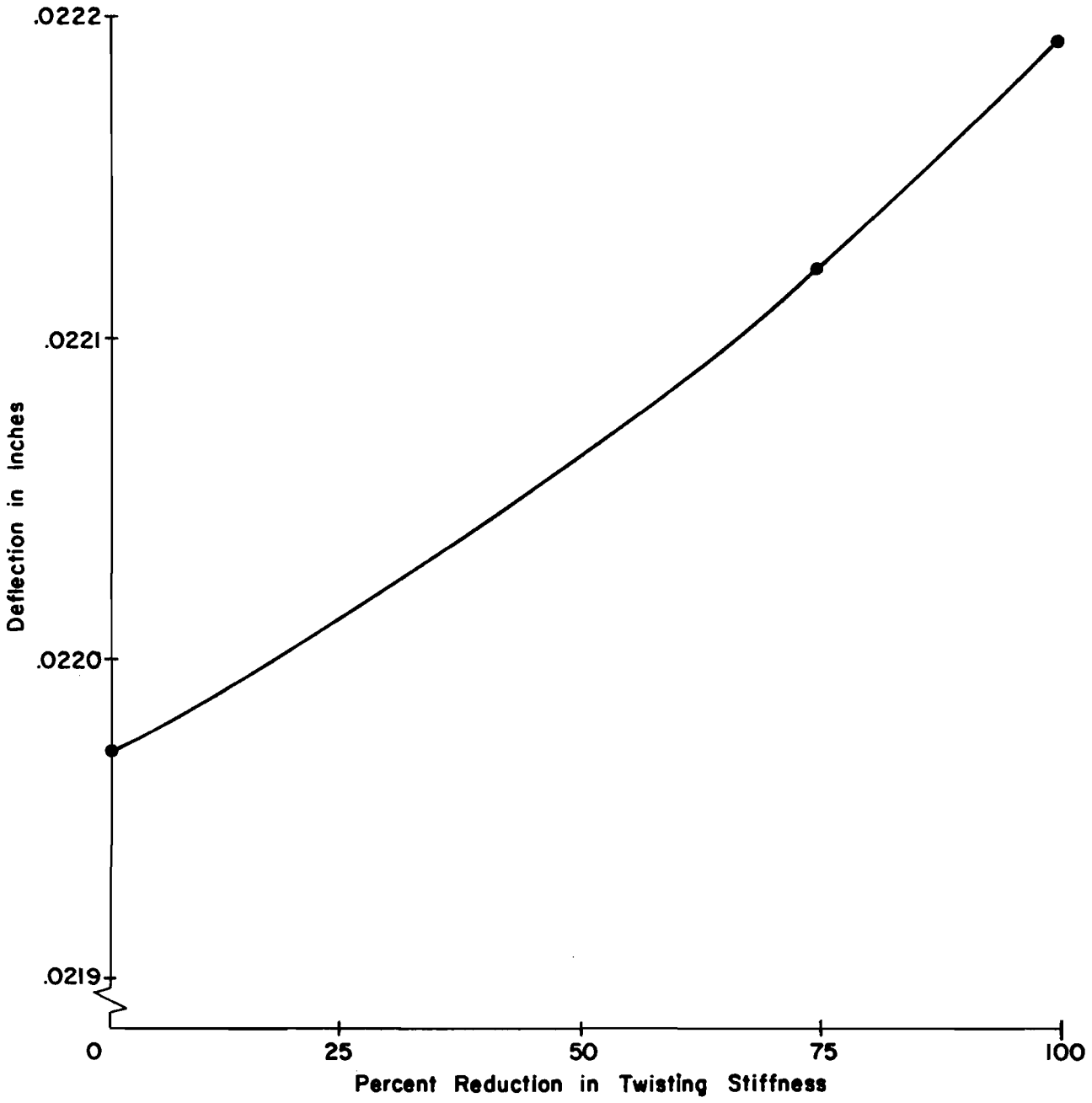

Fig 4.4. Effect of reduction in twisting stiffness on maximum deflections.

figures, it is apparent that a reduction is twisting stiffness with no reduction in bending stiffness has much more effect on maximum stresses than maximum deflections.

Effect of Bending Stiffness Reduction

Previous work by Abou-Ayyash (Ref 23) shows the effect of a crack in continuously reinforced concrete pavements. The result indicates that the percent reduction in bending stiffness over the most appropriate length ranges from 80 to 92 percent of the original value (Ref 23). For jointed pavement, the joint width is usually wider than the crack width. Theoretically, the joint width depends on the spacing of the joint. As the spacing of the joint increases the joint width increases; the joint widths of the reinforced sections are wider than those of the nonreinforced sections. In general, the reduction in bending stiffness depends on the region affected by the joint width. As the joint width increases, the region affected by the joint width, as well as the reduction in stiffness of slab, increases. In fact, when the load passes the joint, the deflection at the joint increases as the joint width increases. To appraoch the actual field conditions for reinforced and nonreinforced sections, the following assumptions were made based on a limited analysis:

(1) for nonreinforced sections, reduce bending stiffness at one station; and

(2) for reinforced sections, reduce bending stiffness at two adjacent stations.

The results of both cases from SLAB 40 are presented in Table 4.1 and also plotted in Figs 4.5 and 4.6. The graphs show the bending stiffness has a significant effect on maximum deflection. The difference in maximum deflection for a reduction at one station is approximately 75 percent, whereas a reduction at two adjacent stations is approximately 140 percent. At the same time, the differences in maximum principal stresses for the reduction at one station and at two adjacent stations are approximately 10 percent and 8 percent, respectively (Table 4.1).

These results reinforce previous assumptions on the best approach to represent the actual condition. In conclusion, it might be valid to assume that a reduction in binding stiffness of one station and two adjacent stations represents the regions affected by the joint width of nonreinforced and reinforced sections, respectively.

TABLE 4.1. EFFECT OF REDUCTION IN BENDING STIFFNESS ON MAXIMUM DEFLECTIONS AND PRINCIPAL STRESSES

Reduction in bending stiffness (percent)	Reduced at one station			Reduced at two adjacent stations		
	Corner deflection (in.)	Maximum deflection (in.)	Maximum stress (psi)	Corner deflection (in.)	Maximum deflection (in.)	Maximum stress (psi)
0	0.02107	0.02243	551.8	0.02051	0.02197	551.8
90	0.03013	0.03281	500.4	0.02038	0.03290	502.8
100	0.03616	0.03943	495.8	0.02039	0.05276	507.7

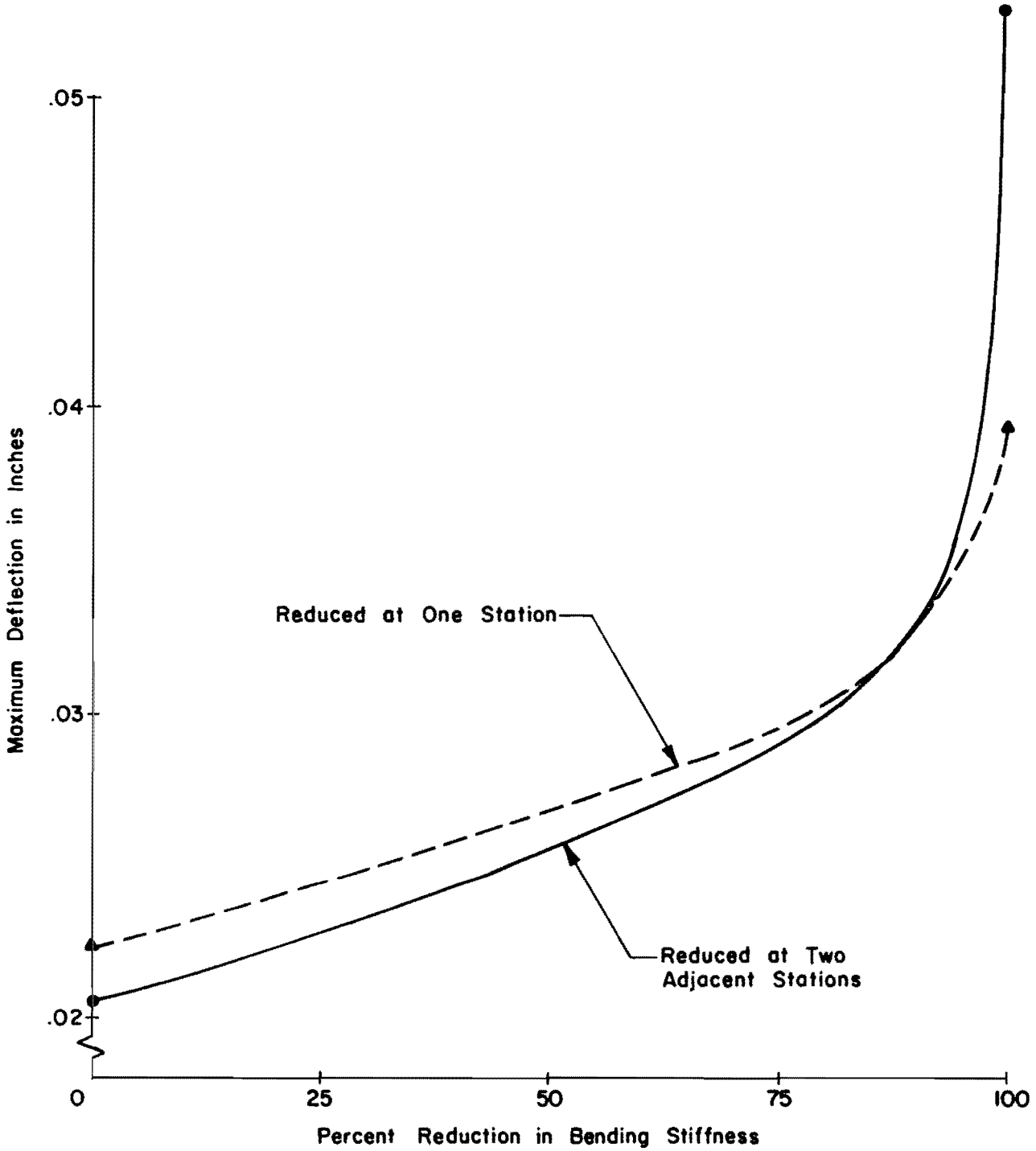

Fig 4.5. Effect of reduction in bending stiffness on maximum deflections.

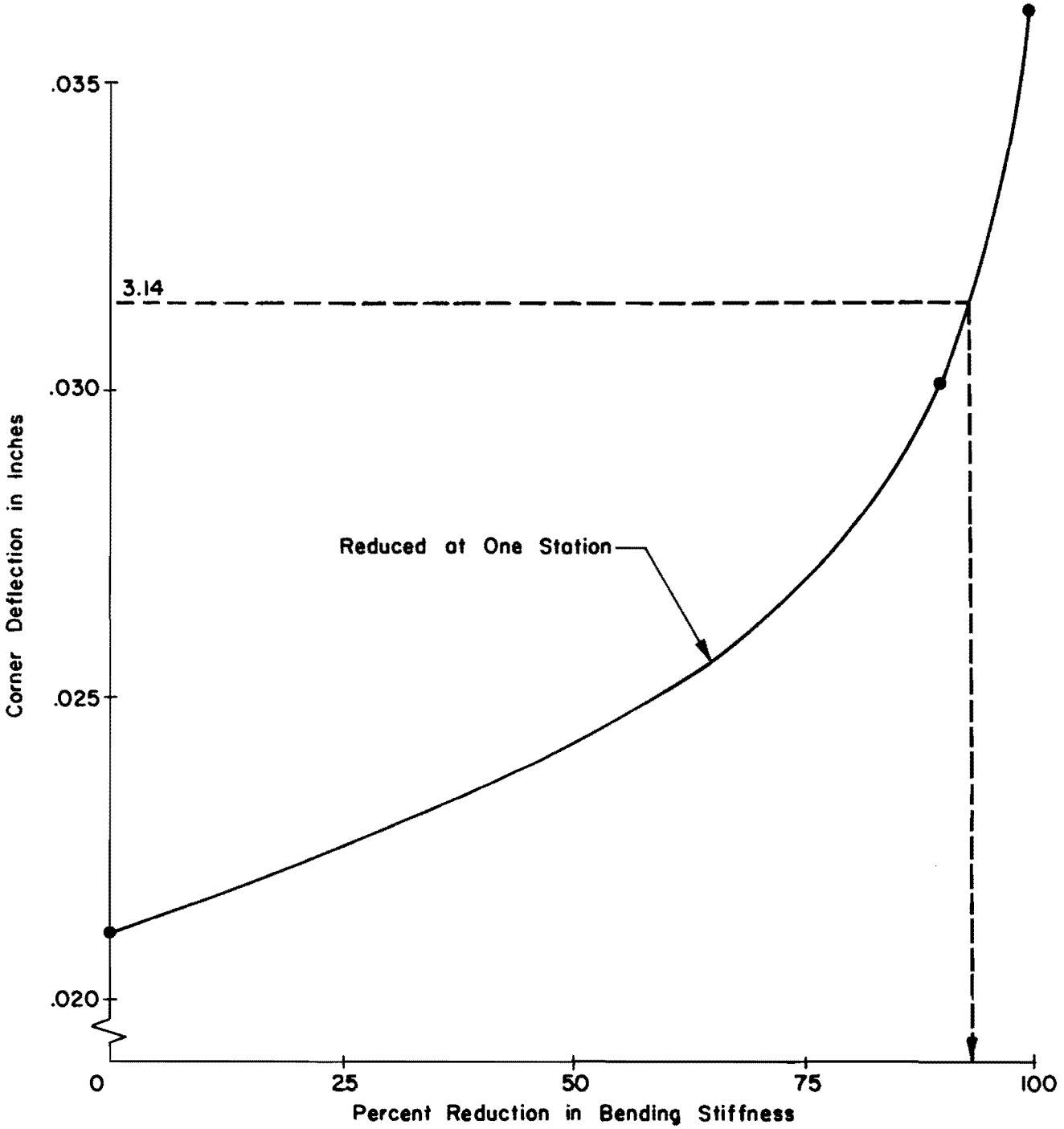

Fig 4.6. Effect of reduction in bending stiffness on corner deflections.

Interaction Between Reduction in Bending Stiffness and Twisting Stiffness

Since the joint width of reinforced sections (40-foot spacing) is large when compared with the crack, it follows that when the load passes the joint, the induced stresses will be higher than interior stresses because of the discontinuity of the pavement section. To attack this problem, the interaction problems were analyzed by SLAB 40 and the results are shown in Table 4.2. As shown in Fig 4.7, the variation of corner deflection due to a reduction in bending stiffness at various levels of twisting stiffness is more or less the same up to 90 percent reduction in bending stiffness, but the deflections vary tremendously from 90 percent to 100 percent reduction in bending stiffness. Figure 4.8 shows the effect of reduction in twisting stiffness on maximum stresses at various percent reductions in bending stiffness. Apparently the maximum stresses increase with an increase in twisting stiffness reduction for any bending stiffness reduction. The rate of change in maximum principal stresses due to reduction in twisting stiffness increases as the percent reduction in bending stiffness increases.

TABLE 4.2. INTERACTION BETWEEN REDUCTION IN BENDING STIFFNESS AND TWISTING STIFFNESS ON MAXIMUM DEFLECTIONS AND STRESSES

Reduction in twisting stiffness (percent)	Results from theoretical analyses	Reduction in bending stiffness at two adjacent stations (percent)		
		0	90	100
0	Maximum deflections	0.02197	0.03290	0.05276
	Corner deflections	0.02051	0.03034	0.05004
	Maximum stresses	551.8	502.8	507.7
75	Maximum deflections	0.02212	0.03360	0.05735
	Corner deflections	0.02038	0.03024	0.05395
	Maximum stresses	584.8	579.8	612.0
100	Maximum deflections	0.02219	0.03406	0.05990
	Corner deflections	0.02029	0.02991	0.05580
	Maximum stresses	600.6	630.4	700.2

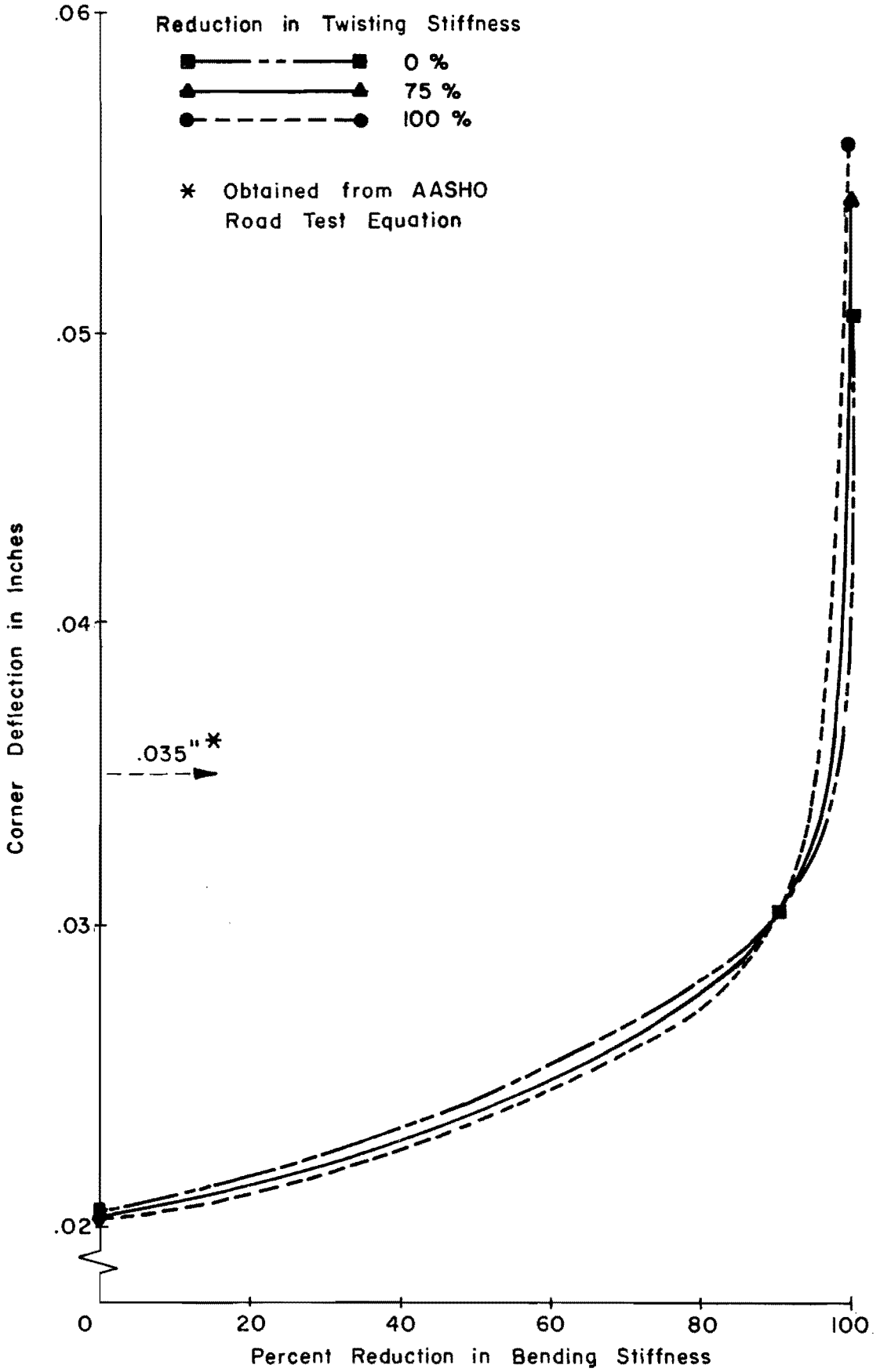

Fig 4.7. Effect of reduction in bending stiffness on corner deflections at various percent reductions in twisting stiffness.

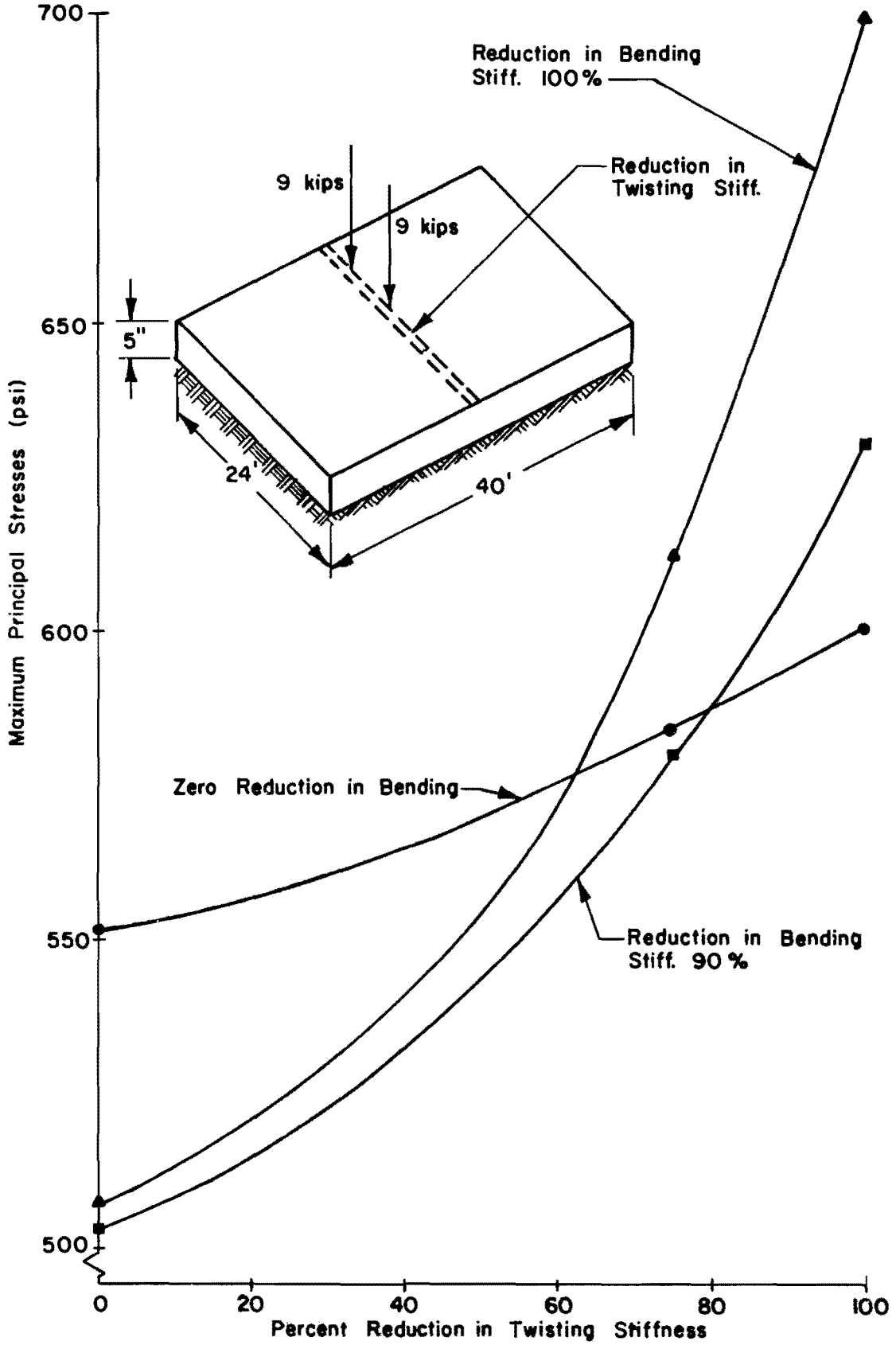

Fig 4.8. Effect of reduction in twisting stiffness on maximum principal stresses at various percent reduction in bending stiffness.

Analysis of the Results by AASHO Road Test Equation

At the AASHO Road Test, static rebound deflections at the corner were measured by means of a Benkelman beam (Appendix D, Ref 32). The equation below was obtained from static rebound corner deflection data from rounds 1 through 3 and 5 through 9, gathered from April to September 1959. The data from loop 2 are excluded from the analysis because the data are not consistent with those from the other loops (Ref 32). Based on these data, for single-axle vehicles on reinforced sections (Ref 32),

$$dc' = \frac{0.013L_1}{10^{0.015T_{D_2}1.18}} \qquad (4.1)$$

where

dc' = static rebound corner deflection, inches;

L_1 = single-axle load, kips;

D_2 = pavement thickness, inches;

T = temperature (^{o} F) at a point 1/4-inch below the top surface of the 6.5-inch slab, minus the temperature at a point 1/2 inch above the bottom surface, determined at the time the deflection was measured.

Since elastic theory was used in this analysis, the static rebound deflection is assumed to be comparable with the static deflection. To analyze using the AASHO equation for 18 kips, a 5-inch pavement thickness single-axle load on a reinforced section was used. The corner deflection at zero temperature is equal to:

$$dc = \frac{0.013 \times 18}{5^{1.18}} = 0.035\text{-inch}$$

This value of corner deflection is entered in Fig 4.7 (deflection computed for AASHO conditions) to obtain the percent reduction in bending stiffness for various percent reductions in twisting stiffness and the results are as follows:

Reduction in Twisting Stiffness	Obtained Percent Reduction in Bending Stiffness
0	95
75	97
100	98

The average value of bending stiffness reduction for all percent reduction in twisting stiffness is approximately 97 percent. With 97 percent bending stiffness reduction, entered on the abscissa of Fig 4.7, corner deflections are as follows:

Percent Reduction in Twisting Stiffness	Corner Deflection, inches
0	0.0330
75	0.0355
100	0.0380

The relation between percent reduction in twisting stiffness and corner deflection at 97 percent reduction in bending stiffness (previously obtained) is plotted in Fig 4.9. With the corner deflection from actual field conditions (equal to 0.035), the reduction of twisting stiffness at the corresponding deflection is about 81 percent.

In conclusion, for a reinforced section to represent the field conditions, the results of the analysis are shown below:

(1) the reduction in bending stiffness at two adjacent stations is 97 percent, and

(2) the reduction in twisting stiffness is 81 percent.

For a nonreinforced section to represent the field condition, the corner deflections were obtained from the AASHO Road Test equation for a single-axle nonreinforced section (Ref 32):

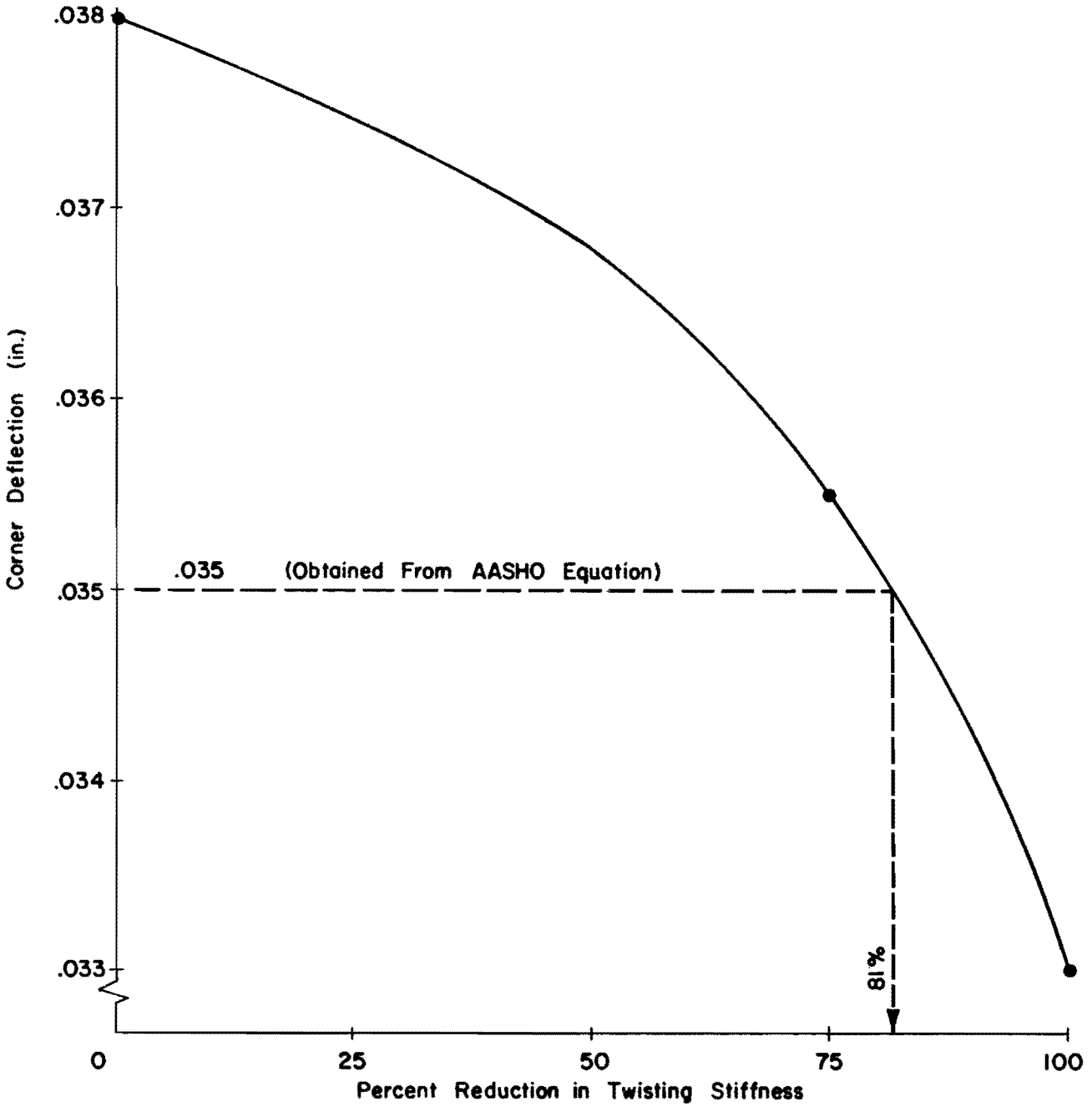

Fig 4.9. Corner deflection versus percent reduction in twisting stiffness at 97 percent reduction in bending stiffness.

$$dc = \frac{0.013L_1}{10^{0.011T}D_2^{1.25}} \qquad (4.2)$$

The terms dc , L_1 , T , and D_2 were previously discussed.

For an 18-kip single-axle and a 5-inch pavement thickness:

dc = 0.0314 inch

Entering this value in Fig 4.6, the percent reduction in bending stiffness at one station is approximately 93 percent, whereas the difference in stresses for 93 percent and 100 percent reduction in bending stiffness is small. It is valid to assume that for nonreinforced sections, 100 percent reduction in bending stiffness at one station is the best approach to simulate actual field conditions.

Summary

From Table 4.2, the difference in maximum deflection at full value of twisting stiffness and zero twisting stiffness is only about 1 percent, whereas the difference in maximum principal stresses is 10 percent. Both deflections and stresses increase as reduction in twisting

stiffness increases, so it may be concluded that reduction in twisting stiffness alone does not have an effect on maximum deflections but has considerable effect on maximum principal stress.

At no reduction in twisting stiffness, the differences in maximum deflection at full value of bending stiffness at one station and two adjacent stations are 75 percent and 140 percent, respectively. The deflection increases as the reduction in bending stiffness increases. In contrast, the maximum principal stress usually decreases as percent reduction of bending stiffness increases. The difference in maximum principal stress is approximately 10 percent.

C H A P T E R V

MODIFICATION OF ERODED AREA BENEATH SLAB FROM PUMPING INDEX

Pumping of rigid pavement is a significant factor in the deterioration of the pavement surface. At the AASHO Road Test, severe pumping occurred in the first and second levels of thickness for all loops. When a rigid pavement with a subbase pumped, the subbase material was ejected and the result was the loss of support beneath the pavement slab. Local stresses increase as the eroded area increases.

To predict the maximum stress of rigid pavement at the AASHO Road Test, pumping must be taken into consideration because pumping usually causes loss of support that leads to increase in maximum stress under loading applications of rigid pavement. To successfully predict the maximum stress in the rigid pavement system, the conversion of pumping index to eroded area beneath slab is required.

The initial step in pumping of the subbase is the creation of a void space under the pavement where

freewater may accumulate after repeated loads are applied to the pavement. Generally, the void space may be caused by plastic deformation of the soil after the more elastic slab rebounds or by warping of the slab due to temperature differential. If the soil is free-draining, when water enters the void space, the water will move through the soil. But if the water does not drain sufficiently, deflection of the slab due to load application will cause the water to be ejected from beneath the pavement slab. After many load applications, the pumping action will produce a large void space beneath the pavement and cause distress in the pavement.

It appears that the pavement distress under moving load is greatest when the load travels close to the pavement edge (causing edge and corner loading conditions). Whenever the slab produces maximum deflection, the maximum pumping action will occur and whenever loss of support of rigid pavement begins, stresses in the pavement will change tremendously, depending on the extent of the area eroded beneath the pavement slab. Since the rigid pavement system is subjected to numerous variables, it is difficult to formulate a clear-cut loading condition representative of actual conditions in the field.

To accommodate the situation of loading in the field, the average anticipated wheel path position (approximately 2 feet from the pavement edge) is considered.

At the AASHO Road Test, a considerable volume of the subbase material was ejected along the edge of the pavement immediately after a rainfall (Ref 32). The amount of pumped material was presented in the form of a pumping index. Based on engineering judgment and experience from field tests, the pumping index is converted to a value for an eroded area beneath the slab by making certain assumptions and establishing boundary conditions. The reason for this conversion is for the feasible use of the SLAB program in the prediction of the maximum principal stresses during the test period at the AASHO Road Test. In the first stage of the report, brief review of observations and findings from the AASHO Road Test are presented.

AASHO Road Test Observations

It was observed that freewater collected under the slab during rains and did not drain laterally through the subbase material in the shoulder to the site ditches at a rate sufficient to prevent pumping action. It was

also observed that subbase material was apparently removed by the erosive action of water moving across the top of the subbase. A pumping index was computed by approximating the accumulated volume of material ejected per unit length of pavement and averaging over the length of the test section. The pumping index is in cubic inches of pumping material per inch of pavement length.

Pumping is generally noted first at the free edge of the pavement near a joint and then progresses along the edge toward the center of the slab. Edge pumping is generally more extensive than joint pumping throughout the life of the pavement. There was no clear-cut evidence from the Road Test to associate pumping index with serviceability of a pavement, since some test sections which failed had a pumping index less than those of the surviving sections. Nevertheless, the average pumping index for failed and surviving sections was 134 and 34, respectively. A great majority of the failed sections pumped severely prior to failure, which seems to confirm the fact that whenever pumping starts, stresses in the pavement increase significantly due to loss of support, which leads to pavement cracks. There are no consistent trends relating the pumping index to subbase thickness

and pavement types (reinforced or nonreinforced sections), but there is some correlation for pavement thickness and load.

Table 5.1 presents the pumping index for loops 4, 5, and 6 under a single load application. Only the sections where the serviceability index dropped to 1.5 will be analyzed because of their complete histories in pumping index and performance.

Based on these studies, the following paragraphs are presented to show the transformation of the pumping index to values of eroded areas beneath pavement slabs.

Transformation of Pumping Index to Eroded Area. The computation for the pumping index was as follows:

$$PI = 144 \frac{PV}{L} \text{ in}^3/\text{in} \qquad (5.1)$$

where

PV = pumping value, in cubic feet;

L = length of pavement section, in feet;

PI = pumping index, in cubic inches per inch.

A number of assumed boundary conditions must be established to convert pumping index to a volume. The more important are as follows:

TABLE 5.1. PUMPING INDEX AT PRESENT SERVICEABILITY INDEX = 1.5 OR N = 1,114,000

Loops	Single Axle Load, in kips	Subbase Thickness, in inches	Reinforced Sections						Nonreinforced Sections					
			Pavement Thickness, in inches						Pavement Thickness, in inches					
			5	6.5	8	9.5	11	12.5	5	6.5	8	9.5	11	12.5
4	18	3	189*	47	19	13			191*	48	24	16		
		6	116*	92	19	5			91*	29	24	20		
		9	98*	117	18	6			147*	209	21	16		
5	22.4	3		207*	146	27	11			133*	33	22	23	
		6		104*	63	20	18			301*	47	52	2	
		9		193*	79	16	4			203*	122	28	3	
6	30	3			122*	18	19	4			150*	32	15	22
		6			237*	45	27	6			159	29	20	20
		9			237*	120	22	1			168	59	12	3

* Present serviceability index equal to 1.5

N Number of traffic applications

1. Relationship between compacted condition of subbase and loose saturated condition of pumped material on the surface,
2. Shape of pumped area beneath the pavement,
3. Loss of pumped material due to water, and
4. Human error in estimating the pumped material volume.

These assumed boundary conditions have a great effect on the calculation of the volume of the pumped material. It seems impossible to obtain the exact calculation of the pumped material. However, based on experience and engineering judgment, the general shape of pumping is assumed to be as presented in Fig. 5.1. From mathematics, the pumping volume beneath the slab is:

$$PV_o = \frac{1}{6} d_x \; d_y \; d_z \quad ft^3 \tag{5.2}$$

where

d_x = length of pavement in longitudinal direction, in feet;

d_z = length of pavement in transverse direction, in feet;

d_y = depth of pumping at the corner, in feet.

The boundary values of d_x, d_y, and d_z for reinforced and nonreinforced sections are:

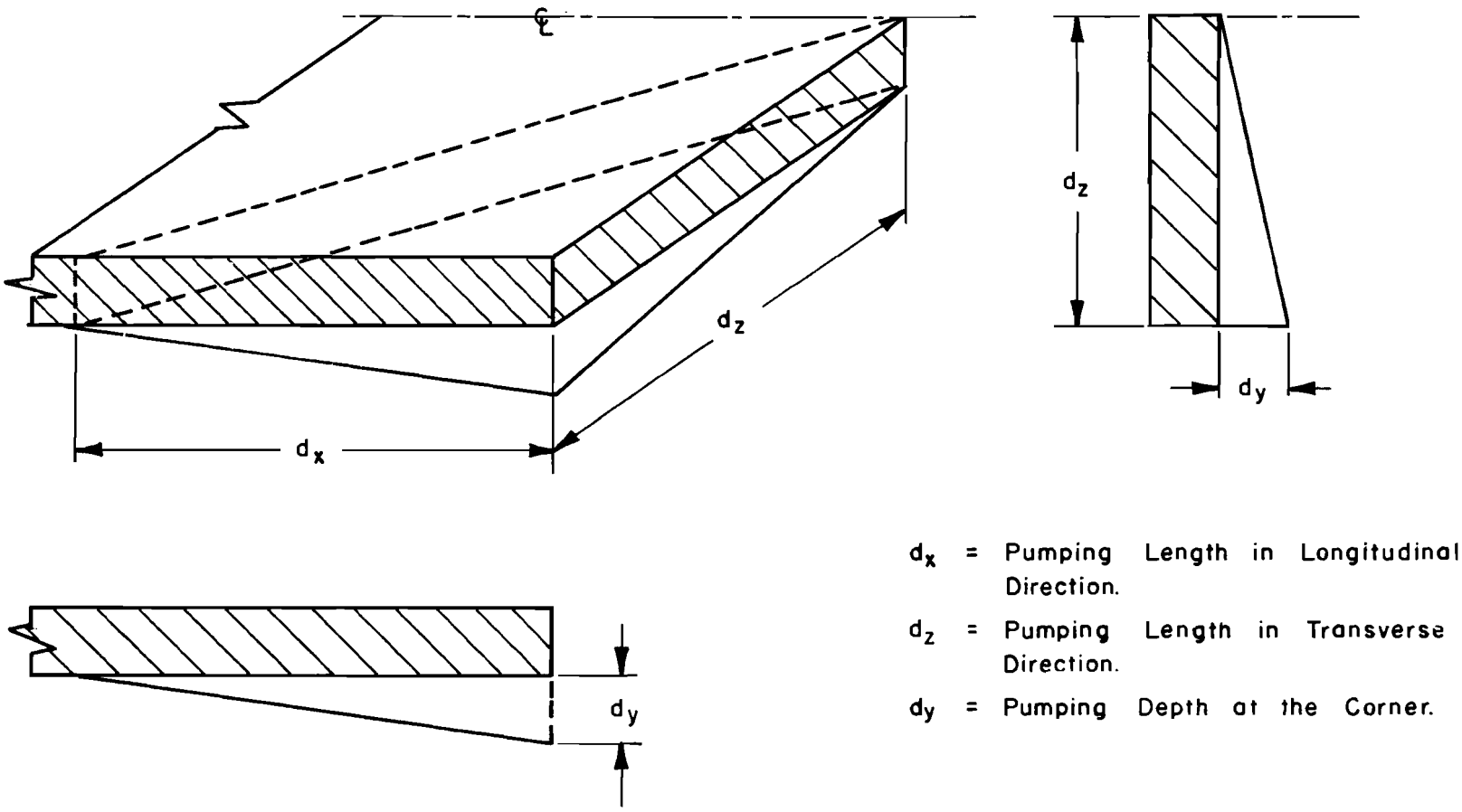

d_x = Pumping Length in Longitudinal Direction.

d_z = Pumping Length in Transverse Direction.

d_y = Pumping Depth at the Corner.

Fig 5.1. Typical shape of eroded area for both reinforced and nonreinforced pavement sections.

40-by-24-Foot Slab Panel (reinforced section) -

(1) For maximum condition

$$0 \leq d_x \leq 15 \text{ feet},$$
$$0 \leq d_y \leq \tfrac{1}{4} \text{ foot},$$
$$0 \leq d_z \leq 12 \text{ feet}.$$

(2) Maximum PI from test data is equal to 237 in^3/in.

15-by-24-Foot Slab Panel (nonreinforced section) -

(1) For maximum condition

$$0 \leq d_x \leq 15 \text{ feet},$$
$$0 \leq d_y \leq \tfrac{1}{4} \text{ foot},$$
$$0 \leq d_z \leq 12 \text{ feet}.$$

(2) Maximum PI from test data is equal to 301 in^3/in.

Recognizing that the pumped volume on top of the slab may not be equal to the eroded area beneath the slab, a modified C-factor is introduced as follows:

$$PV = PV_o C \ in^3/in \qquad (5.3)$$

where

C = modified factor,

PV_o = pumping volume beneath pavement.

Substituting in Eq 5.1, the following equation is obtained:

$$PI = 144\frac{PV_oC}{L} \tag{5.4}$$

To calculate the C-value, the boundary conditions previously established and the shapes in Fig. 5.2 may be used. Different values of C are obtained for each slab size.

For the 40-by-24-foot panel, using the boundary conditions and maximum pumping index of 237 in^3/in, the C-value is computed as follows from Fig. 5.2:

$$PV_o = V_A + V_B = 2(\tfrac{1}{6}\, d_x\, d_y\, d_z)\ ft^3$$

$$PV_o = \tfrac{1}{3}\, d_x\, d_y\, d_z\ ft^3$$

$$PV_o = \tfrac{1}{3} \times 15 \times 12 \times \tfrac{1}{4}\ ft^3 \tag{5.5}$$

Substituting PV_o and maximum PI into Eq 5.4,

$$PI = 237 = 144 \times 15 \times \frac{C}{40}$$

$$C = 4.39$$

Substituting C and PV_o into Eq 5.4,

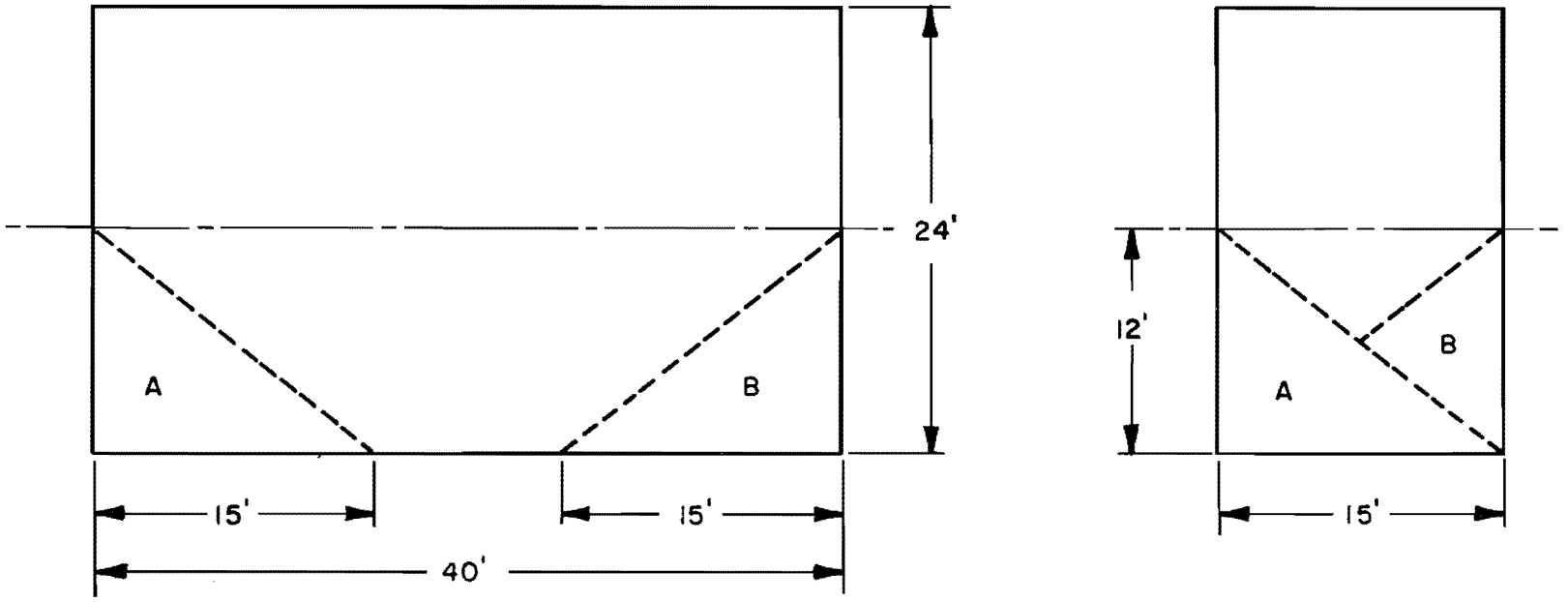

24' by 40' SLAB PANEL

24' by 15' SLAB PANEL

Fig 5.2. Shape of eroded area beneath slab at maximum pumping condition.

$$PI = 144 \times 4.39 \times \frac{1}{3} \frac{d_x \, d_y \, d_z}{L} \text{ in}^3/\text{in}$$

$$PI = 210 \frac{d_x \, d_y \, d_z}{L} \text{ in}^3/\text{in} \qquad (5.6)$$

$$\text{Eroded area} = \frac{1}{2} d_x \, d_z \text{ ft}^2 \qquad (5.7)$$

For the 15-by-24-foot panel, the maximum PI is equal to 301 in^3/in.

$$PV_o = V_A + V_B \text{ ft}^3$$

$$= \frac{1}{6} d_x \, d_y \, d_z + \frac{1}{6} \times \frac{d_x}{2} \times d_y \, d_z \text{ ft}^3$$

$$PV_o = \frac{1}{4} d_x \, d_y \, d_z \text{ ft}^3 \qquad (5.8)$$

$$= \frac{1}{4} \times 12 \times \frac{1}{4} \times 15 \text{ ft}^3$$

$$= 11.25 \text{ ft}^3$$

Substituting PV_o and maximum PI into Eq 5.4,

$$301 = 144 \times C \times \frac{11.25}{15}$$

$$C = 2.8$$

Substituting C and PV_o into Eq 5.4,

$$PI = 144 \times 2.8 \times \frac{1}{4} \frac{d_x\ d_y\ d_z}{L}$$

$$PI = 100 \frac{d_x\ d_y\ d_z}{L} \quad in^3/in \qquad (5.9)$$

$$\text{Eroded area} = \frac{1}{2} d_x\ d_z \quad ft^2 \qquad (5.10)$$

Figures 5.3 and 5.4 present the relation between the pumping index and the eroded area for both 24-by-40-foot and 24-by-15-foot slab panels. The calculations of the plots are presented in Appendix 2.

Summary

From this analysis, the eroded area of reinforced and nonreinforced sections at the AASHO Road Test can be predicted from the pumping index. The analyses were based on data and observations obtained from the AASHO Road Test. The maximum pumping index for reinforced sections is 237 in^3/in. The maximum eroded area obtained from Fig. 5.3 is 87 ft^2. The maximum pumping index for nonreinforced sections is 301 in^3/in. The maximum eroded area obtained from equation 5.10 is 90 ft^2. (See Appendix 2)

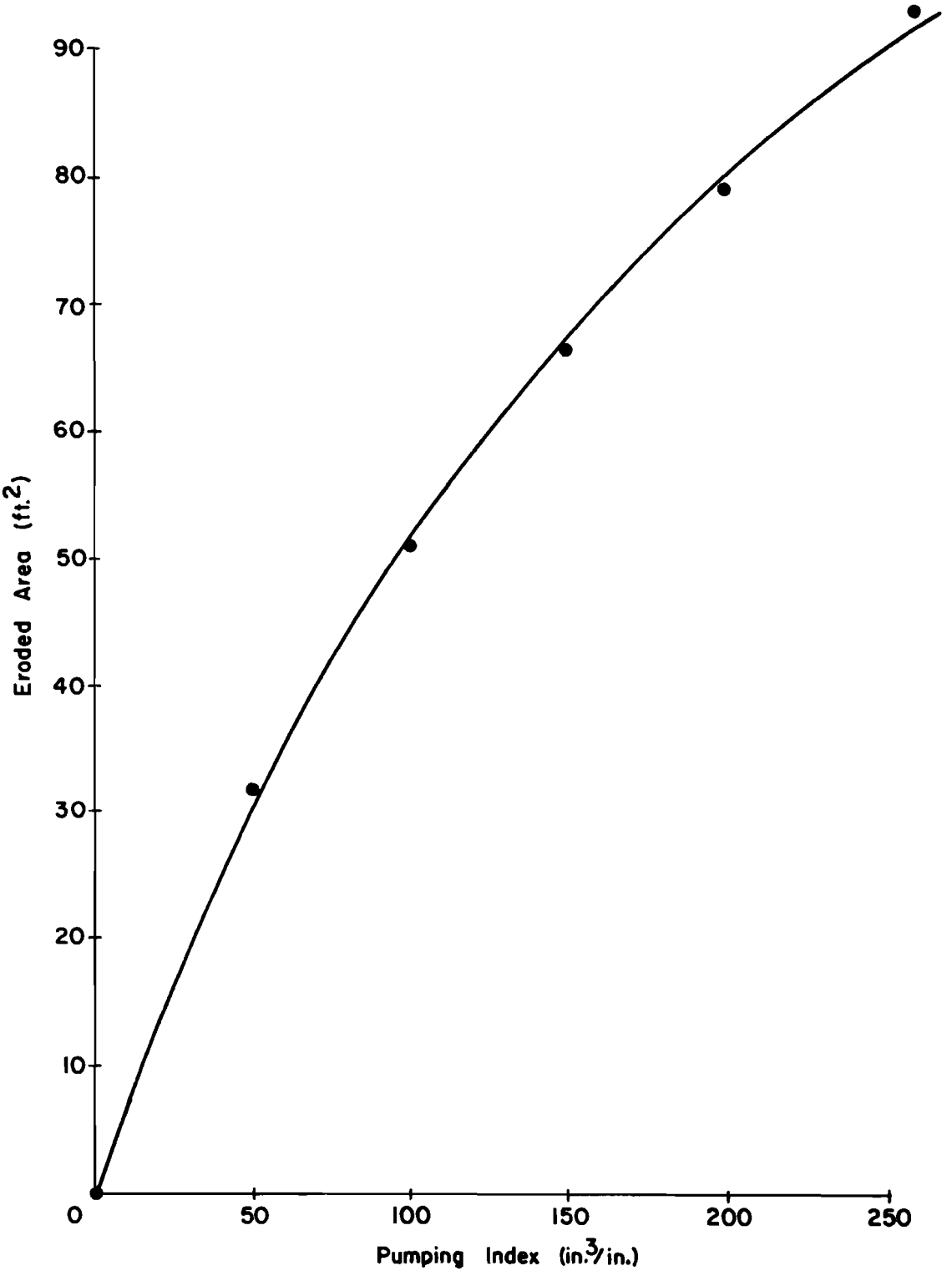

Fig 5.3. Relationship between pumping index and eroded area of reinforced section.

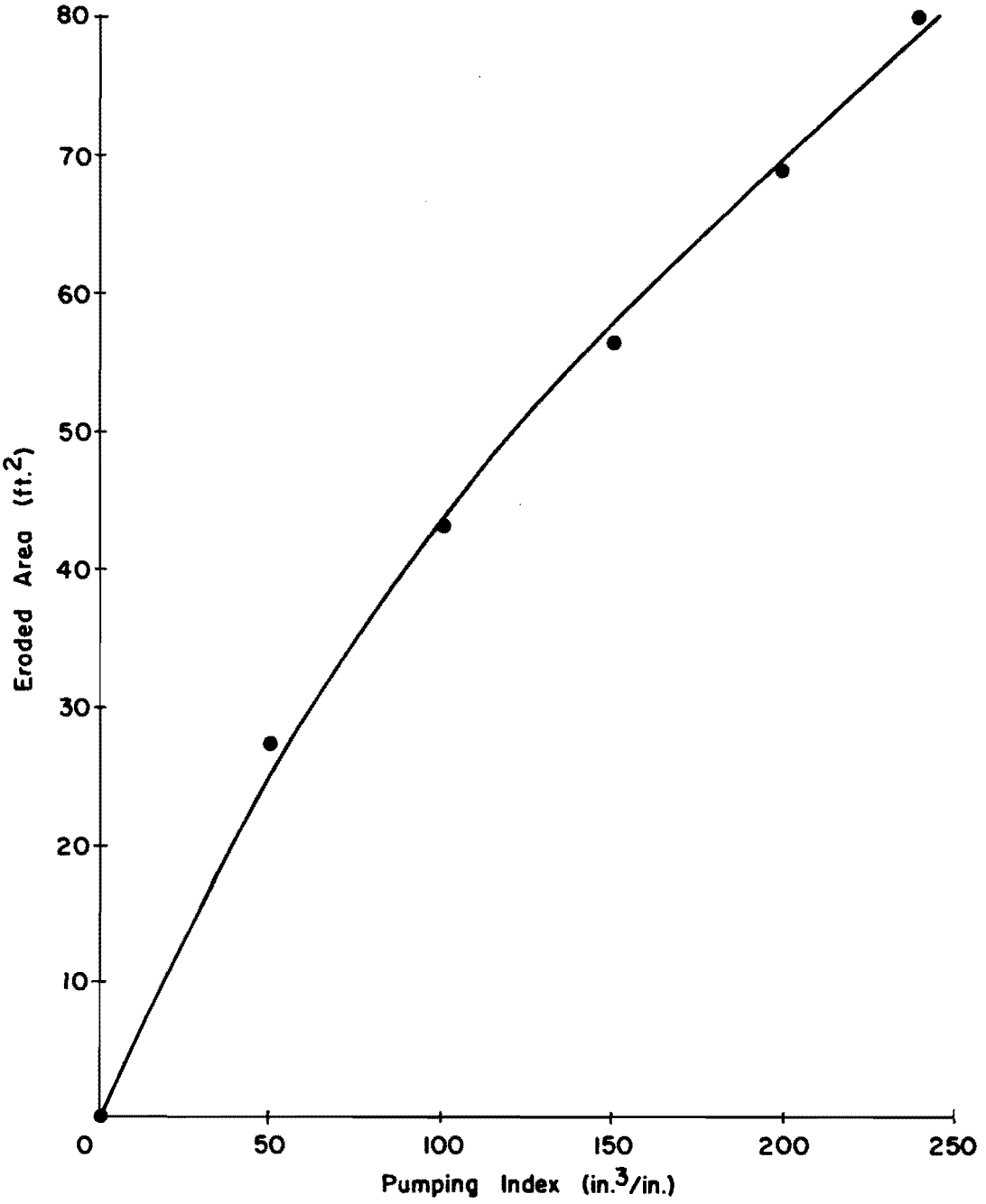

Fig 5.4. Relationship between pumping index and eroded area of nonreinforced section.

C H A P T E R V I

STRESS ANALYSIS FOR REINFORCED AND NONREINFORCED SECTIONS

The analysis of stresses in rigid pavements involves many factors, such as magnitude of load, load placement, temperature changes, pavement stiffness, pavement properties, and support properties. The amount of induced stress that the pavement can sustain is directly related to the concrete strength, based on a hypothesis that when the induced stress exceeds the concrete strength, a crack will occur.

Stress conditions in rigid pavement may be affected by repeated stress due to variation of temperature and moisture during the day, as well as repeated loading conditions. The critical stresses occur when the stresses due to loading condition and climatic conditions are additive. This mechanism of critical stress usually occurs when the temperature on the surface is higher than the temperature at the bottom; then the slab tries to warp downward, but because of restraint forces due to the weight of the slab between surface and subbase, the

initial tensile stress occurs at the bottom of the slab and compressive stress on the top. According to the slab's characteristics, when the load is applied at the interior of the slab, tensile stress occurs at the bottom of the slab. Critical stress occurs when these two conditions are additive. By contrast, when the surface is cooler than the bottom, the slab tries to warp upward, but because of the restraining force between the surface and the subbase, the initial tensile stress occurs on top of the slab. In addition, according to the slab characteristics, when the load is applied at the corner of the slab, tensile stress will occur on the top of the slab. The critical stress of the slab occurs on top of the slab when these two conditions are additive. It may be concluded that critical stress occurs when the slab is warped downward and the load is applied at the interior or when the slab is warped upward and the load is applied at the corner of the slab.

The repeated stress usually leads to the manifestation of cracking. As soon as cracks develop on the surface, the stiffness of the concrete slab decreases and the continued repeated stress applications lead to the damage of the pavement. The amount of reduction in

stiffness depends on the characteristics of the crack, such as degree of cracking, spacing, and crack width. Reduction in stiffness causes a reduction of the load-carrying capacity of the pavement structure. In general, for the first period of traffic applications, few or no cracks will occur. After numerous applications, cracks will develop on the surface due to the following:

1. Fatigue of concrete pavement,
2. Excessive loading,
3. Loss of support caused by high stress concentration, and
4. Additive stresses due to variation of subsurface condition.

From the discussion of stress produced in a concrete slab, it is seen that the effect of variation of subsurface conditions cause increasing stress, and load transfer causes the difference in stresses for reinforced and nonreinforced sections. Since the flexural stresses of concrete are the criterion of the fatigue equation, the best solution of flexural stresses is required.

For this report, the effect of variation of subsurface condition and the loss of support due to pumping are considered in the analysis.

Effect of Variation of Subsurface Condition

The variation of elastic modulus of the subbase (k-value) affects pavement performance, since the stresses in the pavement vary with the k-value of the subbase. In the SLAB program, the elastic modulus of the subbase and Poisson's ratio for the subbase represent the subsurface condition of the pavement. Poisson's ratio for the subsurface condition may vary during the life of a pavement, but its influence is small when compared with other variables and therefore it will be eliminated from further consideration.

In the following paragraphs, the effects of variation of the k-value of the subbase on maximum principal stresses of rigid pavement at the AASHO Road Test will be analyzed on the basis of previous studies (Ref 30).

The effect of variation of the k-value on the maximum principal stress and consequently performance for full support and partial loss of support was indicated by a previous study of the erodability factor (Ref 30). The erodability factors were specified by 0, 1, 2, and 3, which represented the eroded areas beneath the slab of

0, 9.05, 20.25, and 38.90 square feet, respectively. The eroded area was assumed to occur at the corner of the slab and eroded equally in the transverse and longitudinal directions of the pavement slab. A 24-kip single axle with dual tires was placed 1 foot from the pavement edge of the slab which was 24 by 40 feet and 8 inches thick. The results of previous studies are presented in Fig 6.1. The corner condition was selected because it is symmetrical and occurred at the AASHO Road Test.

Figure 6.1 shows the effect of loss of support on maximum principal stresses for various k-values. The average minimum and maximum k-values of loops 4, 5, and 6 at the AASHO Road Test are equal to 108 pci and 155.5 pci, respectively (Chapter III). These two k-values were entered on the abscissa of Fig 6.1 to obtain the values of maximum principal stresses at various erodability factors on the ordinate.

The maximum principal stresses at an erodability factor equal to 0, 1, 2, and 3 for the average minimum k-value are 237.5, 346, 447, and 550 psi, and for the average maximum k-value are 225, 335, 437.5, and 545 psi, respectively. These maximum principal stresses versus eroded area in square feet were plotted in Fig 6.2

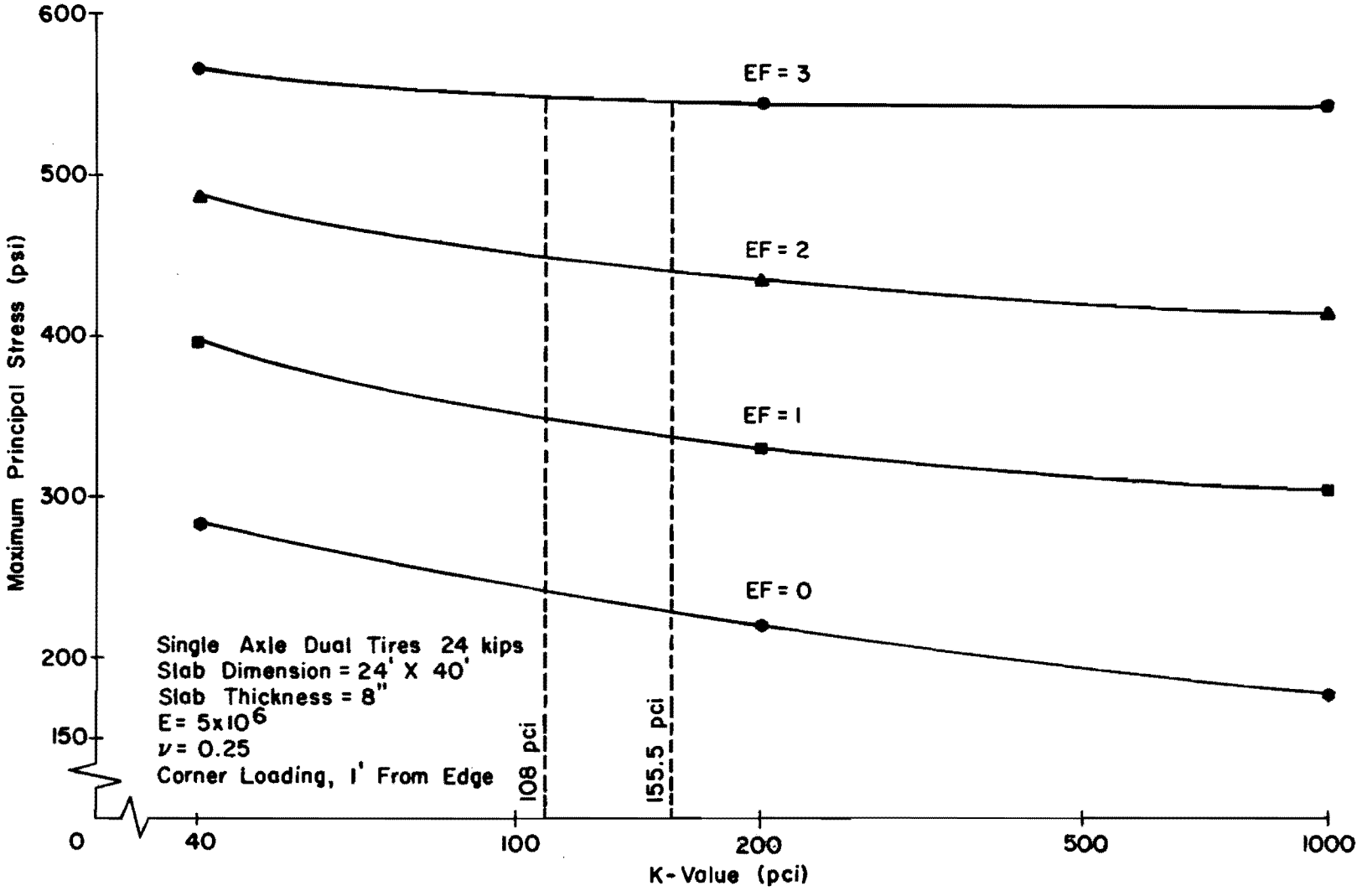

Fig 6.1. Effect of k-value on maximum principal stress at various support conditions (after Ref 30).

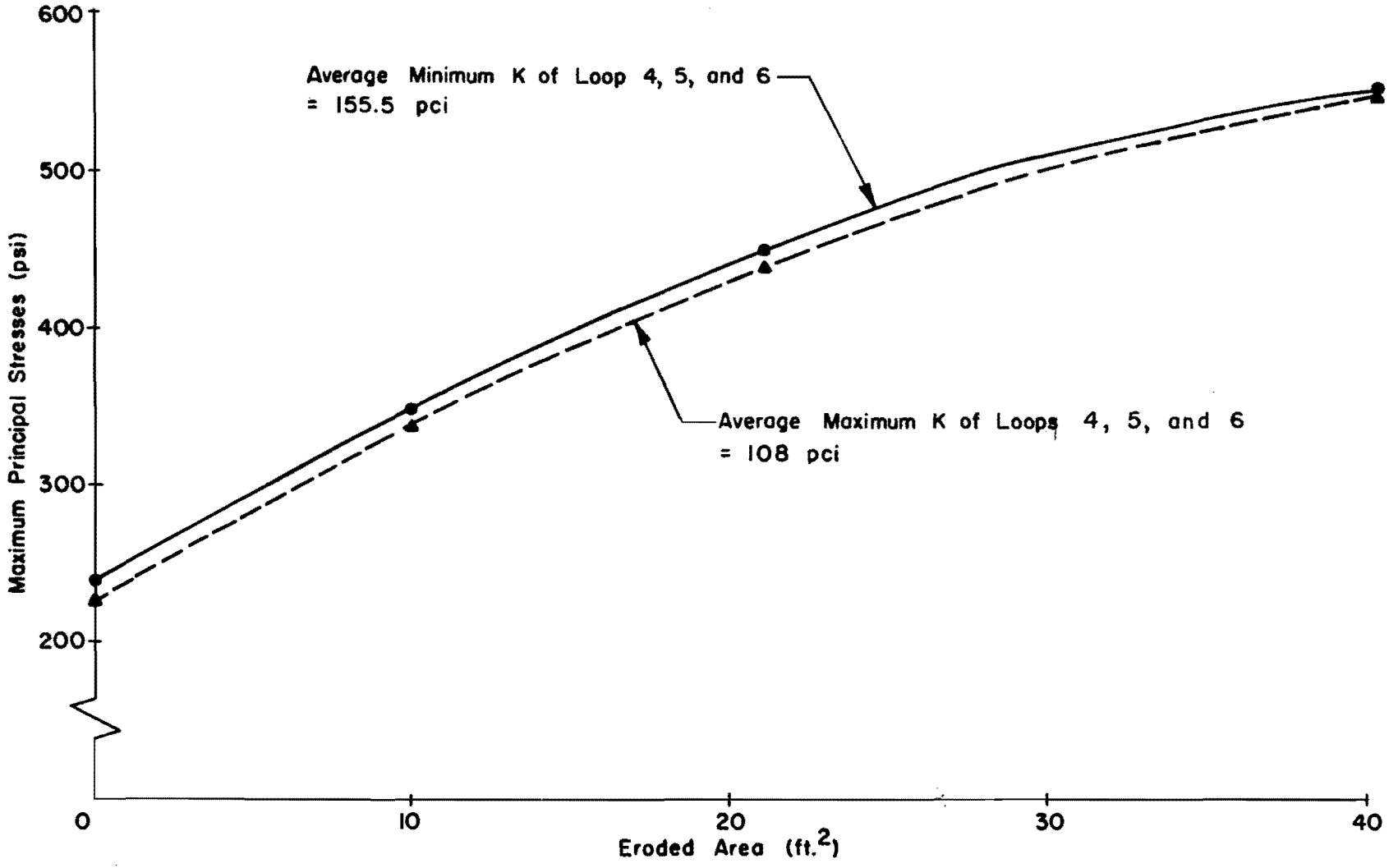

Fig 6.2. Effect of variation of K-subbase at AASHO Road Test on maximum principal stresses.

to illustrate the effect of variation of k-value at the AASHO Road Test. The maximum difference in principal stress was found at full support condition and was approximately equal to 4 percent. From this result, it may be concluded that the effect of variation of k-value during the test period at the AASHO Road Test had little effect on changing maximum principal stress and is considered negligible.

Stress Analysis for Reinforced and Nonreinforced Sections

From previous chapters, the effect of load transfer on pavement stress and the transformation of pumping index to eroded area of reinforced and nonreinforced sections were obtained. At the AASHO Road Test, pumping was generally noted first at the free edge of the pavement and then it progressed along the joint toward the centerline of the pavement. Edge pumping was generally more extensive than joint pumping throughout the life of the pavement. Based on experience and field observation, it is believed that pumping usually starts at the joint of one slab and then moves progressively along the slab. The volume of material pumped by two adjacent slabs is

generally not equal. In analyzing the effect of pumping on maximum principal stresses, it is difficult to make a clear-cut statement about the shape and amount of pumping beneath two adjacent slabs.

Based on previous assumptions about the eroded area beneath pavement slabs, the pumping action at the AASHO Road Test was divided into three parts for this analysis:

1. When the pumping action produced an eroded area beneath the pavement equal to 90 square feet, assume EF = L;
2. When the pumping action produced an eroded area beneath the pavement equal to 40 square feet, assume EF = M; and
3. When the pumping action produced an eroded area beneath the pavement slab equal to 10 square feet, assume EF = S

where EF is defined as the erodability factor.

The facts seem to indicate that no exact solution was available to predict the shape of eroded area beneath two adjacent slabs. Therefore, an attempt was made to simulate the eroded area beneath two adjacent slabs in the field for this analysis.

Based on observations from the AASHO Road Test, it was found that whenever one slab pumps for a period

of time, the adjacent slab will start to pump, but the amount of pumped material for each slab will not be equal. To represent this pumping condition in the field, Fig 6.3 was assumed to be the typical shape of eroded area beneath two adjacent slabs. The slab with the larger eroded area is called the main slab and the slab with the smaller eroded area is called the adjacent slab. The analyses for predicting the maximum stresses and deflections of the two adjacent slabs based on the three pumping conditions are as follows:

1. The main slab and the adjacent slab have the EF equal to L and M, respectively.
2. The main slab and the adjacent slab have the EF equal to M and S, respectively.
3. The main slab and the adjacent slab have the EF equal to S and 3 ft^2, respectively.

Effect of Position of Loading After Pumping

In order to illustrate the effect of position of loading after pumping on maximum principal stresses and deflections, a nonreinforced section from loop 4 of the AASHO Road Test was selected. Since the maximum principal stresses are usually the criterion in rigid

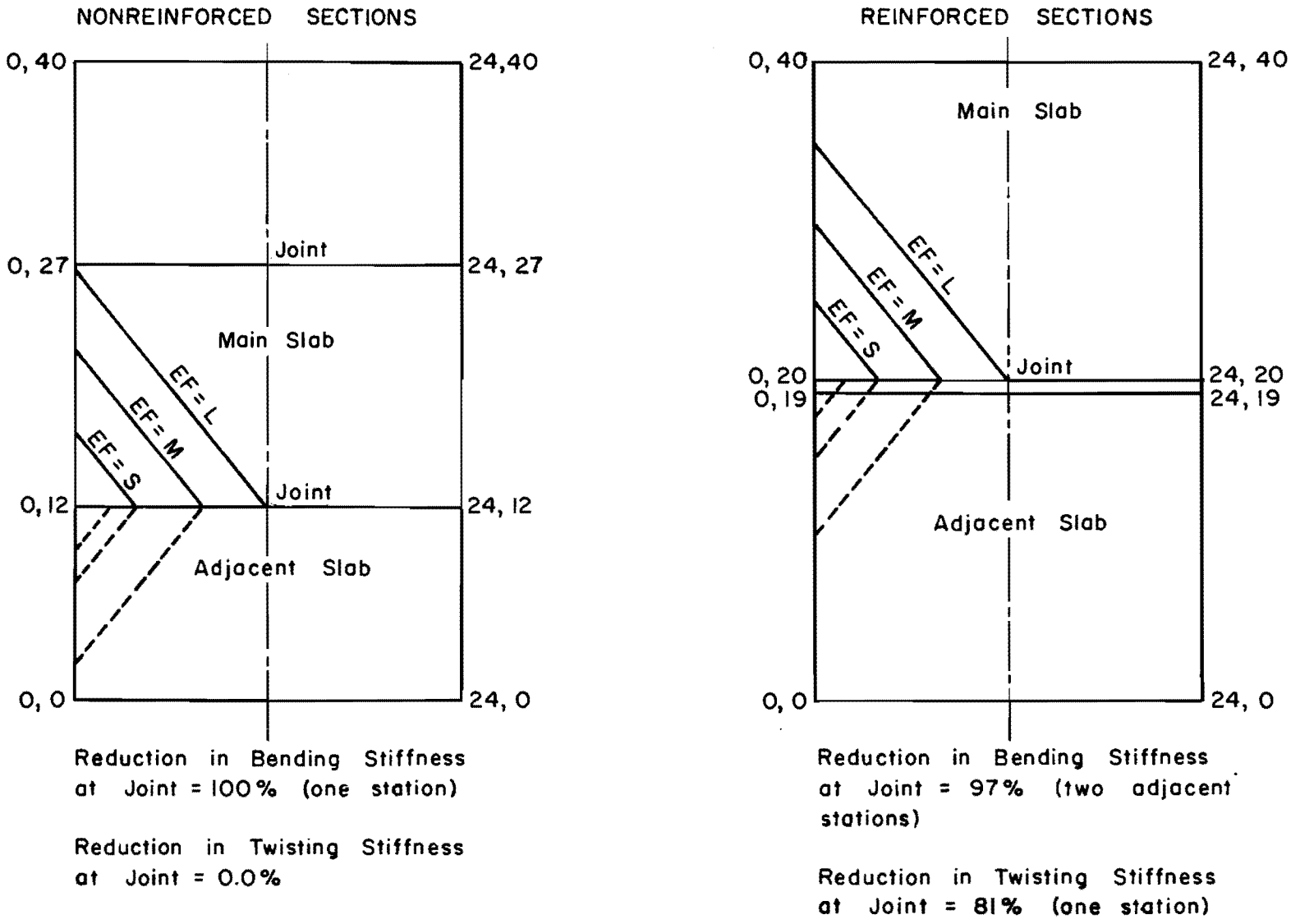

Fig 6.3. Typical shape of eroded area beneath two adjacent slab panels.

pavement systems, the analysis will be concentrated on the maximum principal stresses versus eroded area beneath pavement slab. Based on AASHO Road Test data, the typical conditions of the selected section were:

Pavement thickness	5 inches
Joint spacing	15 feet
Design condition	nonreinforced
E concrete	4.5×10^6 psi
μ	0.2
Axle load	single, 18 kips
Reduction in bending stiffness at the joint (one station)	100 percent
Load position	(1) at joint (2) 1 foot from joint

SLAB 40 was used to predict the maximum stresses and deflections and the results are shown in Table 6.1 for maximum principal stresses and maximum deflections for loading conditions at the joint and 1 foot from the joint. The results are also plotted in Figs 6.4 and 6.5.

As shown by Fig 6.4, the loading condition at 1 foot from the joint produced higher stresses before and at the beginning of pumping action. Joint loading

TABLE 6.1. LOSS OF SUPPORT STUDIES OF NONREINFORCED SECTIONS AT AASHO ROAD TEST

	Erodability Factor	Eroded Area in Main Slab, ft^2	Eroded Area in Adjacent Slab, ft^2	Loop 4		Loop 5	Loop 6
				Load at Joint	1 ft from Joint	Load at Joint	Load at Joint
Max. Principal Stresses, psi	L	90	40	852.2	756.6	609.0	540.3
	M	40	10	583.9	549.0	431.8	375.5
	S	10	3	476.8	491.0	368.2	335.3
Max.Deflections, in.	L	90	40	0.40700	0.36750	0.29820	0.26120
	M	40	10	0.16570	0.14240	0.13420	0.12000
	S	10	3	0.08390	0.06546	0.07368	0.06928

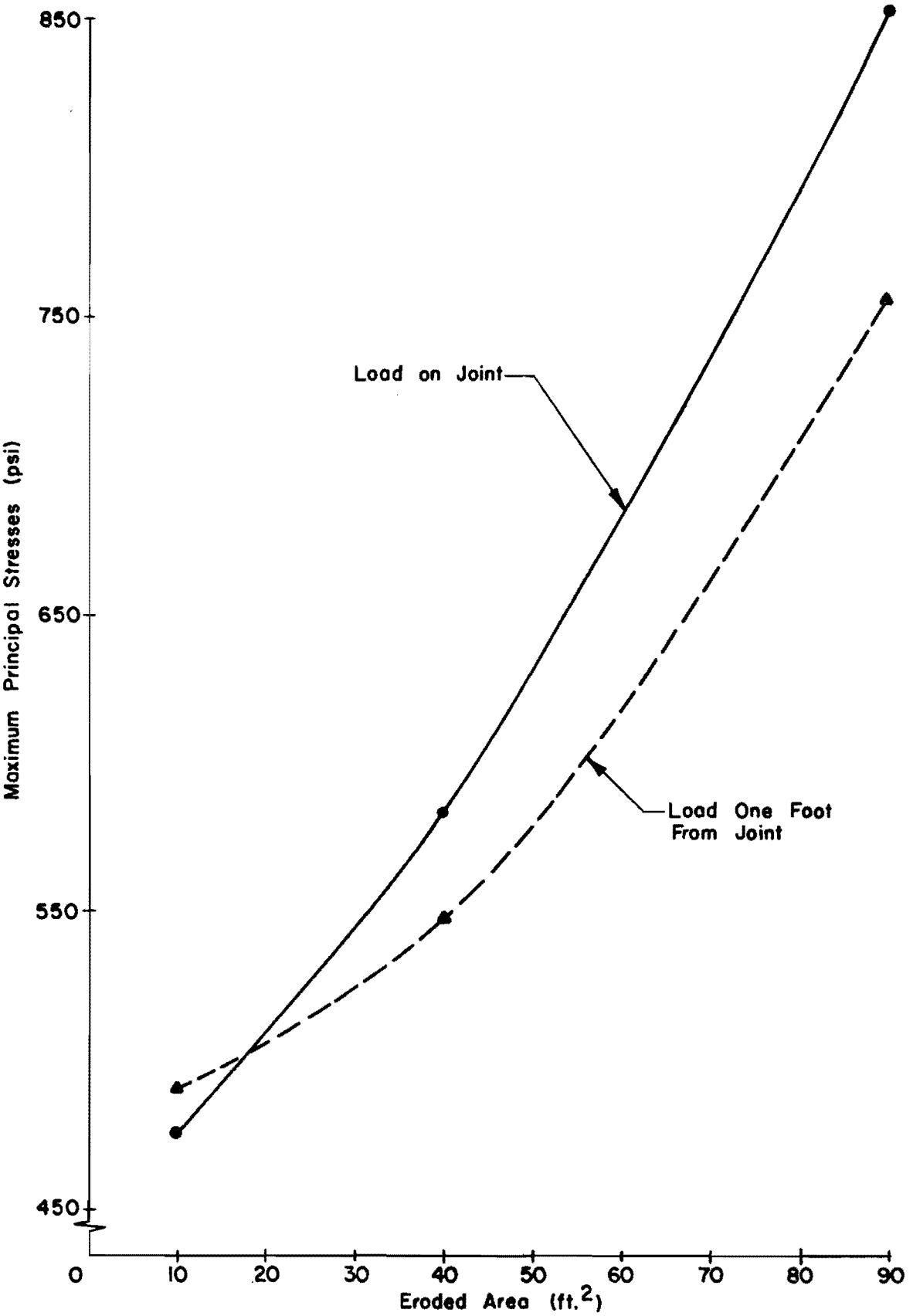

Fig 6.4. Effect of position of loading on maximum principal stresses for eroded pavement.

condition seems to be more critical since it caused increased pumping and produced higher stresses than the load at 1 foot from the joint when the eroded area due to pumping beneath the slab was greater than 18 ft^2 (PI $\approx$ 30 in^3/in). Reinforcing this result by Fig 6.5, it can be seen that the maximum deflections when loading at the joint were higher than those for interior loading conditions at any eroded area.

For reinforced sections, based on previous analysis, the joint loading condition was accepted as the critical loading condition. The maximum principal stress at 97 percent reduction in bending stiffness at two adjacent stations and 81 percent reduction in twisting at one station was 605 psi (extrapolated from Fig 4.8). In comparison with the interior stress (551.8 psi), joint loading condition is approximately 10 percent higher than interior loading condition.

According to these results, it is evident that for loss of support, studies show that in reinforced and nonreinforced sections, the joint loading condition seems to be the best method of approach at the present time.

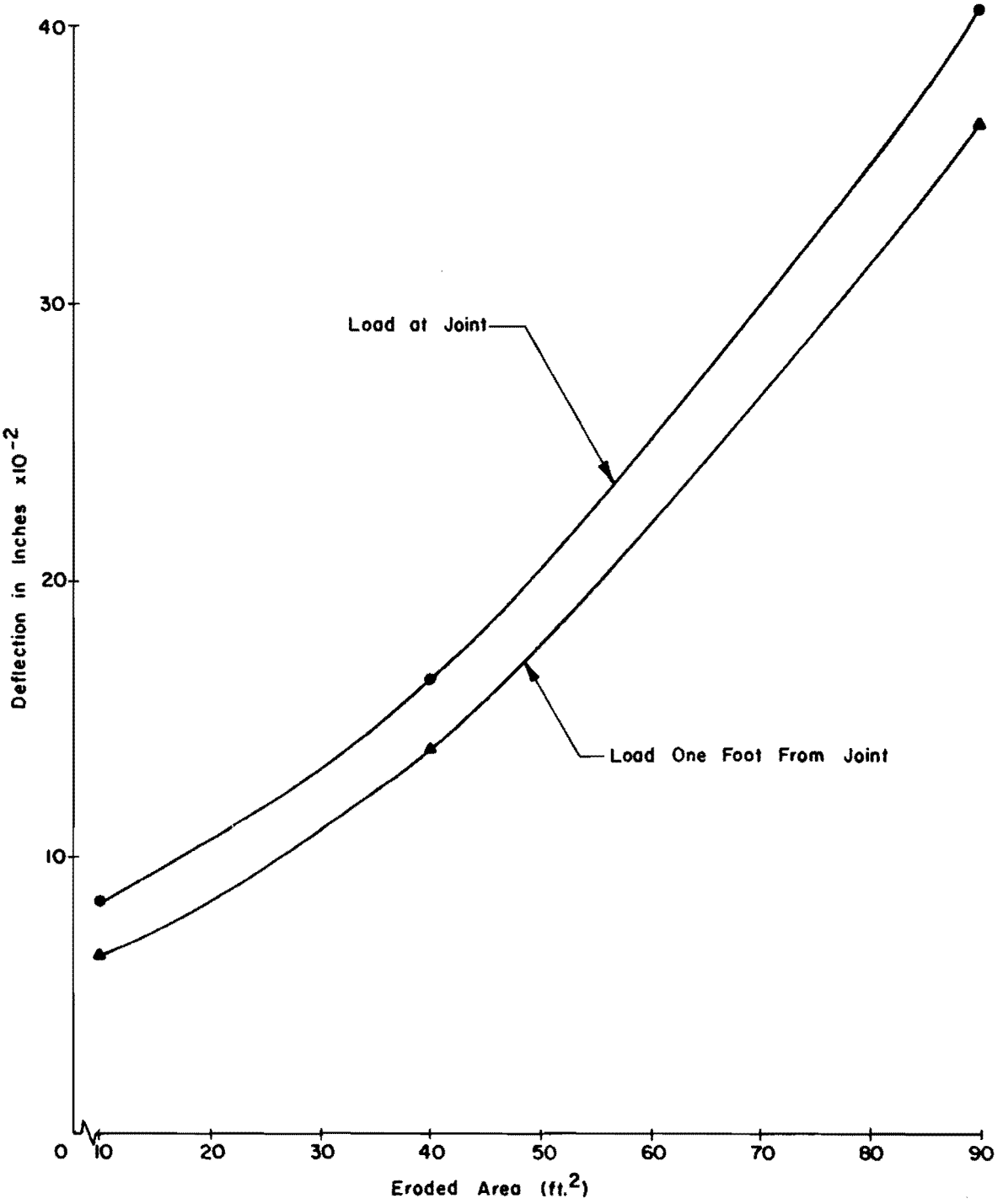

Fig 6.5. Effect of loading position on maximum deflection for eroded pavement.

Effects of Pumping on Maximum Principal Stresses and Maximum Deflections

The purpose of this study was to predict the critical stresses and deflections of rigid pavement for any pumping index. For this analysis, the shapes of eroded areas for reinforced and nonreinforced sections are illustrated in Fig 6.3 and classified below:

EF	Eroded Area in Main Slab, ft^2	Eroded Area in Adjacent Slab, ft^2
L	90	40
M	40	10
S	10	3

For nonreinforced sections, the maximum principal stresses and deflections of loops 4, 5, and 6 were calculated by using SLAB 40. Details on design variables for each loop were presented in Chapter III. The results of the analysis for each loop for a joint loading condition are shown in Table 6.1 and are also plotted in Figs 6.6 and 6.7 to illustrate the effect of eroded area beneath pavement slabs on maximum principal stresses and maximum deflections, respectively.

For reinforced sections, only loop 4 will be analyzed because of the symmetrical characteristics of

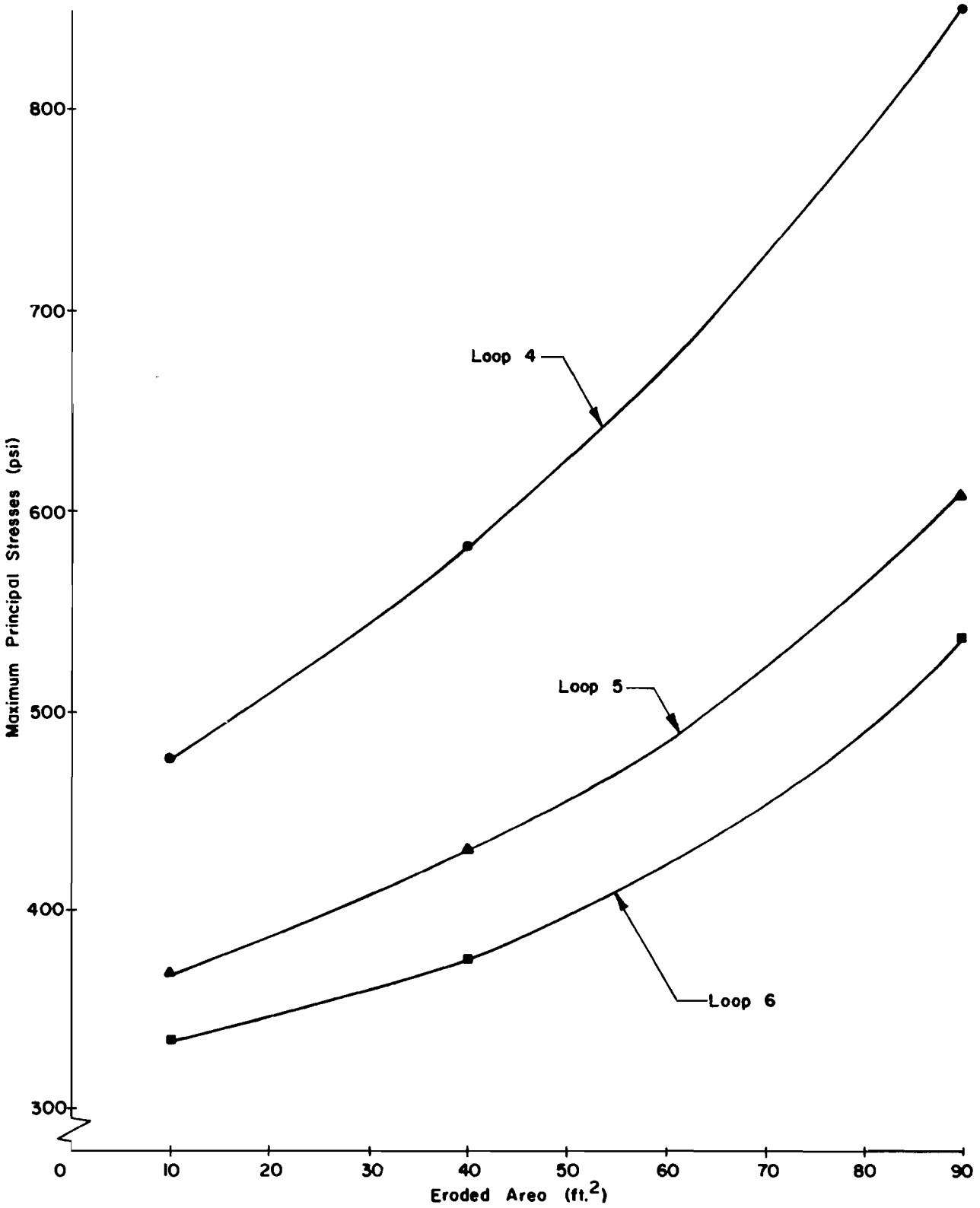

Fig 6.6. Effect of eroded area on maximum principal stresses for nonreinforced sections at AASHO Road Test.

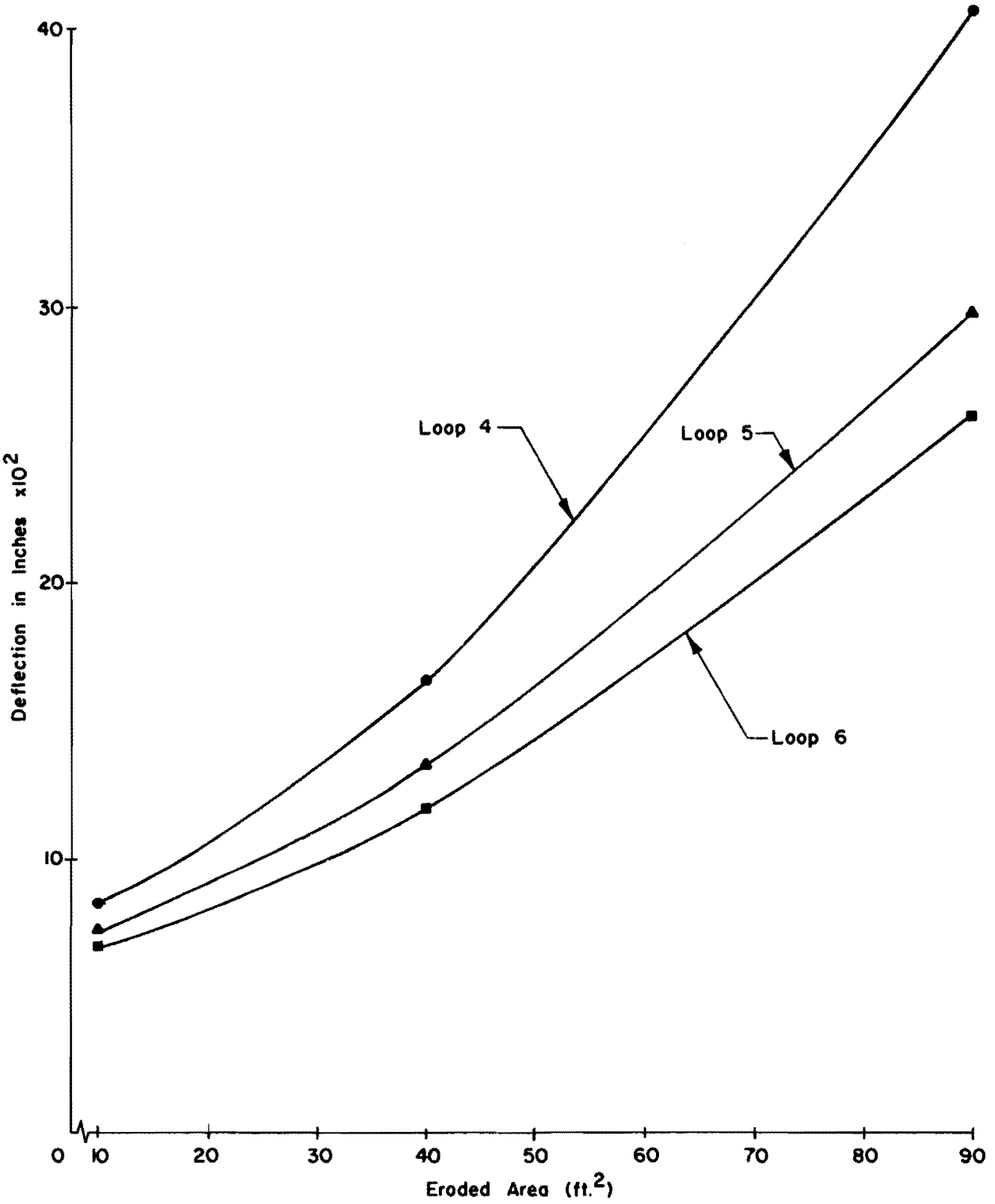

Fig 6.7. Effect of eroded area on maximum deflections for nonreinforced sections at AASHO Road Test.

the stress and deflection analyses of the pavement under pumping conditions. The results of the analysis by SLAB 40 for loop 4 are as follows:

Eroded Area in Main Slab, ft^2	Eroded Area in Adjacent Slab, ft^2	Maximum Deflection, in.	Maximum Stress, psi
90	40	0.3701	708.1
40	10	0.1727	622.2
10	3	0.09199	603.0

To illustrate the effect of pumping on maximum principal stresses and maximum deflections of reinforced sections, these results were plotted in Fig 6.8.

As illustrated by Figs 6.6, Fig 6.7, and 6.8 for both types of pavement, the maximum principal stresses and maximum deflections usually increase as the pumping index increases.

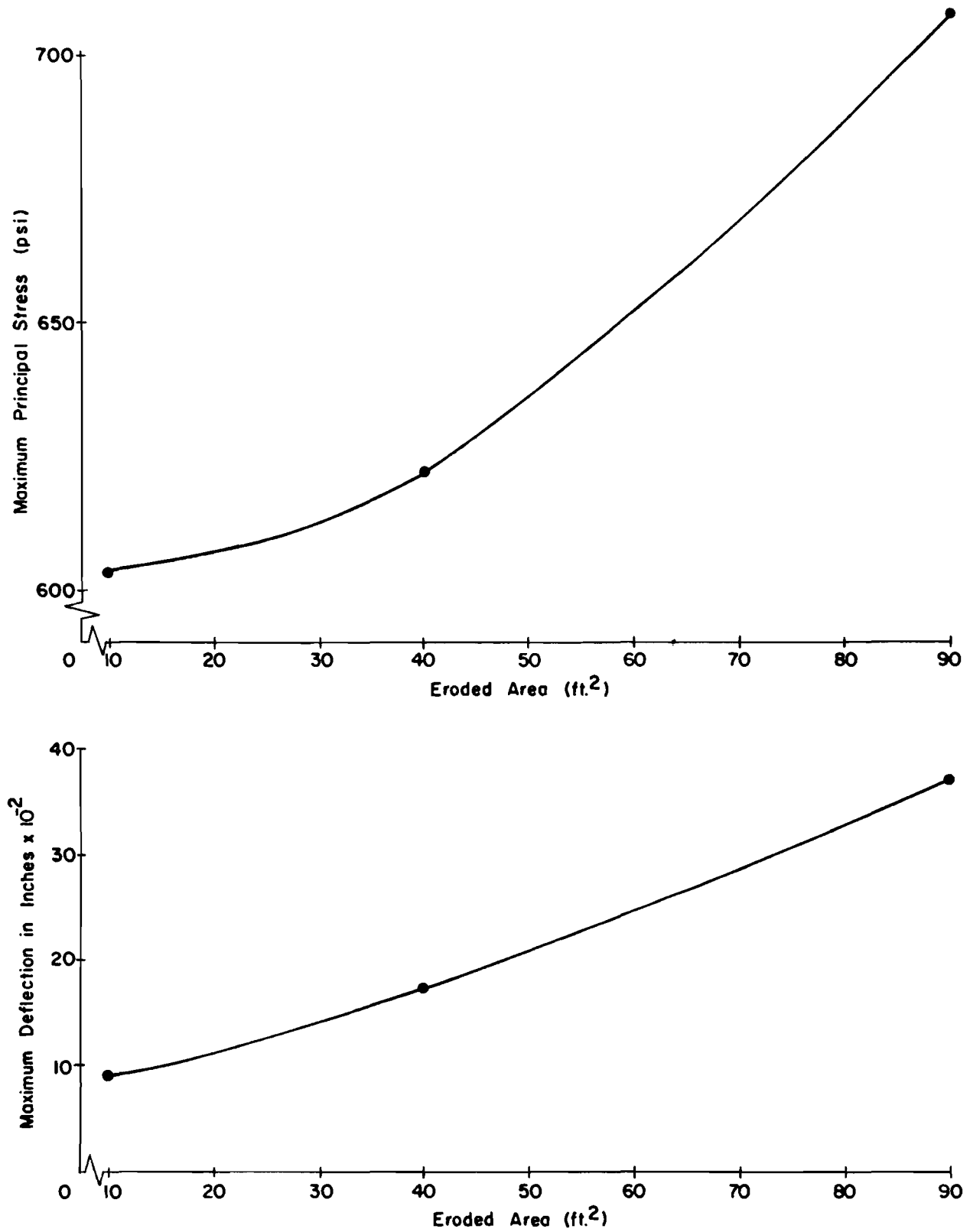

Fig 6.8. Effect of eroded area on maximum stresses and deflections for reinforced sections at AASHO Road Test.

C H A P T E R V I I

CONCLUSIONS AND RECOMMENDATIONS

The study reported herein was conducted for the purpose of modeling the concrete fatigue equation and predicting the maximum principal stress in pavement slabs of reinforced and nonreinforced sections under traffic applications at the AASHO Road Test. This analysis was conducted by use of the discrete-element slab model to determine the sensitivity of pavement stress and deflection to change of slab size and support property. The analysis provides the reasonable predictions on concrete fatigue life from laboratory tests and the maximum principal stress in the slab after any pumping index at the AASHO Road Test.

The following analyses were considered in stress analyses:

(1) The effect of load transfer - This analysis was based on the corner deflection values which were obtained from the AASHO Road Test equation and the theoretical analysis.

(2) The correlation between pumping index and the eroded area - This analysis was based on

engineering judgment and observations from the AASHO Road Test.

(3) The load locations at the joint and 2 feet from the pavement edge.

The following conclusions and recommendations are made on the basis of the results and observations of this analysis.

Conclusions

The conclusions are limited to the range of variables studied in this report and listed as follows:

(1) The effect of applied flexural stress on fatigue life of concrete is highly important.

(2) The effects of concrete properties and speed of test on fatigue life of concrete are negligible.

(3) The probability of failure of concrete increases with an increase in applied flexural stress.

(4) Concrete exhibits no fatigue limit up to ten million applications.

(5) Observations showed that the traffic, material properties, and environmental conditions at the AASHO Road Test varied during the test period.

(6) The effect of joint spacing for reinforced and nonreinforced sections was studied and based on reduction in bending and twisting stiffness.

(7) For nonreinforced sections, a reduction in bending stiffness of 100 percent is required to simulate the AASHO pavements.

(8) For reinforced sections, a reduction in bending and twisting stiffness of 97 and 81 percent, respectively, is required to simulate the AASHO pavements.

(9) A reduction in bending stiffness has a large effect on maximum deflection but only a small effect on maximum principal stress.

(10) A reduction in twisting stiffness has a large effect on maximum principal stress but only a small effect on maximum deflection.

(11) The highest maximum principal stress and deflection are produced when loads are located at the joint.

(12) Variation of elastic modulus of support has a small effect in stress analysis and is negligible.

(13) The maximum principal stress was predicted at full support and at various stages of support losses at two adjacent slabs.

Recommendations

In long-range terms, to develop the more exact and reliable design method for rigid pavement requires the following studies:

(1) Development of a fatigue failure model of rigid pavement.

(2) Understanding the logical mechanism after the first crack has developed. This mechanism seems to be logical at the present time. The difficult problem is what happens to the pavement behavior after the first crack and an increasing number of cracks develop.

(3) Temperature effects should be taken into consideration.

(4) Mode of loading. The AASHO Road Test procedure permitted the performance of each test

section for the repetition of a specific load. In fact, pavement in-service life carries a wide variety of single and tandem-axle loads. This mixed traffic causes more variation in stress level, which definitely influences fatigue life.

(5) Use of stochastic concepts. The variability of all the inputs in the system along with sensitivity analysis might be helpful to approach the more exact and reliable design method.

R E F E R E N C E S

1. "Design and Control of Concrete Mixture," Portland Cement Association, 1952.

2. Jones, Truman R., and T. J. Hirsch, "The Physical Properties of Concrete at Early Ages," Research Project RP-19, Texas Highway Department, August 1961.

3. Jones, Truman R., Jr., and T. J. Hirsch, "The Curing of Portland Cement Concrete," Research Project RP-19, Texas Highway Department, August 1960.

4. "Thickness Design for Concrete Pavements," Portland Cement Association, 1966.

5. Colley, B. E., and W. J. Nowlen, "Performance of Subbase for Concrete Pavement Under Repetitive Loading," Highway Research Record No. 202, Highway Research Board, Washington, D.C., 1967, pp. 32-58.

6. Sinha, B. P., Kurt H. Gerstle, and Leonard G. Tulin, "Stress-Strain Relation for Concrete Under Cyclic Loading," American Concrete Institute, February 1964, pp. 194-210.

7. Kesler, Clyde E., "Effect of Speed of Testing on Flexural Fatigue Strength of Plain Concrete," Proceedings, Vol. 32, Thirty-Second Annual Meeting, Highway Research Board, Washington, D.C., 1953, pp. 251-258.

8. Murdock, John W., and Clyde E. Kesler, "Effect of Range of Stress on Fatigue Strength of Plain Concrete Beams," ACI Report 55-11, American Concrete Institute, August 1958, pp. 221-231.

9. Nordby, Gerre M., "Fatigue of Concrete - A Review of Research," ACI Report 55-11, American Concrete Institute, August 1958, pp. 191-214.

10. Mills, R. E., and R. F. Dawson, "Fatigue of Concrete," Proceedings, Seventh Annual Meeting, Highway Research Board, Washington, D.C., 1928, pp. 160-172.

11. Yoshimoto, Akira, and Skoji Ogino, "Fatigue Strength of Concrete Subjected to Repeated Flexural Stress," Special Report, American Concrete Institute.

12. Chang, Tien S., and Clyde E. Kesler, "Fatigue Behavior of Reinforced Concrete Beam," ACI Report 55-14, American Concrete Institute, August 1958, pp. 245-254.

13. Ruiz, Walter N., and George Winter, "Reinforced Concrete Beam Under Repeated Loads," Structural Design Division, American Society of Civil Engineers, June 1959, pp. 1189-1209.

14. Stelson, Thomas E., and John N. Cernica, "Fatigue Properties of Concrete Beams," ACI Report 55-15, American Concrete Institute, August 1958, pp. 255-259.

15. McCall, John T., "Probability of Fatigue Failure of Plain Concrete," ACI Report 55-13, American Concrete Institute, August 1958, pp. 233-244.

16. Sinha, B. P., Kurt H. Gestle, and Leonard G. Tulin, "Response of Singly Reinforced Beams to Cyclic Loading," American Concrete Institute, August 1964, pp. 1021-1038.

17. Yoder, E. J., Principal of Pavement Design, John Wiley & Sons, New York, Fifth Printing, February 1967.

18. Jain, Surendra Prakash, "Flexible Pavement System - Second Generation, Incorporating Fatigue and Stochastic Concepts," Ph.D. Dissertation, The University of Texas at Austin, December 1971.

19. Fordyce, Phil, and W. E. Teske, "Some Relationships of the AASHO Road Test to Concrete Pavement Design," Highway Research Record No. 44, Highway Research Board, Washington, D.C., December 1963.

20. Hudson, W. R., and B. F. McCullough, "Development of SAMP: An Operational Pavement Design System, Part II," Final Report NCHRP Project 1-10, National Cooperative Highway Research Program, September 1970.

21. "The AASHO Road Test Report 3, Traffic Operation and Pavement Maintenance," Special Report 61C, Highway Research Board, Washington, D.C., 1962.

22. Hudson, W. R., and F. H. Scrivner, "AASHO Road Test Principal Relationships - Performance With Stress, Rigid Pavement," Special Report 73, Highway Research Board, Washington, D.C., 1962.

23. Abou-Ayyash, Adnan, and W. R. Hudson, "Analysis of Bending Stiffness Variation at Cracks in Continuous Pavements," Research Report No. 56-22, Center for Highway Research, The University of Texas at Austin, August 1971.

24. Westergaard, H. M., "Stresses in Concrete Pavements Computed by Theoretical Analysis," Public Roads, Vol. 7, No. 2,

25. Brown, Russel H., and James O. Jirsa, "Reinforced Concrete Beam Under Load Reversals," American Concrete Institute, Vol. 68, No. 68-39, 1971, pp. 380-390.

26. "The AASHO Road Test Report 2, Materials and Constructions," Special Report 61B, Highway Research Board, Washington, D.C., 1962.

27. Roberts, Freddy L., and W. R. Hudson, "Pavement Serviceability Equations Using the Surface Dynamics Profilometer," Research Report No. 73-3, Center for Highway Research, The University of Texas at Austin, April 1970.

28. Carey, W. N., Jr., and P. E. Iric, "The Pavement Serviceability Performance Concepts," Bulletin 250, Highway Research Board, Washington, D.C., 1960.

29. Statistical Computer Program for Stepwise Multiple Regression, Center for Highway Research, The University of Texas at Austin.

30. Kamel, Nabil I., "System Loss of Support in Rigid Pavements," Term Paper, The University of Texas at Austin, May 1971.

31. "The AASHO Road Test Report 1, History and Description of Project," Special Report 61A, Highway Research Board, Washington, D.C., 1961.

32. "The AASHO Road Test Report 5, Pavement Research," Special Report 61E, Highway Research Board, Washington, D.C., 1962.

33. Vesic, Aleksandar, S., and Surendra K. Saxena, "Analysis of Structural Behavior of Road Test Rigid Pavements," NCHRP Project 1-4(1), National Cooperative Highway Research Program, 1968.

34. Panak, John J., and Hudson Matlock, "A Discrete-Element Method of Analysis for Orthogonal Slab and Grid Bridge Floor System," Research Report No. 56-25, Center for Highway Research, The University of Texas at Austin, August 1971.

35. McCullough, B. F., "Design Manual for Continuously Reinforced Concrete Pavement," United States Steel Corporation, Pittsburgh, Pennsylvania, January 1970.

36. Stelzer, C. Fred, Jr., and W. Ronald Hudson, "A Direct Computer Solution for Plates and Pavement Slabs," Research Report No. 56-9, Center for Highway Research, The University of Texas at Austin, October 1967.

37. Hudson, W. R., "Discontinuous Orthotropic Plates and Pavement Slabs," Ph.D. Dissertation, The University of Texas, Austin, August 1962.

APPENDIX 1

SOLUTION FOR CODED DATA INPUT
LOOPS 4, 5, AND 6

APPENDIX 1

SOLUTION FOR CODED DATA INPUT
LOOPS 4, 5, AND 6

Loop 4

Pavement thickness = 5 inches

Single load = 18 inches

Elastic modulus of concrete = 4.5×10^6 psi

k from spring trend program = 112 pci

Solution

Increment in x,y-direction = 12 inches

Slab bending stiffness per unit length $D = \frac{Et^3}{12(1-\mu^2)}$

$$D_x = D_y = \frac{4.5 \times 10^6 \times 5^3}{12(1 - 0.2^2)} = 4.88 \times 10^7 \text{ inch-pounds.}$$

$\frac{D_x}{4} = \frac{D_y}{4}$ = 1.22E + 07 = joint's slab bending stiffness

Support spring S = elastic modulus of support × area of joint

= $112 \times 12 \times 12 = 16.13 \times 10^3$ inch-pounds.

$\frac{S}{4}$ = support spring for each joint

Joint's twisting stiffness:

$$C = \frac{Et^3}{12(1 + \mu)}$$

$$= \frac{4.5 \times 10^6 \times 5^3}{12(1 + 0.2)}$$

$$= 3.9 \times 10^7 \text{ inch-pounds}$$

For 15-foot spacing, for any 24-by-40-foot section at the joint (in x-direction), D_y should be reduced $\approx$ 100 percent.

Reduction in D_y at joint

for 15-foot spacing $= -1.0D_y$

$= -4.88 \times 10^7$ inch-pounds

For 40-foot spacing, for any 24-by-40-foot section, assume reduction of 90 percent at two adjacent joints. Therefore, reduction in D_y at the joint for 40-foot spacing = $-0.9D_y$.

D_y at joint = $0.9 \times 4.88 \times 10^7$

= -4.4×10^7 inch-pounds

$\frac{D_Y}{2}$ = -2.20E + 07 inch-pounds

Loop 5

Pavement thickness = 6.5 inches

Single load = 22.4 kips

k = 103.5 pci

$D_x = D_y = 1.07 \times 10^8$ inch-pounds

$\frac{D_X}{4} = \frac{D_Y}{4}$ = 2.675E + 07 inch-pounds

$S = 14.90 \times 10^3$ inch-pounds

$\frac{S}{4}$ = 3.720E + 03 inch-pounds

C = 8.55E + 07 inch-pounds

Loop 6

Pavement thickness = 8 inches

Single load = 30 kips

k = 117.5 pci

$D_x = D_y = 20 \times 10^7$ inch-pounds

$\frac{D_x}{4} = \frac{D_y}{4} = 5.00E + 07$ inch-pounds

$S = 1.70 \times 10^4$ inch-pounds

$\frac{S}{4} = 4.250E + 03$ inch-pounds

$C = 1.600E + 08$ inch-pounds

APPENDIX 2

ANALYSIS OF THE RELATIONSHIP OF PUMPING INDEX AND ERODED AREA

APPENDIX 2

ANALYSIS OF THE RELATIONSHIP OF PUMPING INDEX AND ERODED AREA

General Equation

$$EA = \frac{1}{2}dx\ dz = \frac{1}{2} \times 48 \times 60 \times dy^2 = 1440 \times dy^2$$

(1) For a 40-foot slab, substitute dx and dz in terms of dy where dy : dz : dz = 1 : 48 : 60.

$$PI = 210 \times \frac{dy \times 48dy \times 60dy}{40}$$

$$= 15100dy^3$$

PI	dy^3	dy	Eroded Area, ft^2
0	-	-	-
50	50/15100 = 1/302	1/6.7	$1440/6.70^2 = 32.10$
100	100/15100 = 1/151	1/5.32	$1440/5.32^2 = 51.00$
150	150/15100 = 1/101	1/4.65	$1440/4.65^2 = 66.70$
200	200/15100 = 1/75.5	1/4.27	$1440/4.27^2 = 79.00$
250	250/15100 = 1/60.4	1/3.92	$1440/3.92^2 = 93.50$

(2) For a 15-foot slab, substitute dx and dz in terms of dy where dy : dz : dx = 1 : 48 : 60.

$$PI = 100 \times 48dy \times \frac{60dy \times dy}{15}$$

$$= 19200dy^3$$

PI	dy^3	dy	Eroded Area, ft^2
50	50/19200 = 1/384	1/7.26	$1440/7.26^2 = 27.40$
100	100/19200 = 1/192	1/5.77	$1440/5.77^2 = 43.20$
150	150/19200 = 1/128	1/5.03	$1440/5.03^2 = 56.80$
200	200/19200 = 1/96	1/4.57	$1440/4.57^2 = 69.00$
250	250/19200 = 1/77	1/4.25	$1440/4.25^2 = 80.00$
300	300/19200 = 1/64	1/4.00	$1440/4.00^2 = 90.00$

THE AUTHORS

Piti Yimprasert was an Assistant Research Engineer while at the Center for Highway Research. His engineering experience also includes work with the Thailand Highway Department, and S.A.E., Inc., in Thailand. His recent research interest has been in analysis and modification of the rigid pavement design system.

B. Frank McCullough is an Assistant Professor of Civil Engineering at The University of Texas at Austin. His engineering experience includes work with the Texas Highway Department and the Center for Highway Research at The University of Texas at Austin. His current research is concerned with (1) systematic pavement design and (2) the evaluation and revision of the Texas Highway Department rigid pavement design procedure. He is the author of numerous publications and a member of several professional societies.